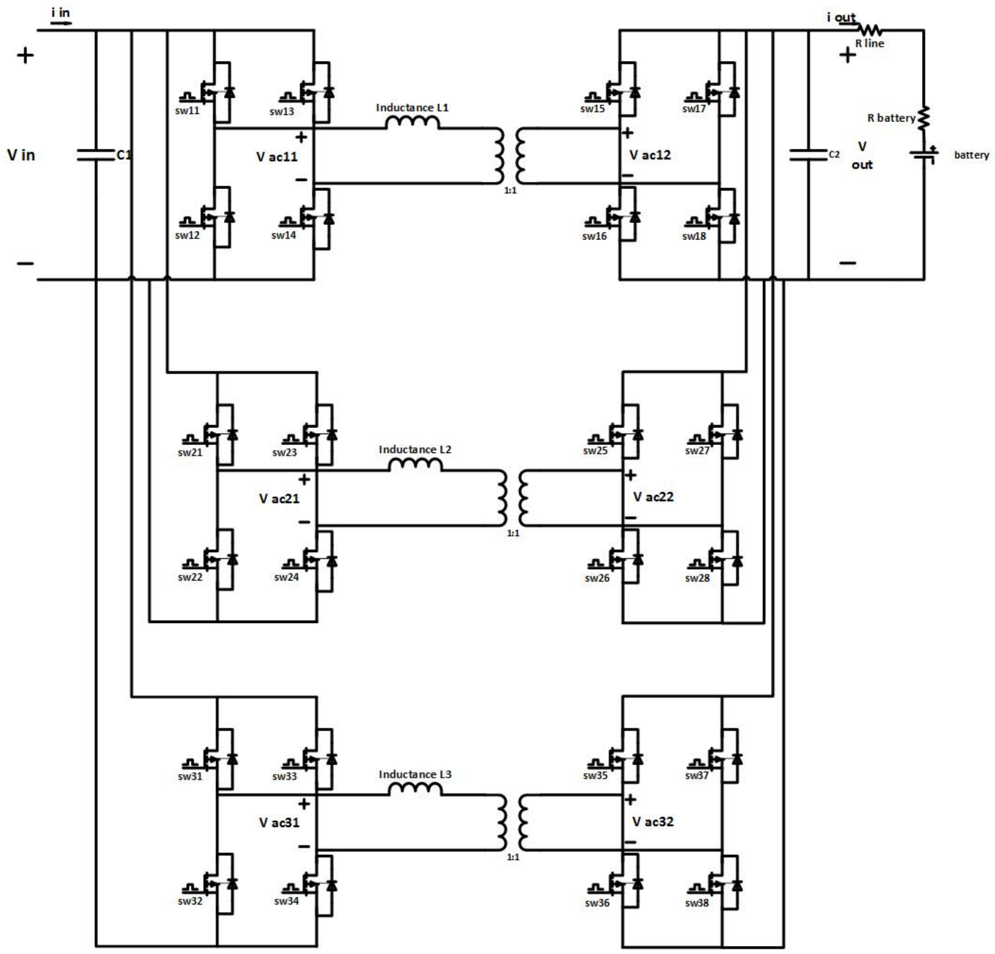

Digital Control of the DC/DC Converter of a 300 kW Fast Charger Station

Master's thesis in Electric Power Engineering

JOSÉ IGNACIO GARCÍA BAJO

Department of Electrical Engineering
CHALMERS UNIVERSITY OF TECHNOLOGY
Gothenburg, Sweden 2018

Master's thesis 2018

Digital control of a DC/DC converter of a 300 kW fast charger station

JOSÉ IGNACIO GARCÍA BAJO

Department of Electrical Engineering

Chalmers University of Technology
Gothenburg, Sweden 2018

A description of the control strategy of the DC/DC converter of a fast charger station for electric vehicles is presented in this report.
The sofware used was Matlab and Simulink.
JOSÉ IGNACIO GARCÍA BAJO

Supervisor: Saeid Haghbin, Elbind Electronik AB.
Examiner: Ola Carlson, Department of Electrical Engineering

Master's Thesis 2018
Department of Electrical Engineering
Chalmers University of Technology
SE-412 96 Gothenburg
Telephone +46 31 772 1000

Cover: Power stage of three parallel connected DC/DC converters.

Typeset in LaTeX
Printed by
Gothenburg, Sweden 2018

A description of the control strategy of the DC/DC converter of a fast charger station for electric vehicles is presented in this report.
The sofware used was Matlab and Simulink.
JOSÉ IGNACIO GARCÍA BAJO
Department of Electrical Engineering
Chalmers University of Technology

Abstract

Nowadays, electric vehicles are the main alternative to traditional vehicles. However, they have some drawbacks, such as the charging time of the batteries.

The digital control of the DC/DC stage of a 300 kW fast charger station including parallel connection of 100 kW modules are subject of this thesis. The goal with fast charging is to drastically reduce the charging time, reducing it to 15-20 min for heavy electric vehicles, such as trucks and buses.

The topology selected for this DC/DC converter is a bidirectional dual active bridge DC/DC converter. Therefore, the main parameter to control in this converter is the phase shift between the voltages of the bridges.

The main objectives of this Master Thesis are: a deeply understanding of the charger's topology, specially the DC/DC converter; a description of the DC/DC converter operation; the selection of the charging strategy; modeling the system; developing the digital control of a single module DC/DC converter; deciding the parallel connection for a 3 modules DC/DC converter and, finally, its control strategy and obtaining the digital control of the 3 modules DC/DC converter.

This objectives were developed along this Master Thesis, and a digital control of a 300 kW DC/DC converter in charging mode was achieved.

As future work, the discharging mode of the DC/DC converter is suggested to be studied as well. Also, the implementation on a DSP can be started, as well as its implementation in a prototype to analyze the behaviour in a real system.

Keywords: power, electronics, digital, control, DC/DC, converter, charging, electrical, vehicles.

Acknowledgements

I would like to express my gratitude to my supervisor Saeid Haghbin, who gave me the opportunity to work in such an interesting topic and gave the support, patience and guidance needed along the Thesis. Also, I would like to thank mi examiner Ola Carlson for his support and suggestions along this time. It was also essential the support received from Elbind Electronik AB, showing the path to follow for new generations of chargers. It was really important as well the support of my Spanish supervisor Carlos Platero, who gave me the opportunity to discuss ideas and finding new alternatives to my Thesis.
I do not want to finish without expressing my gratitude to my colleagues in the department and master program, who gave me support and by contrasting ideas I was able to develop my Thesis.
Finally and really important, I would like to express my gratitude towards my friends, family and Susana for their constant support in any decision I made along these years, giving me opportunity of sharing with them my success.

José Ignacio García Bajo, Gothenburg, June 2018

Contents

List of Figures **xi**

List of Tables **xvii**

1 Introduction **1**

2 Theory **3**
2.1 Charger's topology 3
2.2 Single phase dual active bridge DC/DC converter 4
2.2.1 Topology description 5
2.2.2 Converter operation 6
2.3 The reason of using a 3 modules DC/DC converter 9

3 Digital control of a single module converter **13**
3.1 Average model 15
3.2 Small-signal model 16
3.3 Simulink Block 19
3.4 Control methods 20
3.4.1 Voltage control 21
3.4.2 Current control 30
3.4.3 Cascade control 37

4 Digital control of a three parallel connected DC/DC modules **53**
4.1 Parallel connection and control strategy 56
4.2 Average model 58
4.3 Small-signal model 59
4.4 Simulink Block 60
4.5 Control methods 62
4.5.1 Voltage control 63
4.5.2 Current control 72
4.5.3 Cascade control 81

5 Results **93**
5.1 Digital control of a one module converter 93
5.1.1 Constant current mode with current control. 94
5.1.2 Constant voltage mode with cascade control. 95
5.2 Digital control of a 3 modules converter 97

5.2.1 Constant current mode with current control. 99
5.2.2 Constant voltage mode with cascade control. 101

6 Conclusion and future work **105**

Bibliography **107**

List of Figures

2.1 General structure of the bidirectional 300 kW charger. 4
2.2 The dual active bridge bidirectional DC/DC converter used. 4
2.3 The lossless DAB model. 6
2.4 Simulink system working with a phase shift of 51.47°. 8
2.5 Actual values from variables of the Simulink system working with a phase shift of 51.47°. The variables are, in order: v_{ac1}, v_{ac2}, v_L the voltage across the inductance, i_L the current across the inductance in the AC side and i_{out} the output DC current. 8
2.6 Power as function of the phase shift. 10
2.7 Power as function of the input voltage. 10
2.8 Power as function of the input voltage. 11

3.1 The battery charging strategy. 14
3.2 Average circuit model of a DAB bidirectional DC/DC converter. . . . 16
3.3 Small-signal circuit model of a DAB bidirectional DC/DC converter. . 18
3.4 Simplified small-signal circuit model of a DAB bidirectional DC/DC converter. 19
3.5 Simulink block for a one module DC/DC converter. 19
3.6 Step response for voltage control for a one module DAB bidirectional DC-DC converter. Simulink program. 22
3.7 Step response for voltage control for a one module DAB bidirectional DC-DC converter. 22
3.8 Voltage control strategy. Simulink model. 23
3.9 Bode diagram of T and total system (sys). Case: one module and voltage control. 25
3.10 Voltage control strategy for a one module DAB bidirectional DC-DC converter. Results. 26
3.11 Simulink block of the digital voltage control strategy for a one module DAB bidirectional DC-DC converter. 27
3.12 Results from the step response for voltage control for a one module DAB bidirectional DC-DC converter. Comparison between G(s) and G(z). 28
3.13 Results of the digital voltage control strategy for a one module DAB bidirectional DC-DC converter. 29
3.14 Simulink program of the step response for current control for a one module DAB bidirectional DC-DC converter. 31

3.15 Results of the step response for current control for a one module DAB bidirectional DC-DC converter. 31
3.16 Simulink model of the current control strategy. 32
3.17 Bode diagram of T and total system (sys). Case: one module and current control. 33
3.18 Results of the current control strategy for a one module DAB bidirectional DC-DC converter. 34
3.19 Simulink block of the digital current control strategy for a one module DAB bidirectional DC-DC converter. 35
3.20 Results of the step response for current control for a one module DAB bidirectional DC-DC converter. Comparison between G(s) and G(z). 35
3.21 Digital current control strategy for a one module DAB bidirectional DC-DC converter. Results. 36
3.22 Cascade scheme. 37
3.23 Inner loop. 38
3.24 Bode diagram of T and total system in the inner loop. Case: one module and cascade control. 39
3.25 Results of the cascade control for a one module DAB bidirectional DC-DC converter. Inner loop design. 40
3.26 Outer loop of the cascade control for a one module DAB DC/DC converter. 40
3.27 Rote locus of GT, the first one, and $GT_{simplified}$, the second one. . . . 42
3.28 Step response of GT and $GT_{simplified}$. 43
3.29 Bode diagram of T and total system in the outer loop. Case: one module and cascade control. 44
3.30 Simulink block for a one module DAB DC-DC converter of the cascade control. 45
3.31 Simulink results of the cascade control for a one module DAB DC-DC converter. First graph is the output voltage, second one the current output and third one the phase shifts. Blue curves are the references, red curves the output from the real system and yellow ones the output from the transfer function system. 46
3.32 Simulink block of the digital cascade control strategy for a one module DAB bidirectional DC-DC converter. 47
3.33 Inner loop in the discrete mode. 47
3.34 Discrete mode. Cascade control for a one module DAB bidirectional DC-DC converter. Inner loop design. Results. 48
3.35 Outer loop. Discrete mode. 49
3.36 Results of the discrete mode. Cascade control for a one module DAB bidirectional DC-DC converter. Outer loop design. 50

3.37 Results of the digital cascade control strategy for a one module DAB bidirectional DC-DC converter. First graph is the output voltage, second one is the output current and the third one the phase shift. Curves in order, according to the legend: 1. Output converter reference. 2. Output from a real system model controlled with a PI(z). 3. Output from a continuous-time transfer function model controlled with a PI(z). 4. Output from a discrete-dime transfer function model controlled with a PI(z). 5. Output from a continuous-time transfer function model controlled with a PI(s). 6. Output from a real system model controlled with a PI(s). 51

4.1 Parallel strategy I: isolated inputs. 53
4.2 Parallel strategy II: ISOP configuration. 54
4.3 Parallel strategy III: IPOP configuration. 54
4.4 IPOP configuration of the 300 kW DC/DC converter. 55
4.5 $\frac{\Delta I_{tot}}{I_{tot}}$ as a function of α and β. The one with the lowest starting point corresponds to α = -0.1. Then the others are, in order: -0.02, 0, 0.02 and 0.1. 57
4.6 Average circuit model of a 3 modules DAB bidirectional DC/DC converter. 59
4.7 Simplified output port of the small-signal circuit model of a 3 modules DAB bidirectional DC/DC converter. 60
4.8 Simulink block for the 3 modules DAB DC/DC converter. 61
4.9 Simulink program of the step response for voltage control for a 3 modules DAB bidirectional DC-DC converter. 64
4.10 Results of the step response for voltage control for a 3 modules DAB bidirectional DC-DC converter. 65
4.11 Simulink model of the voltage control strategy for a 3 modules converter. 66
4.12 Bode diagram of T and total system (sys). Case: 3 modules and current control. 67
4.13 Results of the voltage control strategy for a 3 modules DAB bidirectional DC-DC converter. 68
4.14 Simulink block of the digital voltage control strategy for a 3 modules DAB bidirectional DC-DC converter. 69
4.15 Results of the step response for voltage control for a 3 modules DAB bidirectional DC-DC converter. Comparison between G(s) and G(z). 70
4.16 Results of the digital voltage control strategy for a 3 modules DAB bidirectional DC-DC converter. First graph is the output voltage and second one the phase shift. Curves, in order, according to the legend: 1. Output converter reference. 2. Output from a real system model controlled with a PI(z). 3. Output from a continuous-time transfer function model controlled with a PI(z). 4. Output from a discrete-dime transfer function model controlled with a PI(z). 5. Output from a continuous-time transfer function model controlled with a PI(s). 6. Output from a real system model controlled with a PI(s). 71

4.17 Simulink program for the step response for current control for a 3 modules DAB bidirectional DC-DC converter. 73
4.18 Results for the step response for current control for a 3 modules DAB bidirectional DC-DC converter. 74
4.19 Simulink model for the current control strategy for a 3 modules converter. 75
4.20 Bode diagram of T and total system (sys) for the case of 3 modules and current control. 76
4.21 Results of the current control strategy for a 3 modules DAB bidirectional DC-DC converter. 77
4.22 Simulink block of the digital current control strategy for a 3 modules DAB bidirectional DC-DC converter. 78
4.23 Results of the step response for current control for a 3 modules DAB bidirectional DC-DC converter. Comparison between G(s) and G(z). 79
4.24 Results of the digital current control strategy for a 3 modules DAB bidirectional DC-DC converter. First graph is the output current and second one the phase shift. 80
4.25 Bode diagram of T and total system in the inner loop for the case of 3 modules and cascade control. 82
4.26 Results of the cascade control for a 3 modules DAB bidirectional DC/DC converter. Inner loop design. 83
4.27 Bode diagram of T and total system in the outer loop for the case of one module and cascade control. 85
4.28 Simulink block for a 3 modules DAB DC-DC converter of the cascade control. 86
4.29 Simulink results for a 3 modules DAB DC-DC converter of the cascade control. First graph is the output voltage, second one the current output and third one the phase shifts. Blue curves are the references, red curves the output from the real system and yellow ones the output from the transfer function system. 87
4.30 Simulink block of the digital cascade control strategy for a 3 modules DAB bidirectional DC-DC converter. 88
4.31 Results of the cascade control in the discrete mode for a 3 modules DAB bidirectional DC-DC converter. Inner loop design. 89
4.32 Results of the cascade control in the discrete mode for a 3 modules DAB bidirectional DC-DC converter. Outer loop design. 90
4.33 Results of the digital cascade control strategy for a 3 modules DAB bidirectional DC-DC converter. 91

5.1 Simplified small-signal circuit model of a DAB bidirectional DC/DC converter. 93
5.2 Simulink block of the digital current control strategy for a one module DAB bidirectional DC-DC converter. 94
5.3 Results of the digital current control strategy for a one module DAB bidirectional DC-DC converter. 94

5.4 Simulink block of the digital cascade control strategy for a one module DAB bidirectional DC-DC converter. 95
5.5 Results of the digital cascade control strategy for a one module DAB bidirectional DC-DC converter. 96
5.6 IPOP configuration of the 300 kW DC/DC converter. 97
5.7 Simplified output port of the small-signal circuit model of a 3 modules DAB bidirectional DC/DC converter. 98
5.8 Simulink block of the digital current control strategy for a 3 modules DAB bidirectional DC-DC converter. 99
5.9 Results of the digital current control strategy for a 3 modules DAB bidirectional DC-DC converter. 100
5.10 Simulink block of the digital cascade control strategy for a 3 modules DAB bidirectional DC-DC converter. 101
5.11 Results of the digital cascade control strategy for a 3 modules DAB bidirectional DC-DC converter. 102

List of Tables

3.1 Small signal equivalents for modeling the DC/DC converter [14]. . . . 17

4.1 Mismatches introduced in the different modules. 58
4.2 Results obtained from mismatches introduced in the different modules. 58

1 Introduction

Nowadays, pollution is one important challenge in the society that needs special attention. Climate change is already a global issue that needs to be solved with technology. Also, fossil fuels are being exhausted. Therefore, finding alternatives to traditional combustion engines vehicles is urgent.

For that purpose, several alternatives to fossil fuels and traditional vehicles have appeared, such as biofuels, natural gas, hydrogen or LPG. However, the one that have taken advantage is the electric vehicle. Among other reasons, some advantages of electric vehicles are that they do not have in situ emissions, they do not have gear box or that they are independent of fossil fuels. However, they have some drawbacks as well, such as the batteries' autonomy or the long charging time.

Also, due to the ongoing research it seems that, in the future, electric vehicles are going to play an important role in the decentralized electric market. In order to fully implement the renewable energies in our society, it seems extremely important to be able to store the energy from those solar panels of the roofs or any other discontinuous renewable energy sources. For that purpose, electric vehicles could play the role of portable batteries, where they can be used as batteries when there is an exceed of energy production and, at the same time, they can provide energy and behave as energy sources when needed.

Besides, it is at this point where this project appeared. This Master Thesis is involved in a bigger project held by Elbind Electronik and Chalmers University of Technology, where a fast charging station for heavy electric vehicles is being developed. The aim of this project is to charge batteries of trucks and buses in about 15-20 minutes, drastically reducing the charging time. Therefore, the charger is going to have a power level of 300 kW. But, also, due to the reason previously mentioned, this charger needs to be bidirectional, in order to fulfill that requirement.

Finally, the aim of this Master Thesis is developing a digital control for the DC/DC converter of the charger using Simulink and Matlab.

Therefore, the goals of this Master Thesis are:

1. Understanding of the charger's topology, specially the DC/DC converter.

2. Description of the DC/DC converter operation.

3. Selection of the charging strategy.
4. Modeling the system.
5. Developing the digital control of a single module DC/DC converter.
6. Deciding the parallel connection for a 3 modules DC/DC converter and its control strategy.
7. Obtaining the digital control of the 3 modules DC/DC converter.

Thesis outline

After this introduction, in chapter 2 an explanation of the converter's topology and operation is presented, highlighting the importance of the DC/DC converter. In chapter 3, the digital control of a single module DC/DC converter is discussed. In chapter 4, the digital control of a 3 modules module DC/DC converter is developed, where it was necessary also to decide the parallel connection of the modules and the control strategy for them. In chapter 5, the results from previous discuss are exposed. Finally, in chapter 6, the conclusions and future work are proposed as a continuation of this Master Thesis.

2

Theory

2.1 Charger's topology

In this section, a general description of the charger is presented.

This charger is aim to charge batteries of heavy electric vehicles, such as electric trucks or buses, where the battery is considerably big. Specifically, the batteries that this charger is supposed to feed are those with voltage around 700 V and capacity of 100 kWh. The aim of this charger is to charge them fast, in order to have them fully charged in 15-20 minutes. For that purpose, a 300 kW charger was decided to be developed.

Due to the relevant role that electric cars are going to play in the integration of renewable energies in the cities, it is important to develop bidirectional chargers which are able to feed the battery but, also, feed the grid with the energy from the vehicle when needed. Therefore, even though it makes more complex the development of the charger, a bidirectional 300 kW charger was decided to be developed.

Besides, based on previous research, the selected structure is the one shown in Figure 2.1.

The elements shown in Figure 2.1 are, from the left to the right:

- The grid, with a AC line-to-line voltage of 400 V.
- A voltage source converter (VSC) to provide a DC voltage of 700 V to the DC-link between the VSC and the DC/DC converter.
- The DC-link with a capacitor to provide smooth current and voltage from the VSC to the DC/DC converter.
- A DC/DC converter, to regulate the power supplied to the battery.
- Finally, the battery itself, with a previous capacitor to provide again smooth current and voltage to the battery.

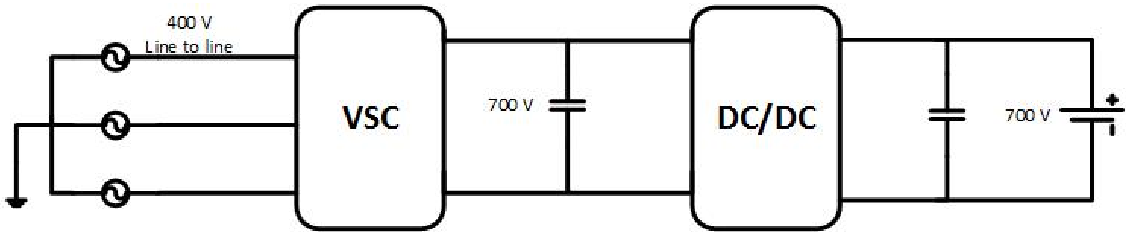

Figure 2.1: General structure of the bidirectional 300 kW charger.

The aim of this thesis is developing the digital control of the DC/DC converter in order to regulate the power supplied to the battery. Therefore, from now onwards, only the DC/DC converter is going to be considered. However, it was important to have a general picture of the charger before focusing on the DC/DC converter.

2.2 Single phase dual active bridge DC/DC converter

The dual active bridge (DAB) topology is a bidirectional topology that cam have a compact and efficient design. Also, one of the main advantages of a DAB converter is the low number of passive elements and its soft switching properties. In addition, with a DAB converter, high power density is feasible [1]. As a result, the structure used is shown in Figure 2.2.

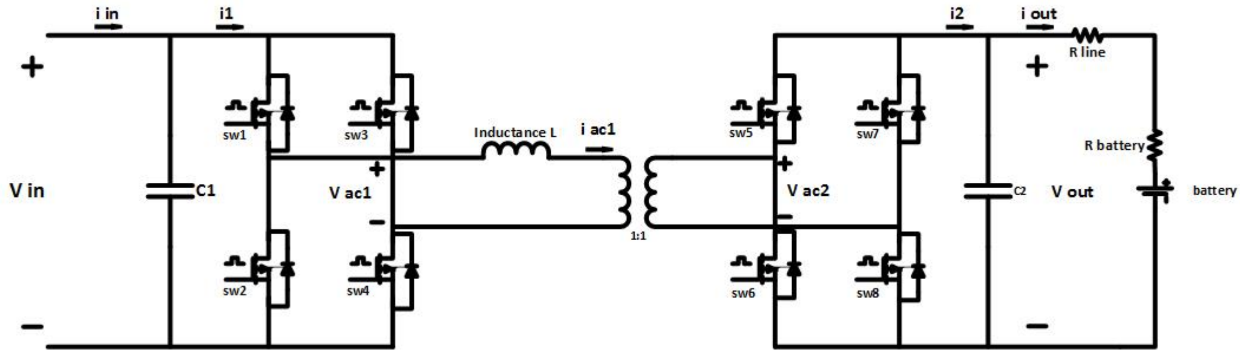

Figure 2.2: The dual active bridge bidirectional DC/DC converter used.

Since a 300 kW level power is desired, instead of building a single module charger of 300 kW, which is not possible as it is explained in section 2.3, a parallel configuration is implemented. Therefore, each module will handle 100 kW. To achieve that power, the main characteristics of the converter are:

- Voltage of 700 V.
- Power of 100 kW.

- Peak current of 160 A.
- Switching frequency of 25 kHz.

In the following two sections, a description of the converter from Figure 2.2 is going to be exposed followed in the next section by the converter operation.

2.2.1 Topology description

In this section, a description of the components of the converter is going to be presented. Based on Figure 2.2 and going from the left to the right, the next elements are presented:

- V_{in} is the DC voltage that comes from the VSC. It is 700 V.
- C_1 is the input filter based on a single capacitor. It is used to provide a smooth current and voltage to the converter.
- The first full bridge is in charge of converting the DC system into the AC system. It is built by MOSFETs since it is going to deal with voltages of 700 V, current peaks of 160 A and switching frequencies of 25 kHz. Each one can be in short circuit (1) or open circuit (0). In order, they are: sw1, sw2, sw3, sw4.
- The inductance L selected to obtain the desired current, This inductance is the key of the system, as it will be seen later.
- Transformer with a ratio of 1:1. It is required to achieve electric isolation and protect both sides of the charger and the charger itself.
- The second full bridge is in charge of converting the AC system back again to the DC system. It is built by MOSFETs since it is going to deal with voltages of 700 V, current peaks of 160 A and switching frequencies of 25 kHz. Each one can be in short circuit (1) or open circuit (0). In order, they are: sw5, sw6, sw7, sw8.
- C_2 is the output filter based on a single capacitor. It is used to provide a smooth current and voltage to the battery.
- Finally, a load that represents the battery of 700 V.

More specific information cannot be provided due to confidential reasons.

2.2.2 Converter operation

In this section the converter operation is going to be explained. This explication is based on the lossless model, which is the same shown in Figure 2.2.

To simplify the analysis, the dual active bridge can be seen as shown in Figure 2.3.

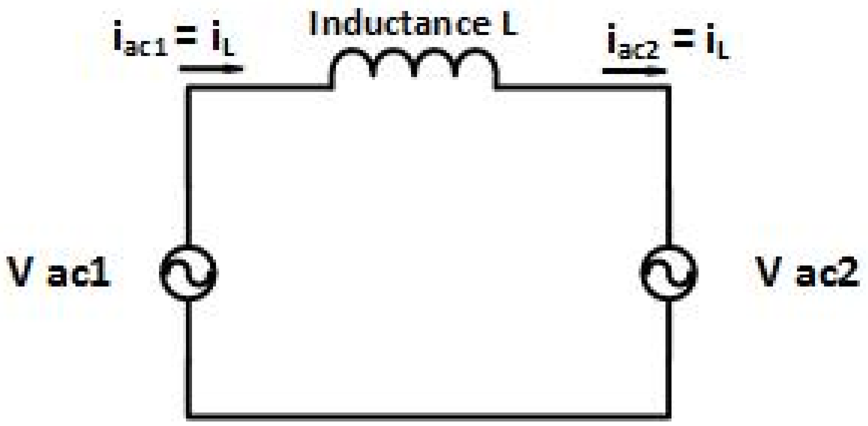

Figure 2.3: The lossless DAB model.

Where each bridge represents a voltage source. Therefore, in order to appear some current in the system, both have to be time varying and have a delay between them. Otherwise, the voltage across the inductance would be 0 and no current would circulate in the system.

The three possible voltages of v_{ac1}, depending on the switching operation, are:

$$v_{ac1} = \begin{cases} +V_{in}, & sw1 \;\; sw4 \;\; ON, \;\; sw2 \;\; sw3 \;\; OFF \\ 0, & sw1 \;\; sw3 \;\; ON, \;\; sw2 \;\; sw4 \;\; OFF \\ 0, & sw2 \;\; sw4 \;\; ON, \;\; sw1 \;\; sw3 \;\; OFF \\ -V_{in}, & sw2 \;\; sw3 \;\; ON, \;\; sw1 \;\; sw4 \;\; OFF \end{cases} \tag{2.1}$$

and similar with v_{ac2}, where for this converter, both are going to be square waves. The difference between them,

$$v_L = v_{ac1} - v_{ac2} \tag{2.2}$$

is applied to the inductance, that generates a current in the circuit, which is:

$$i_L = i_l(t_0) + \frac{1}{L}\int_{t_1}^{t_0} v_L \, dt \; \forall \; t_1 > t_0. \tag{2.3}$$

Thus, by controlling the voltage difference between v_{ac1} and v_{ac2}, the current through the inductance and, therefore, the current through the system can be controlled [1]. Finally, the average value of i_L is 0 but, since it is rectified afterwards by any of the bridges, the DC output current can be controlled as well, as it is going to be shown in equations 2.5 and 2.6.

Besides, since v_{ac1} and v_{ac2} are square waves, the controlled parameter is going to be the phase shift between the two of them.

Finally, following the process in [1] about the phase shift modulation, the following equation about power as a function of the phase shift was obtained:

$$P = P_1 = P_2 = \frac{n\ V_1\ V_2\ \phi\ (\pi\ -\ |\phi|\ )}{2\ \pi^2\ f_s\ L} \tag{2.4}$$

Where n is the transformer ratio, V_1 and V_2 the DC voltages, ϕ is the phase shift, f_s is the switching frequency and L the inductance.

Moreover, since the power, in the DC side, is $P = V_2 I_{out}$, the conclusion is that there is a direct relationship between the output current and the phase shift:

$$I_1 = \frac{P_1}{V_1} = \frac{n\ V_2\ \phi\ (\pi\ -\ |\phi|\ )}{2\ \pi^2\ f_s\ L} \tag{2.5}$$

$$I_2 = \frac{P_2}{V_2} = \frac{n\ V_1\ \phi\ (\pi\ -\ |\phi|\ )}{2\ \pi^2\ f_s\ L} \tag{2.6}$$

On the other hand, there is another important equation [1] that provides the phase shift needed to achieve a certain amount of power:

$$\phi = \frac{\pi}{2}\left[1 - \sqrt{1 - \frac{8\ f_s\ L\ |P|}{n\ V_1\ V_2}}\right] \tag{2.7}$$

Finally, the circuit from Figure 2.2 was developed in Simulink and it was verified that the circuit behaves as it was expected from formulas, as it can been seen in Figure 2.4 and Figure 2.5.

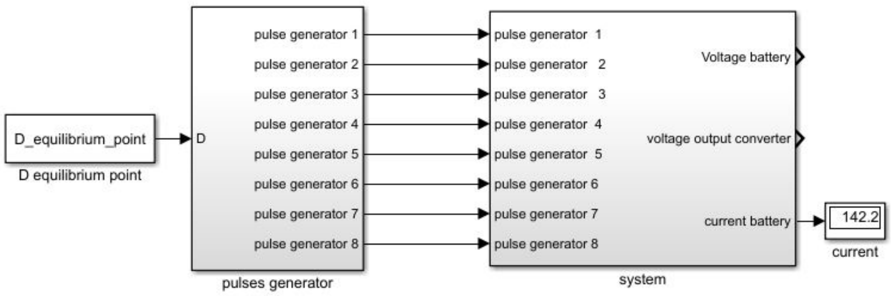

Figure 2.4: Simulink system working with a phase shift of 51.47°.

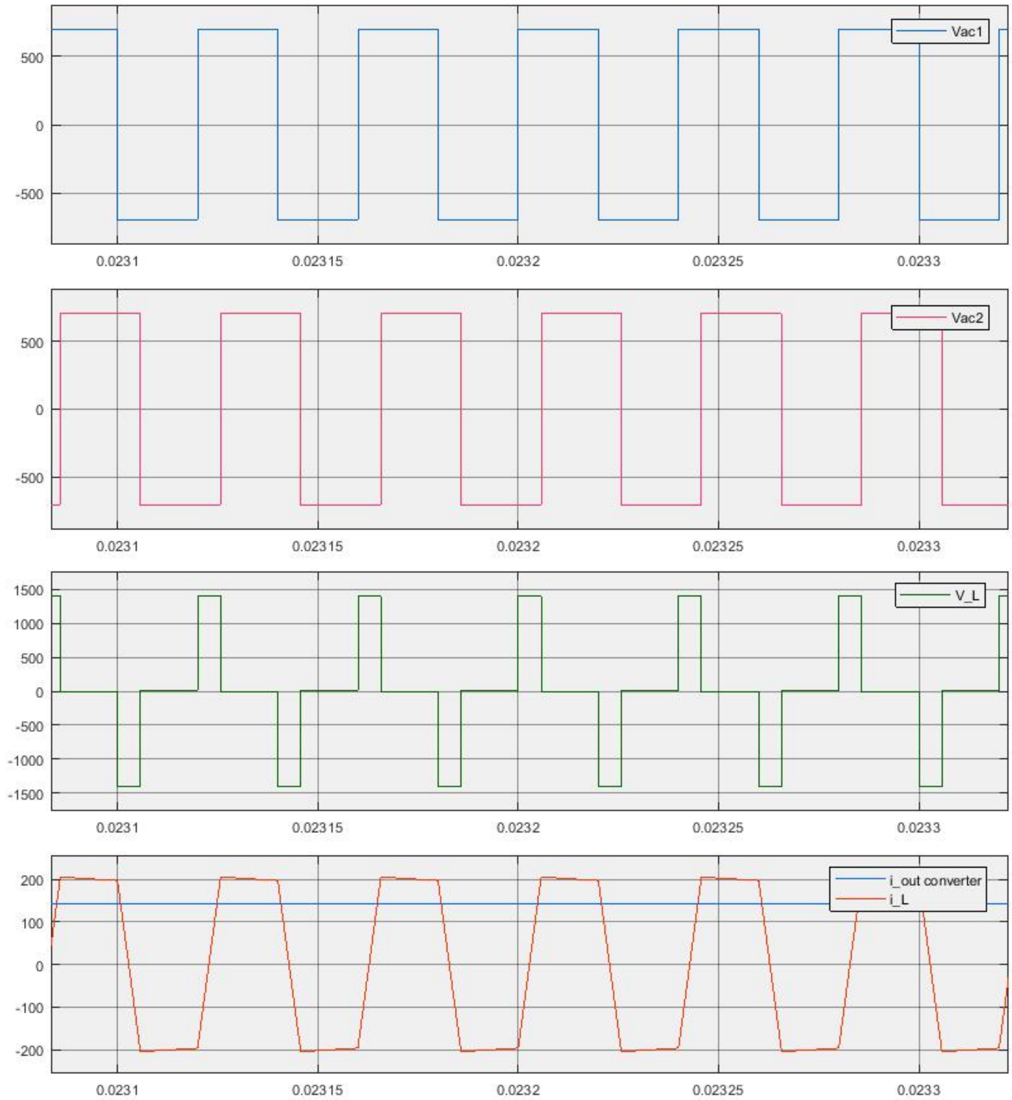

Figure 2.5: Actual values from variables of the Simulink system working with a phase shift of 51.47°. The variables are, in order: v_{ac1}, v_{ac2}, v_L the voltage across the inductance, i_L the current across the inductance in the AC side and i_{out} the output DC current.

The Simulink blocks from Figure 2.4 are explained in the section 3.3. For this verification process, all the parameters previously mentioned were used and the phase shift was settled in 51.47°. According to the equation 2.6, the expected output current from a lossless model is 142.92 A, which means that the Simulink system has an error or 0.5 %. It is important to remark that some resistance were needed to be introduced in order to be the system realizable.

Therefore, the Simulink model was validated since the values obtained were the ones expected from formulas, according to the phase shift introduced. Besides, the losses of the system where introduced and finally the Simulink circuit was ready to represent the real system. Once again, these values cannot be given due to the confidential agreement.

In the next chapter, the development of the digital control of the DC/DC converter is going to be presented. First, the control of a one module DC/DC converter is going to be presented. After that, the parallel connection of 3 modules is going to be studied. Finally, the digital control of the 3 modules DC/DC converter is going to be shown.

2.3 The reason of using a 3 modules DC/DC converter

In this section an answer to the question about why not using a big one module DC/DC converter instead of a 3 modules DC/DC converter is going to be solved.

As a direct answer, it is important to point out that the current power modules are not capable to held currents above 300A. Therefore, even if the module was able to produce those 300A, the maximum power would be 210kW.

However, based on equation 2.4, it is going to be studied why is convenience to have several modules rather than one but big. According to equation 2.4, the parameters that could be changed are: V_1, the phase shift ϕ, the switching frequency f_s or the inductance L.

First, as it is shown in Figure 2.6, just changing the phase shift, the maximum power that could be provided with this module would be 122.5kW. Therefore, it is not enough. But not only this, that situation happens when the phase shift is 90°, which is an undesired point due to safety stability interval, where it is not desired to have phase shifts bigger than 70°.

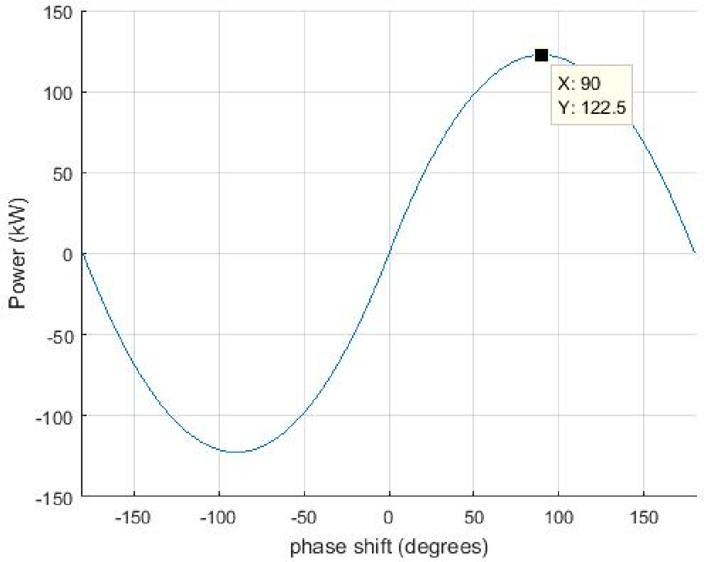

Figure 2.6: Power as function of the phase shift.

Another parameter that could be changed would be the input voltage V_1. As it can be seen in Figure 2.7. For reaching those 300kW, an input voltage of 1.95kV would be needed. However, it would not be sensible at all since it would be necessary to connect to another point of the grid and it would be more expensive since high voltage protections and safety measures would be needed. Moreover, there would still be 700V, which is impost by the battery, on the secondary side of the converter and, therefore, the first restriction mentioned would still apply.

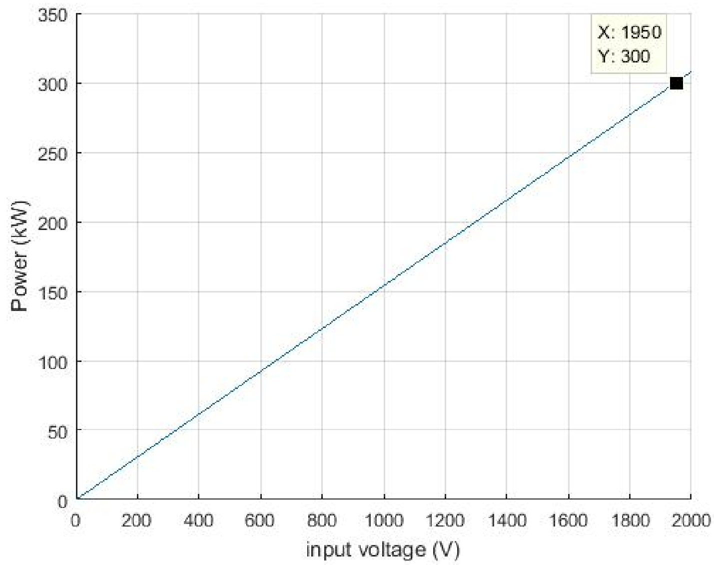

Figure 2.7: Power as function of the input voltage.

The next parameter that could be changed would be the switching frequency f_s. As it can be seen in Figure 2.8, to achieve a power of 300kW, a switching frequency of 8.97 kHz would be needed. However, by decreasing the switching frequency, the controllability of the converter would be decreased as well. Even more, nowadays the general trend in power electronic systems is towards a higher frequency operation. Therefore, it would be a nonsense decreasing the switching frequency.

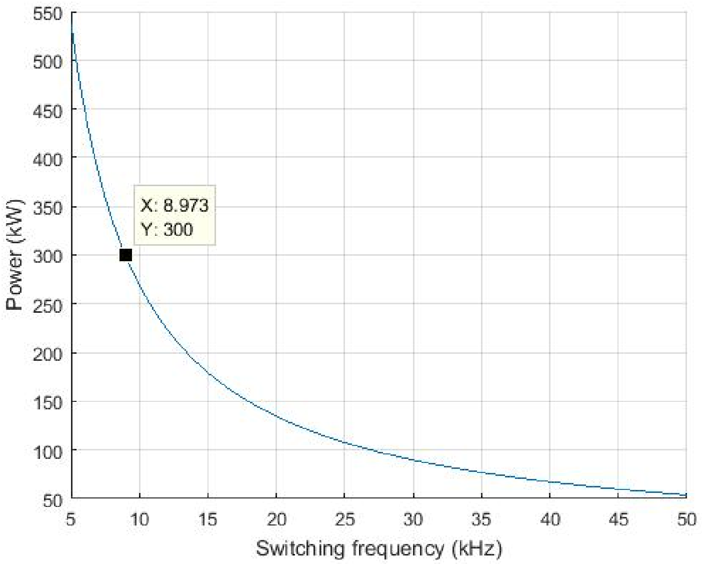

Figure 2.8: Power as function of the input voltage.

The final parameter that could be changed would be the inductance L. However, this graph can not be shown, although the shape is the same as before with the switching frequency. Therefore, by decreasing that inductance, the power would be increased. On the other hand, low values of inductance increases the current ripple. Therefore, it is fundamental to find a balance between those two phenomenons, concluding that the value selected was the most suitable for this converter.

All things considered, it has been demonstrated that using several modules in parallel is needed.

3

Digital control of a single module converter

As it is mentioned before, a single module converter was studied. A digital control is developed in order control the power supplied to the battery of the vehicle. Therefore, in this section, different digital control methods of a one module converter are shown. The aim of this section is to show when to use a voltage control, current control or controlling both at the same time with a cascade control. First, an analog control was implemented. Once it was developed, the digital control was finally studied, base on the analog control. This is because, nowadays, digital signal processors (DSPs) are being implemented for high power converters, due to the fact that a high computational performance is available. Among other reasons, some advantages of the digital control are that it has higher flexibility and a higher electromagnetic interference immunity [1].

The first decision made was whether to use an open-loop control or a close-loop control. On one hand, an open-loop control is easier to implement and cheaper, since any measurement equipment is required. However, even though a good converter model can be obtained, it is never guaranteed that the applied input signal is supplying the expected output power, since the real model is never going to be completely the same as expected throughout its operating life. On the other hand, a close-loop control is more difficult to implement and more expensive. Nevertheless, since the output is always controlled, it is completely guarantee that the applied input is the necessary to obtain the required output. Not only this, because of safety reasons, measuring the output is needed. Therefore, a close-loop control was decided to be implemented in this converter.

Secondly, the control strategy was studied. In order to decide it, it was necessary to first understand the battery charging characteristics. In this case, the main batteries' characteristics are: nominal voltage of 700V and capacity of 100kWh. According to [3], [13], and [15], the usual Li-ion battery charge cycle consists on a constant-current (CC) region, until it reaches a voltage limit, and then it is followed by a constant-voltage (CV) region, as it is shown in Figure 3.1.

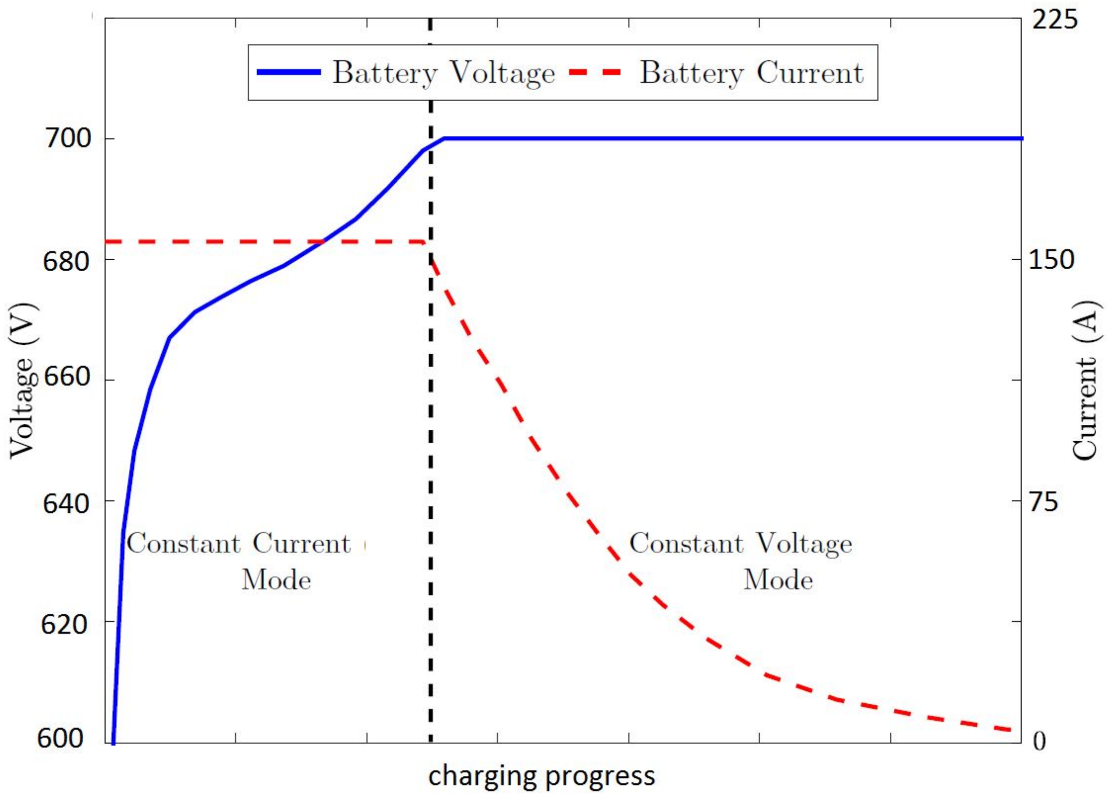

Figure 3.1: The battery charging strategy.

Therefore, a current control mode and a voltage control mode had to be implemented. Furthermore, the voltage control mode was implemented through a cascade mode, so both voltage and current were controlled.

At this point, it was necessary to choose the way the controller was going to be designed. For that purpose, a model of the converter had to be obtained and, after checking that it represents the real system, an accurate controller could be obtained. According to [5], there are several ways of doing it, each one with different accuracy. The different techniques mentioned in [5] can be divided as follow: simplified averaged model, discrete-time model and continuous-time model.

In this thesis, the selected technique is included in the category of simplified averaged model. By this technique, losses are neglected, leading, on one hand, to a lower accurate model. But, on the other hand, a simpler model makes easier the design of the controllers. Moreover, even though the model is less accurate, it is enough for this purpose, specially because the system does not need a super fast response. Therefore, the simplified averaged model was chosen because it makes the modelling easier and at the same time it is accurate enough. Besides, it is the most common technique in the literature [1][2][4][5][6][7][8].

In the next subsections, the model based on the simplified averaged model is developed. First, an average model is presented follow by the small signal model.

3.1 Average model

The average model was based on the lossless converter model [3] shown in figure 2.2. According to this circuit, the transferred power [1] by the converter is

$$P = P_1 = P_2 = \frac{n\ V_1\ V_2\ \phi \cdot (\pi - |\phi|)}{2\ \pi^2\ f_s\ L} \tag{3.1}$$

as it was explained in section 2.2. However, for practical reasons, the transformation $D = \dfrac{\phi}{\pi}$ is used. By this, instead of working with intervals from $-\frac{\pi}{2}$ to $\frac{\pi}{2}$, the more practical interval $(-\frac{1}{2}, \frac{1}{2})$ was used. Therefore, the transferred power is:

$$P = P_1 = P_2 = \frac{n\ V_1\ V_2\ D\ (1 - |D|)}{2\ f_s\ L}. \tag{3.2}$$

From equation 3.2, the DC current that flows in both DC sides of the DC/DC converter are shown in equations 3.3 and 3.4. This currents correspond to the average value of $i1$ and $i2$ from Figure 2.2. Therefore, it is possible to end up with the same equations as 3.3 and 3.4 by averaging the DAB input and output port current [3].

$$I_1 = \frac{P_1}{V_1} = \frac{n\ V_2\ D\ (1 - |D|)}{2\ f_s\ L} \tag{3.3}$$

$$I_2 = \frac{P_2}{V_2} = \frac{n\ V_1\ D\ (1 - |D|)}{2\ f_s\ L} \tag{3.4}$$

With equations 3.3 and 3.4 and Figure 2.2, the average circuit could be obtained, as shown in Figure 3.2.

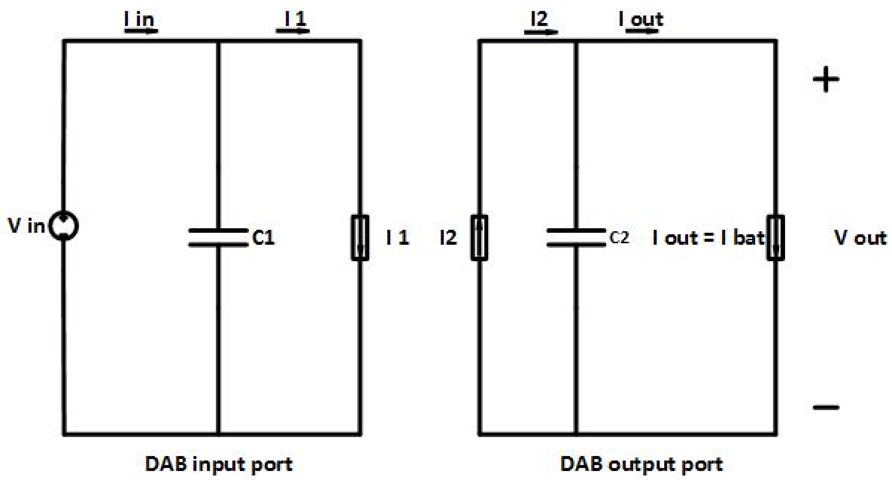

Figure 3.2: Average circuit model of a DAB bidirectional DC/DC converter.

3.2 Small-signal model

Small-signal modeling consists on developing a model that provides information about how the system reacts to a small perturbation in some variables. Consequently, the average model can be perturbed and linearized around an equilibrium point to obtain a small-signal model of the converter [3]. Therefore, any variable of the circuit can be expressed as:

$$i_2 = I_2 + \widehat{i}_2. \tag{3.5}$$

Where i_2 is the actual value, I_2 denotes the equilibrium point value and $\widehat{i}_2$ the small signal term [7].

Focusing on the DAB bidirectional DC/DC converter, the equations 3.3 and 3.4 were perturbed. It is known that in order to control i_2, the perturbation $\widehat{i}_2$ has to be known. Therefore, the variables that could affect $\widehat{i}_2$ were the phase shift and input and output voltage, as it is shown in the following equations:

$$\widehat{i}_1 = \left.\frac{\partial i_1}{\partial d}\right|_{Eq.P} \cdot \widehat{d} + \left.\frac{\partial i_1}{\partial v_{out}}\right|_{Eq.P} \cdot \widehat{v}_{out} \tag{3.6}$$

$$\widehat{i}_2 = \left.\frac{\partial i_2}{\partial d}\right|_{Eq.P} \cdot \widehat{d} + \left.\frac{\partial i_2}{\partial v_{in}}\right|_{Eq.P} \cdot \widehat{v}_{in}. \tag{3.7}$$

Eq.P means around the equilibrium point.

According to 3.6 and 3.7, the following constants were defined:

$$K_1 = \left.\frac{\partial i_1}{\partial d}\right|_{Eq.P} = \frac{(1-2\ |D|)\ n\ V_{out}}{2\ f_s\ L} \tag{3.8}$$

$$K_2 = \left.\frac{\partial i_1}{\partial v_{out}}\right|_{Eq.P} = \frac{D\ (1-\ |D|)\ n}{2 \cdot f_s\ L} \tag{3.9}$$

$$K_3 = \left.\frac{\partial i_2}{\partial d}\right|_{Eq.P} = \frac{(1-2\ |D|)\ n\ V_{in}}{2\ f_s\ L} \tag{3.10}$$

$$K_4 = \left.\frac{\partial i_2}{\partial v_{in}}\right|_{Eq.P} = \frac{D\ (1-\ |D|)\ n}{2\ f_s\ L}. \tag{3.11}$$

Therefore,

$$\widehat{i}_1 = K_1 \cdot \widehat{d} + K_2 \cdot \widehat{v}_{out} \tag{3.12}$$

$$\widehat{i}_2 = K_3 \cdot \widehat{d} + K_4 \cdot \widehat{v}_{in}. \tag{3.13}$$

Now, the small-signal model of the DC/DC converter has been defined. To complete the small-signal model of the whole circuit, the table 3.1 was followed.

Real device	Small-signal equivalent
Resistors and capacitors	Same
Independent voltage source	Effectively grounded
Independent current source	Effectively open circuit
Dependent sources	Same
Non linear elements	Different (converter)

Table 3.1: Small signal equivalents for modeling the DC/DC converter [14].

All things considered, the small-circuit model is achieved and shown in figure 3.3.

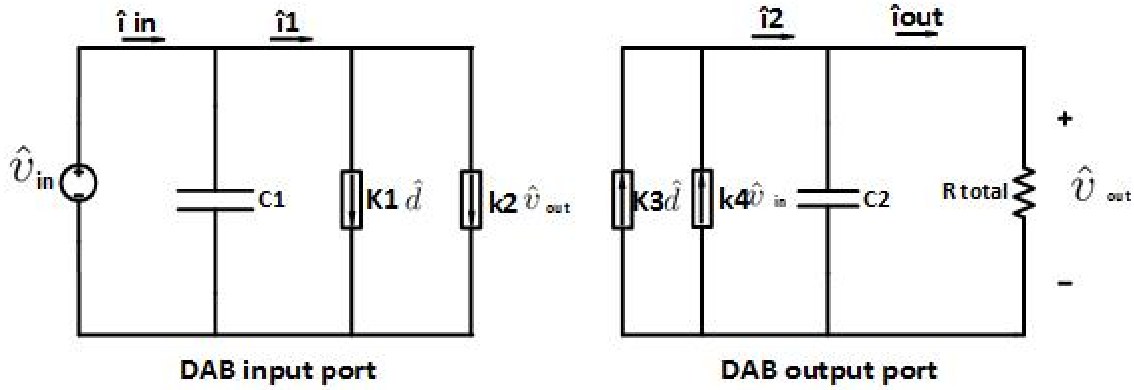

Figure 3.3: Small-signal circuit model of a DAB bidirectional DC/DC converter.

In this figure Rtotal represents the sum of Rline and Rbattery from figure 2.2.

Assumption

The VSC or the DC/DC converter had to be in charge of keeping the voltage of the common DC-link constant. Since the converter was already in charge of feeding the battery, this task was held by the VSC. Therefore, for further investigation, the voltage across the capacitor C_1, the one that comes from the VSC part, was assumed as constant. Thus, $\widehat{v}_{in} = 0$ and, then, the small-signal model finally was:

$$\widehat{i}_1 = K_1 \cdot \widehat{d} + K_2 \cdot \widehat{v}_{out} \tag{3.14}$$

$$\widehat{i}_2 = K_3 \cdot \widehat{d} \tag{3.15}$$

$$C_2 \cdot \frac{dv_{out}}{dt} = \widehat{i}_2 - \widehat{i}_{out}. \tag{3.16}$$

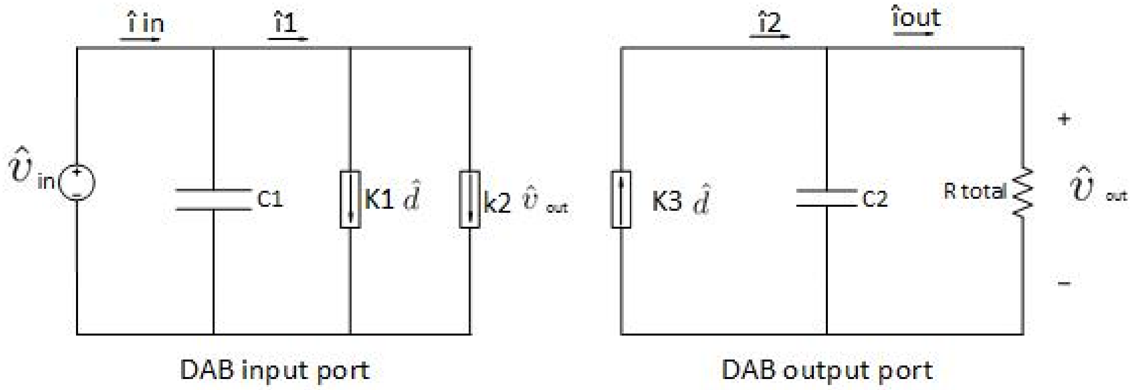

Figure 3.4: Simplified small-signal circuit model of a DAB bidirectional DC/DC converter.

3.3 Simulink Block

The Simulink block developed for this purpose is shown in Figure 3.5.

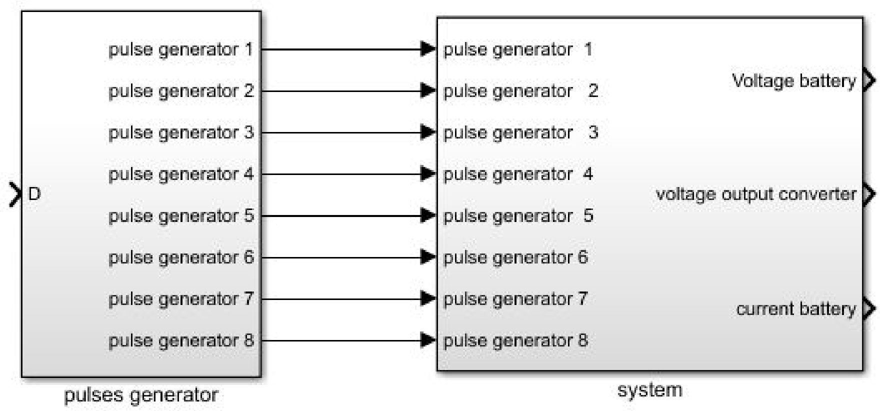

Figure 3.5: Simulink block for a one module DC/DC converter.

The first block from Figure 3.5 is the pulses generator. This block did not exist before and it was created in order to provide the appropriate 8 pulses to the 8 MOSFETs of the converter according to the phase shift needed at each time.

The second block, the system block, includes the system from Figure 2.2, where it has as inputs the pulses and the outputs are the current and voltage from the battery side.

3.4 Control methods

In this section the different control methods are shown. First, a simple voltage control is going to be presented. Even though this method was finally improved for the converter, as it will be explained at the end of this section, it is shown since it was the one that other authors started with. Besides, it was a way to verify that this method works. Then, the current control method is shown followed, finally, by the cascade control.

The three methods had the same structure, which is the one followed in this report:

1. Development of the transfer function desired.
2. Step response. Comparison between real system and transfer function.
3. Close loop control. PI controller development. Analysis of stability. Comparison between formulas, transfer function and real system.

Equilibrium points

Since the system is linearized around an equilibrium point, it had to be defined previously. That equilibrium point is different depending on the charging process phase. As it is said in 3, there are mainly two charging steps: constant current mode and constant voltage control.

In the first step, the current is fixed and controlled. As it was mentioned in section 2.2, there is a direct relationship between the output current and the phase shift. Besides, keeping current fixed means, at the end, keeping phase shift fixed.

Since in this phase the voltage is still not a problem, the maximum current can be applied until battery's voltage reaches its upper limit. Therefore, the next equilibrium point was assumed:

1. $i_{bat} = i_{out} = 153.82\,A$
2. $phase\,shift = 58.69°$
3. $V_{initial}\,battery = 650\,V$
4. $Power_{output\,converter} = 100.87\,kW$

This mode can last more or less, depending on the initial SOC of the battery and until the battery is close to a full charge state.

However, when the charging mode was switched to constant voltage mode, the next equilibrium point was used:

1. $i_{bat} = i_{out} = 142.94\,A$

2. $phase\,shift = 51.48°$
3. $V_{initial}\,battery = 700\,V$
4. $Power_{output\,converter} = 100.81\,kW$

3.4.1 Voltage control

The first control strategy developed is the voltage control. First, the analog development is going to be presented. Then, the digital implementation of the previous system is going to be shown.

3.4.1.1 Analog development

In this section, the transfer function, step response and close loop control for the voltage control is going to be presented.

3.4.1.1.1 Transfer function

Based on the small signal model from Figure 3.4, the transfer function that relates voltage with phase shift is:

$$G = \frac{\widehat{v}_{out}}{\widehat{d}} = K_3\,\frac{Rline + Rbattery}{1 + s\,C_2\,(Rline + Rbattery)}. \tag{3.17}$$

3.4.1.1.2 Step response. Comparison

Before doing any control strategy, the previous transfer function was tested to check if the linearized model behaves as the real system does.

For that purpose, the Simulink model from Figure 3.6 was developed, obtaining the results shown in Figure 3.7. A step of 10 % the phase shift in the equilibrium point was introduced.

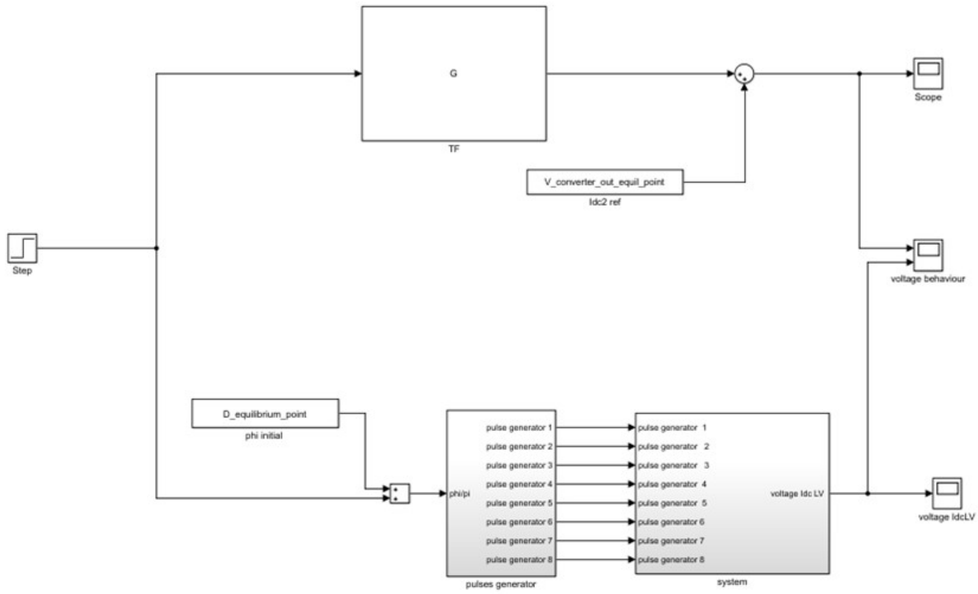

Figure 3.6: Step response for voltage control for a one module DAB bidirectional DC-DC converter. Simulink program.

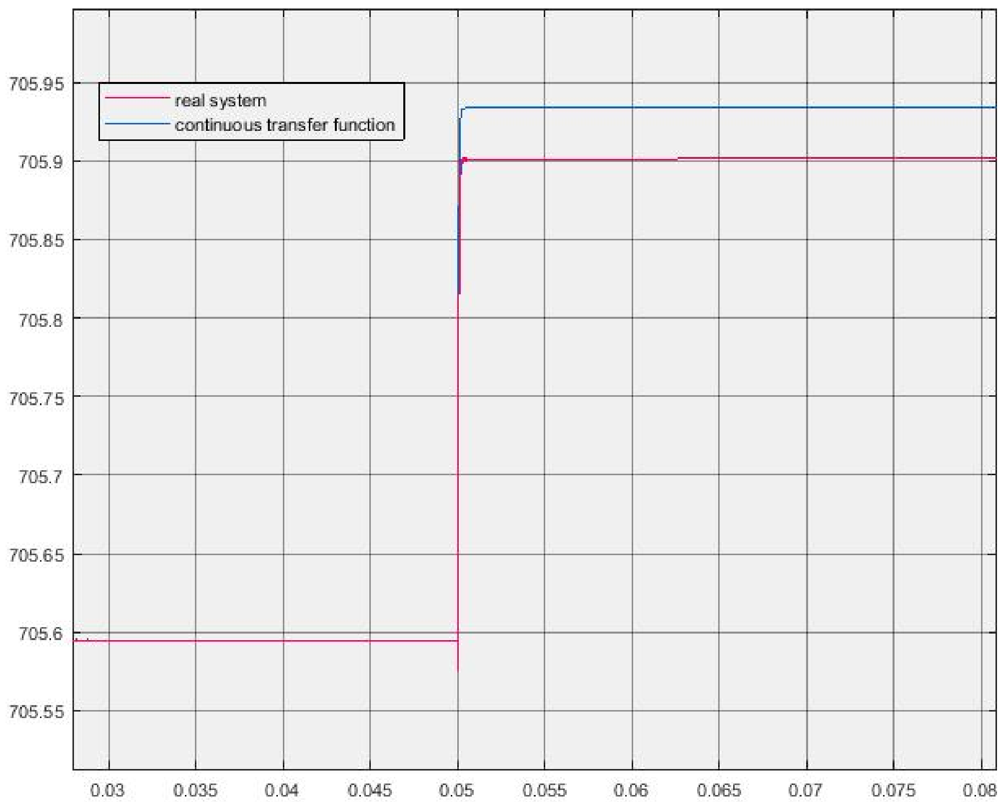

Figure 3.7: Step response for voltage control for a one module DAB bidirectional DC-DC converter.

As it can be observed, both systems behave similar to each other (deviation lower than 10 %). At this point it is important to remark that the real system takes into account the system losses meanwhile the transfer function is based on the lossless model and the assumption of constant input voltage. Therefore, the similarity was even better than expected.

Once it is demonstrated that the linearized system was accurate enough, the control system based on the linearized system is developed.

3.4.1.1.3 Closed loop voltage control. Comparison

The control strategy followed here and onwards was the one shown in Figure 3.8.

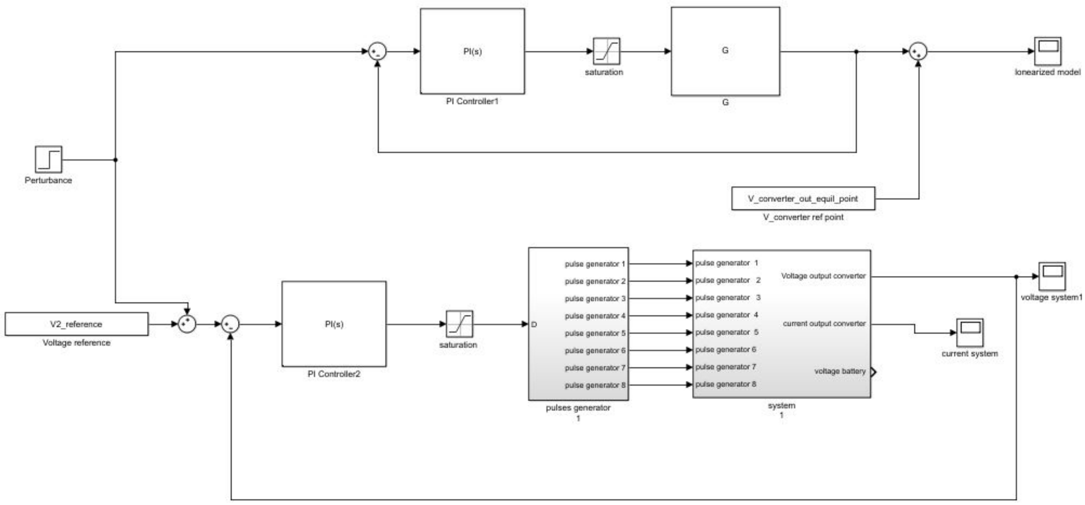

Figure 3.8: Voltage control strategy. Simulink model.

Besides, the control strategy is based on a close loop method where the voltage from the output of the converter is compared with the reference. This difference is received by a PI controller which generates the appropriate phase shift for the converter. This loop is implemented with the real system and the transfer function system.

For the PI tuning, although PI controllers are specially useful for almost every feedback systems, it is specially effective and simple for systems with just one pole [2], as this case.

Based on [2], the PI tuning method was the one that follows.

The PI controller has the following structure:

$$R(s) = K \cdot (1 + \omega_L \cdot \frac{1}{s}) \tag{3.18}$$

Being the system represented by $G(s)$, the following transfer functions were defined:

$$G(s) = \frac{G_{u0}}{(1 + \frac{s}{w_0})} \tag{3.19}$$

$$T(s) = R(s) \cdot G(s). \tag{3.20}$$

Consequently, the closed loop transfer function can be written as:

$$sys = \frac{T}{1+T}. \tag{3.21}$$

Then, the proportional constant of the PI controller is chosen to obtain a desired crossover frequency f_c [2]

$$K = \frac{f_c}{G_{u0} \cdot f_0}. \tag{3.22}$$

And, finally, f_L is chosen lower enough than f_c such that an adequate phase margin is maintained. At frequencies lower than f_L, the PI controller improves the rejection of disturbances, specifically, in DC.

Therefore, this procedure was followed to design the PI compensator for the voltage control system, and these were the parameters obtained:

1. $K = 0.0069$
2. $w_L = 5236$

However, before applying this controller to the system, studying the stability of the total system was necessary. According to the Phase Margin Theorem, a special case of the Nyquist stability theorem [2], the system is stable if the phase margin of T at the crossover frequency is positive. The phase margin is defined as

$$\varphi_m = 180^\circ + < T(j2\pi f_c). \tag{3.23}$$

Besides, in this case the bode diagram is:

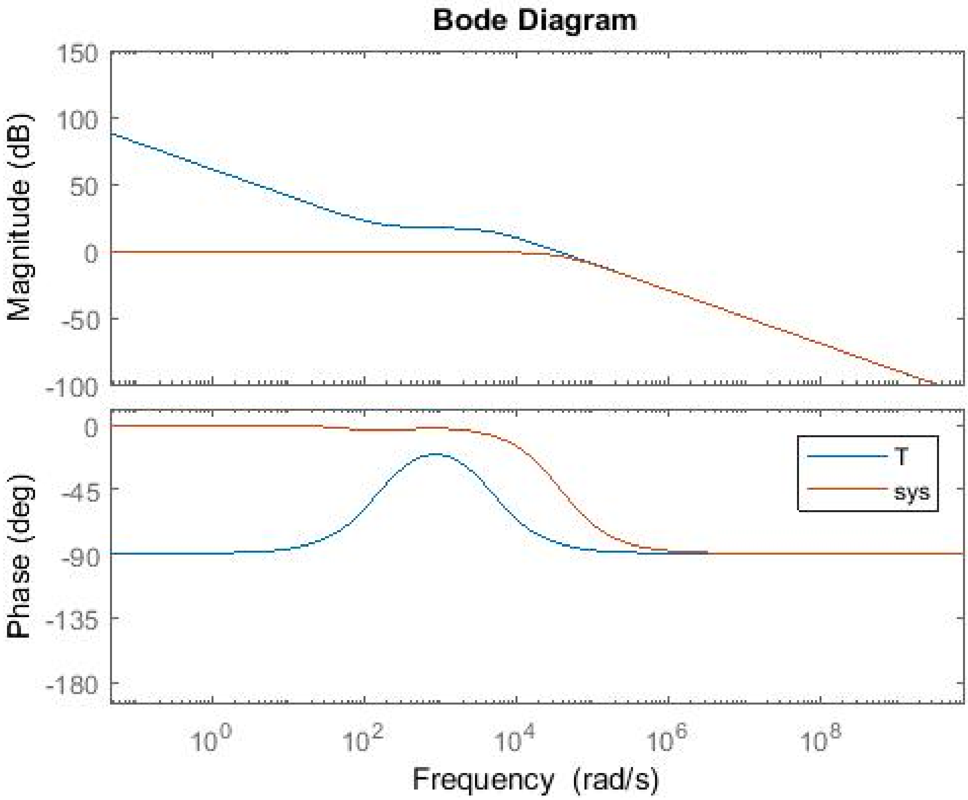

Figure 3.9: Bode diagram of T and total system (sys). Case: one module and voltage control.

As it can be seen, the phase margin φ_m is 94°, positive, and the system is stable.

Once it was demonstrated that the system was stable, the controller was configured and the Simulink program from Figure 3.8 was run around the equilibrium point previously defined in this report.

A small disturbance around the equilibrium point was introduced to observe the behaviour of both systems, and these were the results obtained:

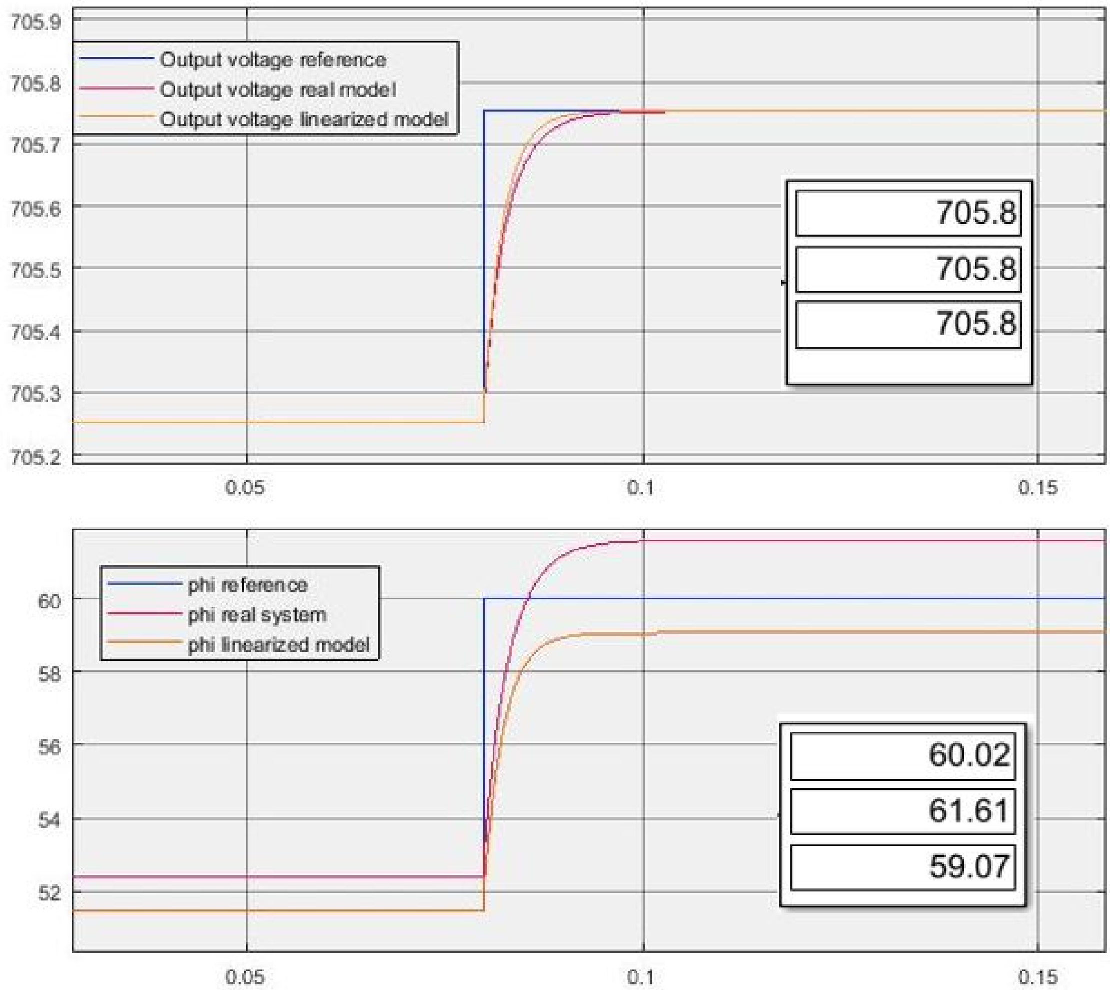

Figure 3.10: Voltage control strategy for a one module DAB bidirectional DC-DC converter. Results.

In Figure 3.10 it is shown, in the first graph, the output voltage of the converter and, in the second graph, the phase shift. Blue curves are the references from formulas, red curves the output from the real system and the yellow curves the output from the transfer function system. As it can be seen, both systems followed perfectly the voltage reference, with just slight differences in the phase shift, since the real system had a difference of 2.65 % respect to the reference from formulas and the transfer function system a difference of -1.58 %. However, this difference were expected and it behaves as it had to do: on one hand, the real system, since it considers the looses, it needed a higher phase shift to achieve the same power. On the other hand, the transfer function is based on the loosless model, as the formulas do, but also it had the assumption of constant input voltage, and that is why it needed less phase shift to achieve the same voltage.

3.4.1.2 Digital control

Once the analog control is accomplished, the digital control is developed. Due to the fact that any system is usually a continuous-time system, an analog design was developed first. Then, since usually controllers are developed in discrete-time domain, the digital control is studied, based on the analog control previously designed.

First, it is important to take into account that the frequency of the digital controller has to be lower enough than the switching frequency in order the system to be able to reach the reference before it has changed. Besides, the frequency decided to use, based on previous experience from literature [1] [18] [19], is 10 % of the switching frequency.

Therefore, the structure used in the digital control is the one shown in Figure 3.11.

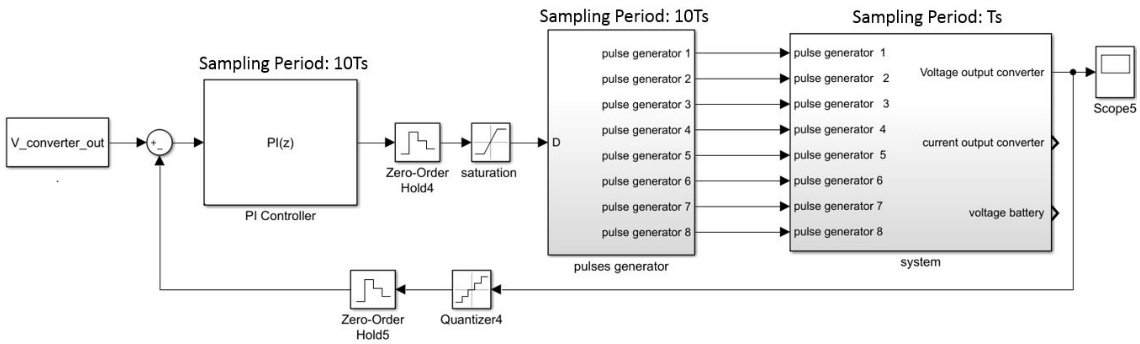

Figure 3.11: Simulink block of the digital voltage control strategy for a one module DAB bidirectional DC-DC converter.

In this new Simulink model, new blocks were used, such as the zero-order hold and quantizer. Both blocks were used to discretized the continuous-time signal from the real system. Also, the zoh was used to hold the values for the pulse generator. Moreover, the PI controller in this case is tuned in the z-domain for the digital control (PI(z)).

It is important to be aware of not incurring in the aliasing effect. However, for this purpose where the converter works in DC, it is not an important problem.

For tuning the PI controller, first the model of the system in the z-domain was developed. For that purpose, several discretizing methods were studied. Among them, the one chosen was the zero-order hold which provides exact discretization in the time domain for staircase inputs [18]. Besides, for a first order transfer function in the s-domain, the type of transfer function from formula 3.24 were obtained.

$$G(z) = \frac{G_{z0}}{z - q} \tag{3.24}$$

Where G_{z0} and q are constants.

The step-response procedure was realized to check if both transfer functions behaves the same way. As it can be seen in Figure 3.12, they behave exactly the same way.

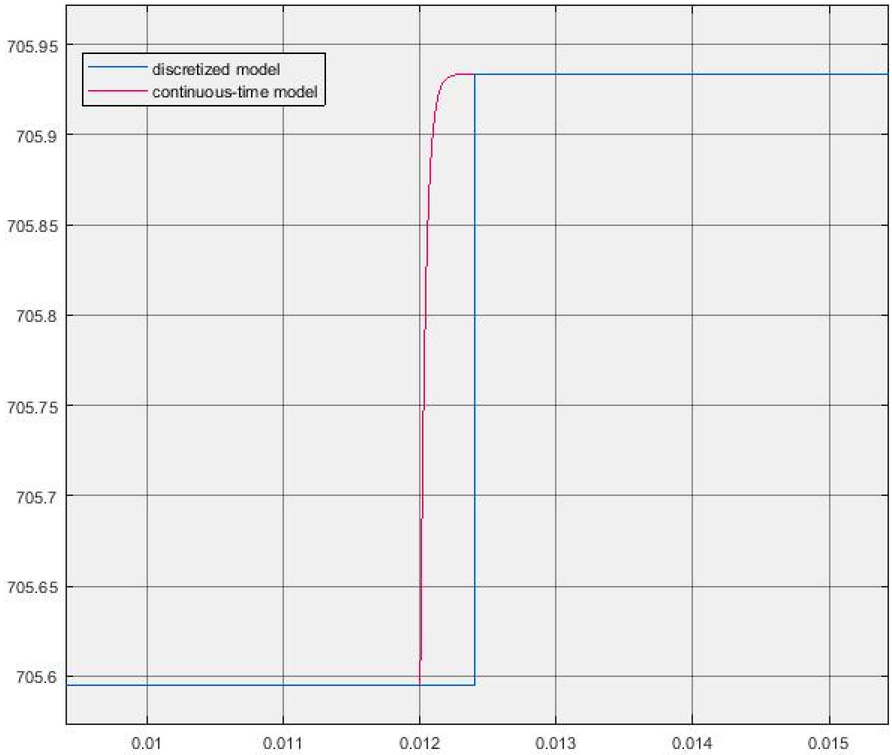

Figure 3.12: Results from the step response for voltage control for a one module DAB bidirectional DC-DC converter. Comparison between G(s) and G(z).

In order to control the system as it was done in the analog mode, a PI(z) controller was developed. This PI controller has the structure from formula 3.25.

$$R(z) = V_p + V_i \, \frac{1}{z-1} \tag{3.25}$$

Based on literature [18], the procedure followed for tuning the PI(z) parameters are shown in formulas 3.26 and 3.27.

$$V_p = K \tag{3.26}$$

$$V_i = K \; (w_L \; T_{sample} \; const - 1) \tag{3.27}$$

Where const is a constant to adjust the integrator to make it faster or slower.

Therefore, for the voltage control, the parameters were:

1. $V_p = 0.0069$
2. $V_i = 57.889$

Thus, the PI(Z) is:

$$R(z) = 0.0069 + 57.889\,\frac{1}{z-1} \tag{3.28}$$

All in all, with the structure from Figure 3.11 and the PI(z) controller, the system was tested. For that purpose, a small step disturbance was introduced to observe the systems behaviour. Moreover, it was compared with some other structures, as it is going to be explained. The results are shown in Figure 3.13.

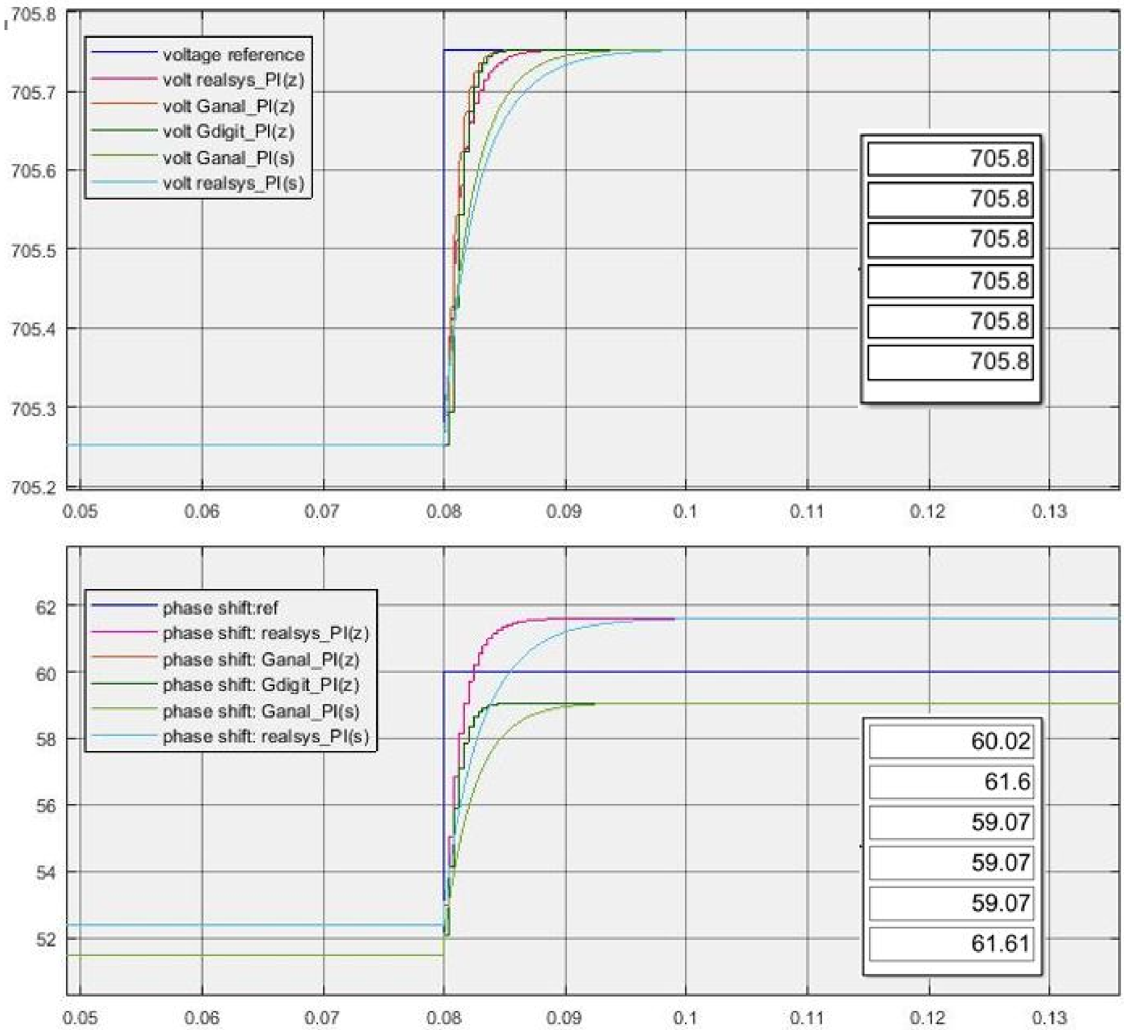

Figure 3.13: Results of the digital voltage control strategy for a one module DAB bidirectional DC-DC converter.

First graph is the output voltage and second one is the phase shift. The curves are, in order according to the legend: 1. Output converter reference. 2. Output from a real system model controlled with a PI(z). 3. Output from a continuous-time transfer function model controlled with a PI(z). 4. Output from a discrete-dime transfer function model controlled with a PI(z). 5. Output from a continuous-time transfer function model controlled with a PI(s). 6. Output from a real system model controlled with a PI(s).

As it can be seen in Figure 3.13, it is totally coherent. On one hand, all the models controlled with a discrete PI(z), reaches the new steady state at the same time. Same happens with the continuous-time PI(s), but with different setting time, related to the controller used. On the other hand, those based on the real system, reach the same phase shift and higher (deviation of 2.65 %) than the one expected from formulas, as explained before. Also, those based on a transfer function system, reach the same phase shift and lower (deviation of -1.58 %) than the expected from formulas, also explained before.

All things considered, the digital voltage control has been presented in the section.

3.4.2 Current control

The second control strategy developed was the current control strategy, corresponding to the first step in the charging strategy: constant current mode.

First, the analog development is presented. Then, the digital implementation of the previous system is shown.

3.4.2.1 Analog development

In this section, the transfer function, step response and close loop control for the current control is presented.

3.4.2.1.1 Transfer function

Based on the small signal model from Figure 3.4, the transfer function that relates current with phase shift was:

$$G = \frac{\widehat{i}_{out}}{\widehat{d}} = \frac{\widehat{i}_{bat}}{\widehat{d}} = K3 \cdot \frac{1}{1 + s \cdot C_2 \cdot (Rline + Rbattery)}. \tag{3.29}$$

3.4.2.1.2 Step response.

Here again, the previous transfer function was tested to check if the linearized model behaves as the real system does.

For that purpose, the Simulink model from Figure 3.14 was developed, obtaining the results shown in Figure 3.15. A step of 10 % the phase shift in the equilibrium point was introduced.

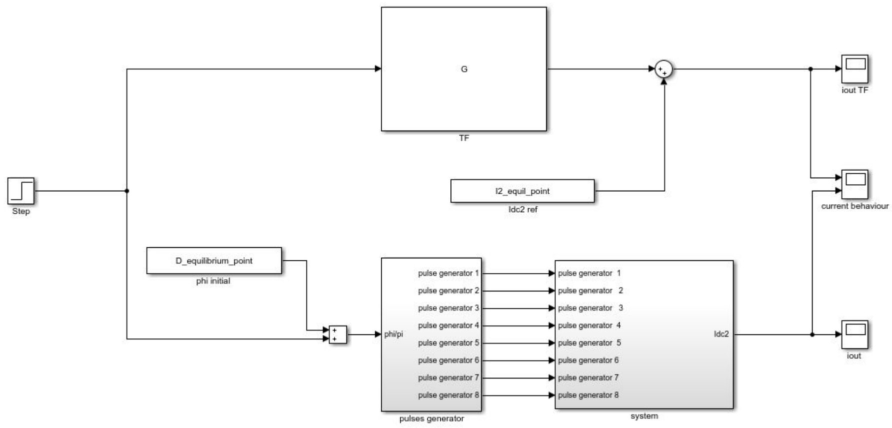

Figure 3.14: Simulink program of the step response for current control for a one module DAB bidirectional DC-DC converter.

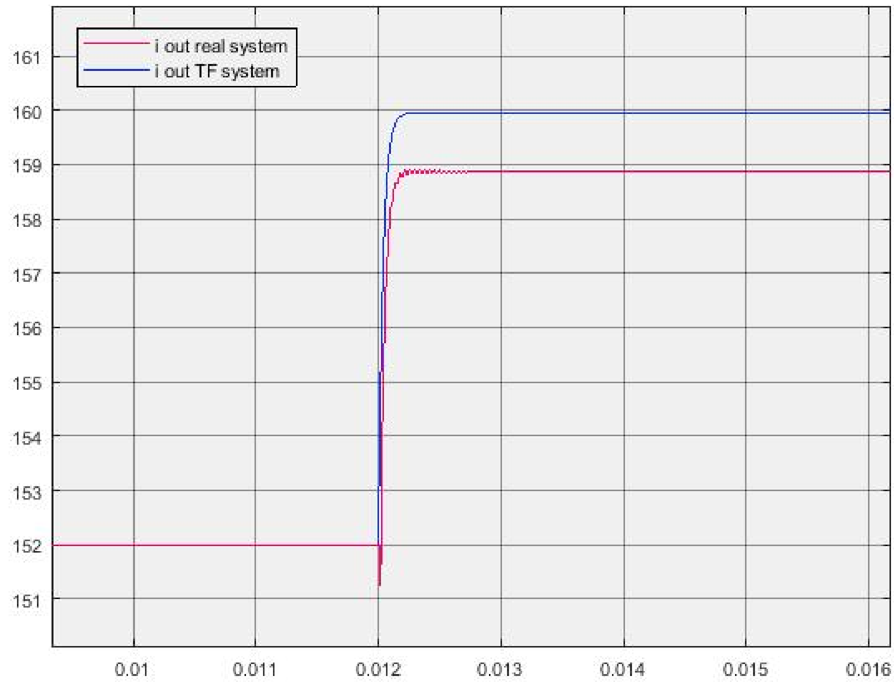

Figure 3.15: Results of the step response for current control for a one module DAB bidirectional DC-DC converter.

Here again, it can be seen that the transfer function system is accurate enough (deviation lower than 13 %), even more if the fact that the real system takes into account the system losses is considered.

3.4.2.1.3 Closed loop current control. Comparison

The control strategy followed was again the one shown in Figure 3.16

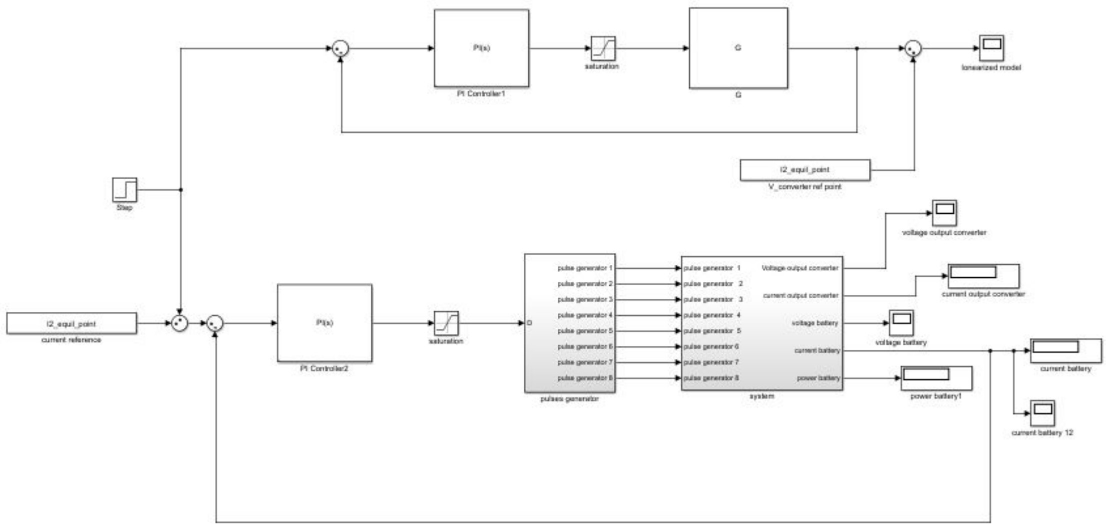

Figure 3.16: Simulink model of the current control strategy.

The steps and theory behind how the PI controller was defined are the same as explained in section 3.4.1.

Therefore, the PI parameters obtained are:

1. $K = 0.0013$

2. $w_L = 872.66$

Besides, the PI controller is:

$$R(s) = 0.0013 \cdot (1 + 872.66 \cdot \frac{1}{s}) \tag{3.30}$$

According to the Phase Margin Theorem, previously discussed to study the stability of the system, and based on equation 3.23 and Figure 3.17, it can be guaranteed that the system was stable since φ_m is 98°, positive.

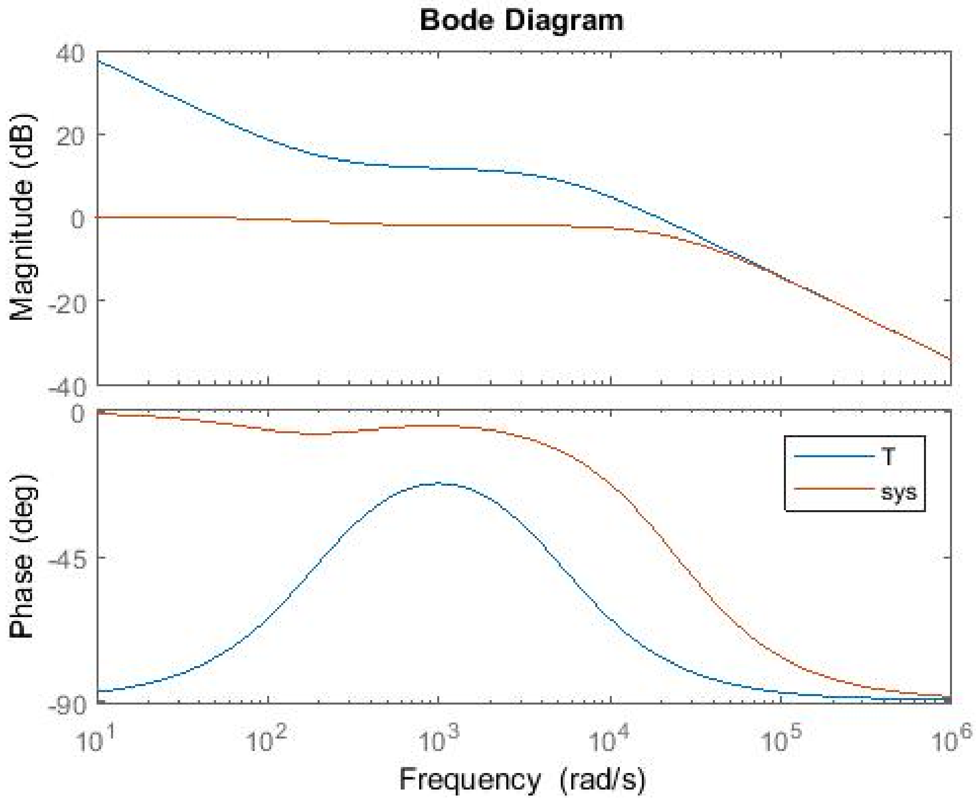

Figure 3.17: Bode diagram of T and total system (sys). Case: one module and current control.

Once it was demonstrated that the system was stable, the controller was configured and the Simulink program from Figure 3.16 was run around the equilibrium point previously defined in this report.

A small disturbance around the equilibrium point was introduced to observe the behaviour of both systems, and this were the results obtained:

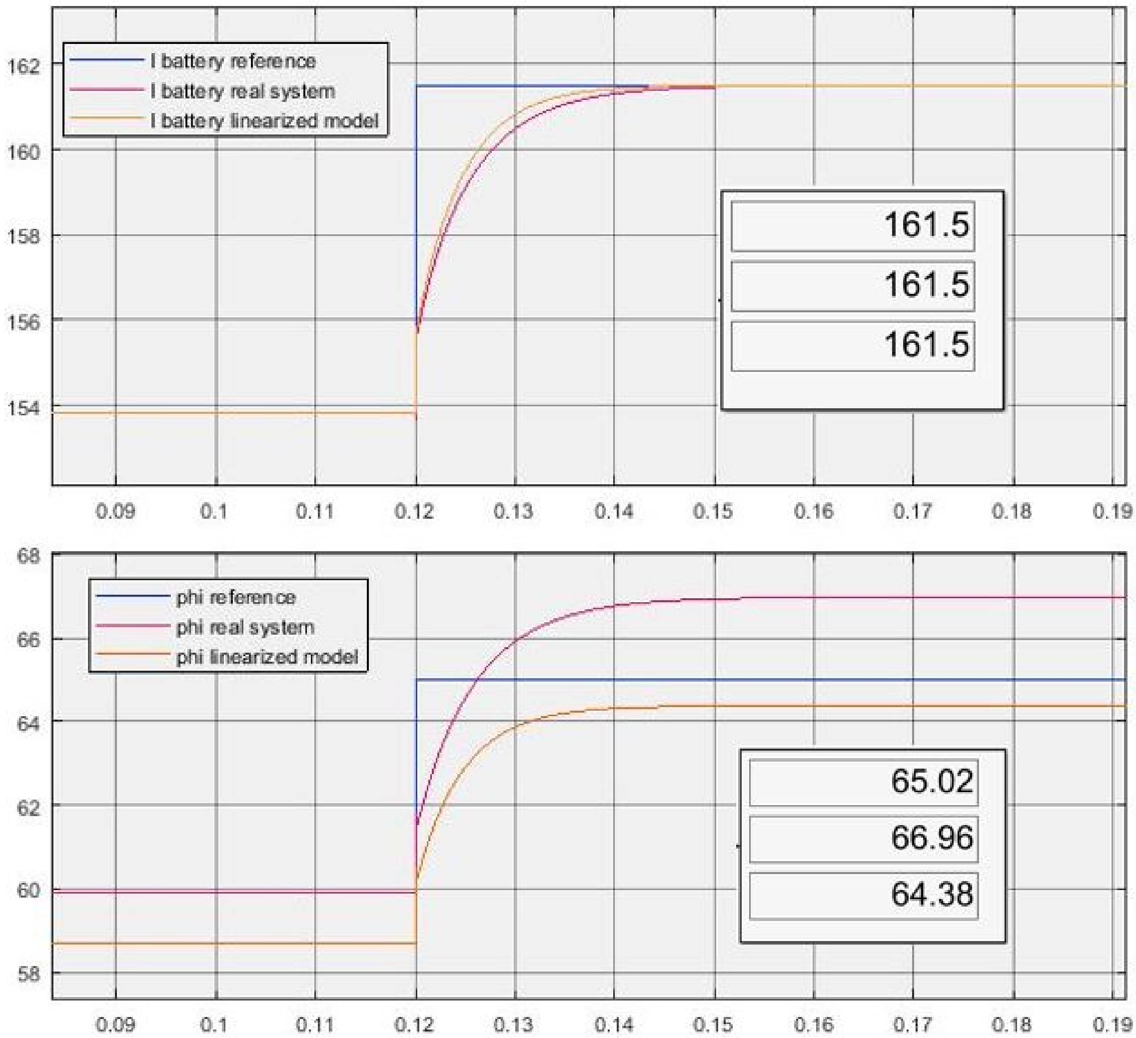

Figure 3.18: Results of the current control strategy for a one module DAB bidirectional DC-DC converter.

In Figure 3.18 it is shown, in the first graph, the output current and, in the second graph, the phase shift. Blue curves are the references from formulas, red curves the output from the real system and the yellow curves the output from the transfer function system. As it can be seen, both systems followed perfectly the current reference, with just slight differences in the phase shift, since the real system had a difference of 2.98 % respect to the reference from formulas and the transfer function system a difference of -0.98 %. However, this differences were expected and it behaved as it had to do: on one hand, the real system, since it considers the looses, it needed a higher phase shift to achieve the same power. On the other hand, the transfer function is based on the lossless model, as the formulas do, but also it had the assumption of constant input voltage, and that is why it needed less phase shift to achieve the same current.

3.4.2.2 Digital control

Here again, once the analog control is accomplished, it is time to focus on the digital control. The same procedure as the one shown in section 3.4.1.2 is followed.

Thus, the structure followed is the one shown in Figure 3.19.

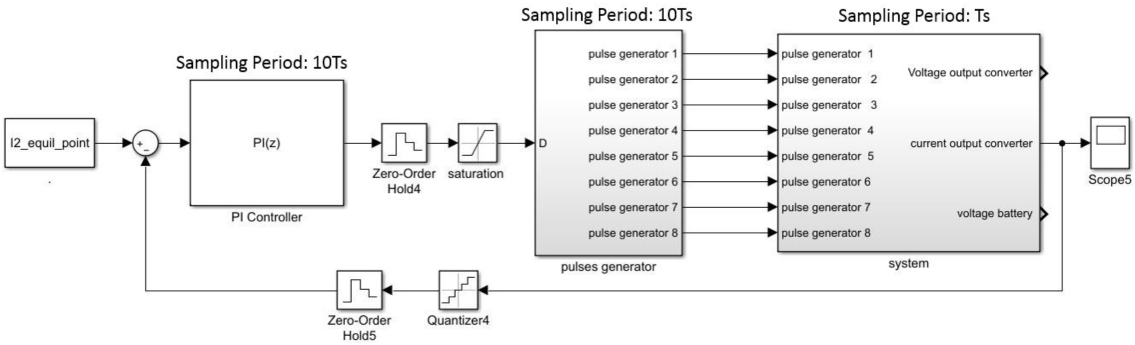

Figure 3.19: Simulink block of the digital current control strategy for a one module DAB bidirectional DC-DC converter.

First, the transfer function G(z) was obtained from the one discussed in section 3.4.2.1.1. To guarantee that it behaves as the continuous-time transfer function, the step-response was studied and shown in Figure 3.20.

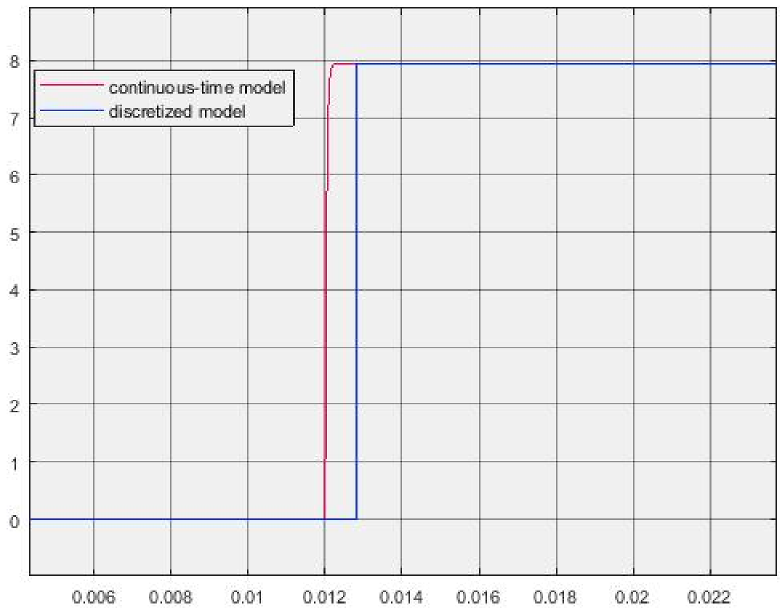

Figure 3.20: Results of the step response for current control for a one module DAB bidirectional DC-DC converter. Comparison between G(s) and G(z).

Following the formulas 3.26 and 3.27, the parameters of the PI(z) used this time were:

1. $V_p = 0.0013$
2. $V_i = 1.61$

Thus, the PI(z) is:

$$R(z) = 0.0013 + 1.61\,\frac{1}{z-1} \tag{3.31}$$

All in all, with the structure from Figure 3.19 and the PI(z) controller, the system was tested. For that purpose, a small step disturbance was introduced to observe the systems behaviour. Moreover, it was compared with some other structures, as it is going to be explained. The results are shown in Figure 3.21.

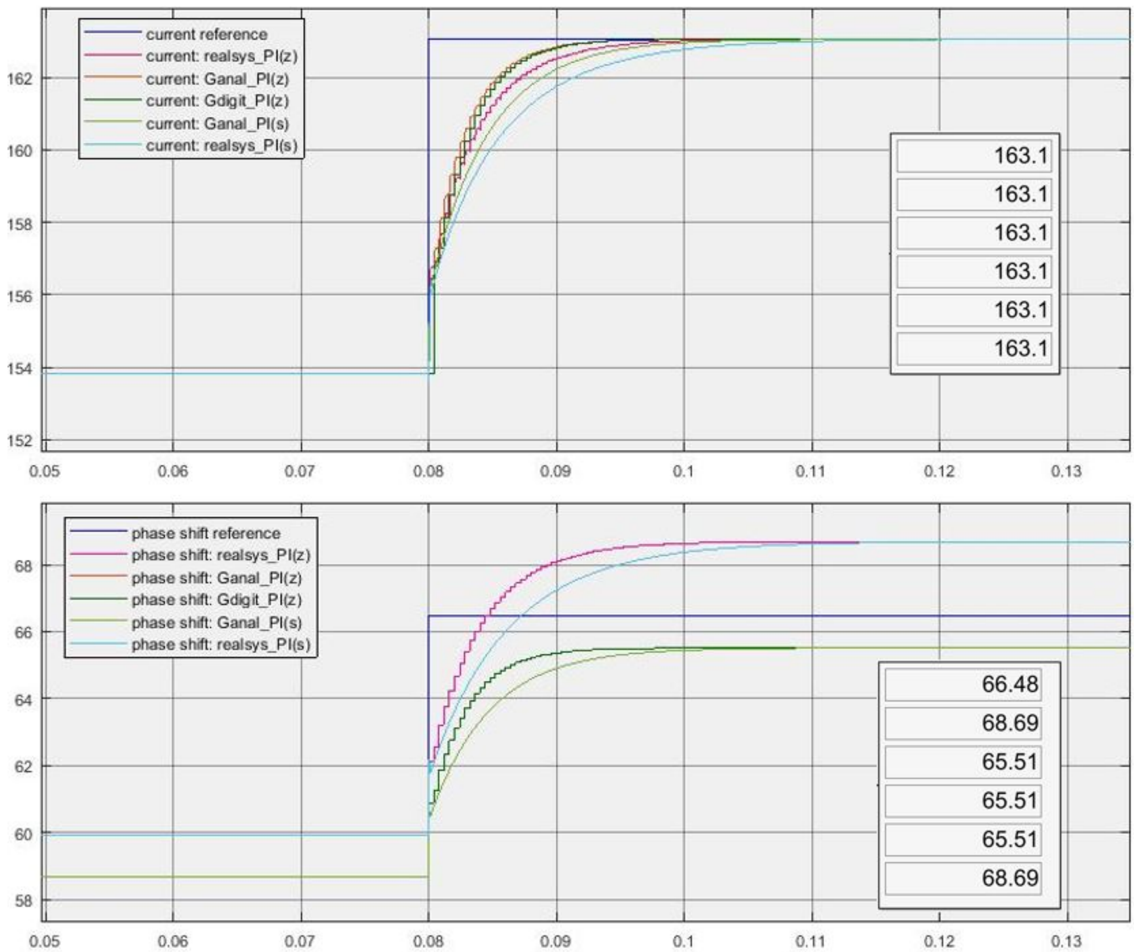

Figure 3.21: Digital current control strategy for a one module DAB bidirectional DC-DC converter. Results.

First graph is the output current and second one is the phase shift. Curves in order, according to the legend: 1. Output converter reference. 2. Output from a real system model controlled with a PI(z). 3. Output from a continuous-time transfer function model controlled with a PI(z). 4. Output from a discrete-dime transfer function model controlled with a PI(z). 5. Output from a continuous-time transfer function model controlled with a PI(s). 6. Output from a real system model controlled with a PI(s)

Here again, as it can be seen in Figure 3.21, it is totally coherent. On one hand, all the models controlled with a discrete PI(z), reaches the new steady state at the same time. Same happens with the continuous-time PI(s), but with different setting time, related to the controller used. On the other hand, those based on the real system, reach the same phase shift and higher (deviation of 2.98 %) than the one expected from formulas, as explained before. Also, those based on a transfer function system, reach the same phase shift and lower (deviation of -0.98 %) than the expected from formulas, also explained before.

3.4.3 Cascade control

The third control strategy developed was the cascade control strategy, corresponding to the second step in the charging strategy: constant voltage mode.

First, the analog development is presented. Then, the digital implementation of the previous system is shown.

3.4.3.1 Analog development

When the end of the first step of the charging strategy is triggered, the constant voltage mode starts. Therefore, the output voltage in controlled. Nevertheless, in this case is also important to keep the track of the output current. Besides, a cascade control strategy was implemented. This cascade control is shown in Figure 3.22.

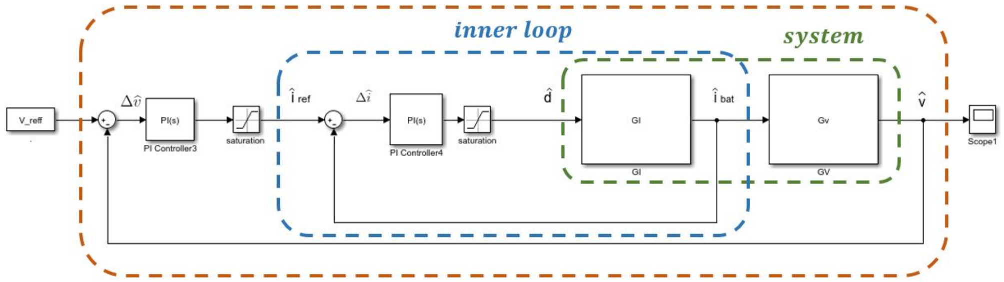

Figure 3.22: Cascade scheme.

Where the master controller controls the output voltage meanwhile the slave controller is in charge of the output current. It is important to remark that the inner loop has to be faster than the outer loop in order to be stable the system.

3.4.3.1.1 Transfer function

In this special case, first GV(s) and GI(s) are defined:

$$GI = \frac{\widehat{i}_{out}}{\widehat{d}} = \frac{\widehat{i}_{bat}}{\widehat{d}} = K3\,\frac{1}{1 + s\,C_2\,(Rline + Rbattery)} \tag{3.32}$$

$$GV = \frac{\widehat{v}_{out}}{\widehat{i}_{out}} = Rline + Rbattery \tag{3.33}$$

Where GI(s) is the transfer function of the inner loop and GV(s) completes the total system.

The process this time was slightly different: first, the inner loop had to be tuned and, after that, it was possible to tun the outer loop.

3.4.3.1.2 Tuning phase

Inner loop

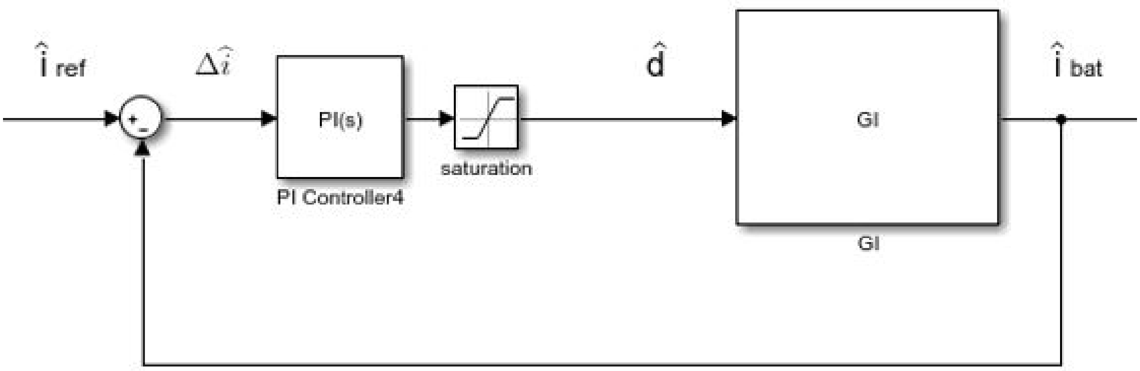

Figure 3.23: Inner loop.

As it can be seen in Figure 3.23, the inner loop is the same system as in section 3.4.2

and, therefore, the transfer function represents the real system. However, the equilibrium point here is different since it is in the second phase of the charging strategy. Besides, a different PI controller was defined. In this case, the PI parameters were:

1. $K = 0.0021$
2. $w_L = a = 1570.8$

Thus, the PI controller was:

$$RI(s) = 0.0021 \cdot (1 + 1570.8 \cdot \frac{1}{s}) \tag{3.34}$$

According to the Phase Margin Theorem, previously discussed to study the stability of the system, and based on equation 3.23 and Figure 3.24, it can be guaranteed that the system was stable since φ_m is 106°, positive.

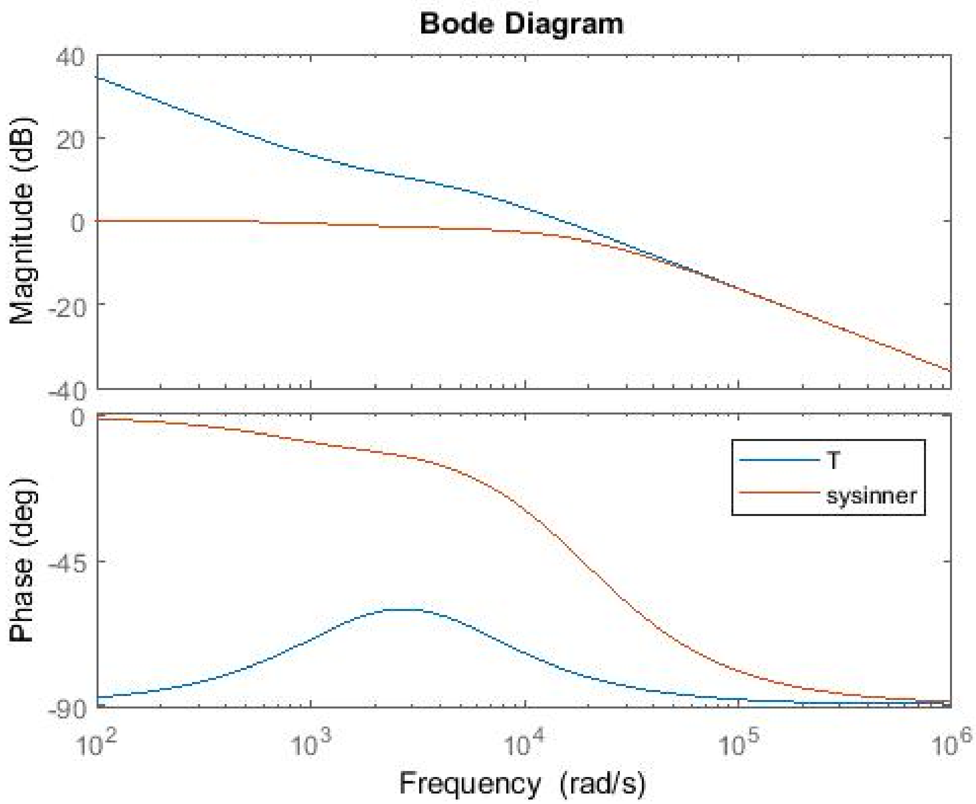

Figure 3.24: Bode diagram of T and total system in the inner loop. Case: one module and cascade control.

In this case, T and sysinner represents:

$$T(s) = RI(s) \cdot GI(s) \tag{3.35}$$

Consequently, the closed loop transfer function can be written as:

$$sysinner = \frac{T}{1+T} \tag{3.36}$$

And applying the PI controller to the system from Figure 3.23 it can be seen in Figure 3.25 that the inner loop was correctly tuned.

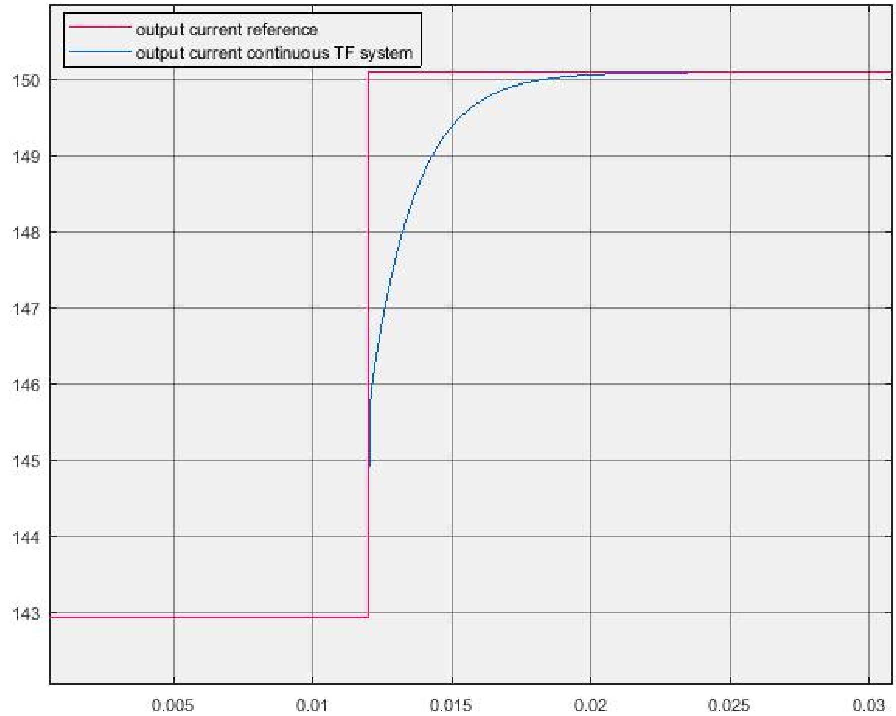

Figure 3.25: Results of the cascade control for a one module DAB bidirectional DC-DC converter. Inner loop design.

Outer loop

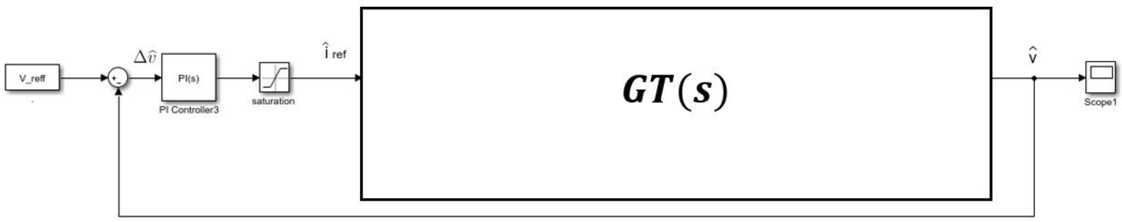

Figure 3.26: Outer loop of the cascade control for a one module DAB DC/DC converter.

The first thing to do is obtaining the transfer function GT(s) in order to design the

PI controller.

$$T(s) = RI(s)\ GI(s) = K3\ K\ \frac{s+a}{s + (R_{bat} + R_{line})\ C_2\ s^2} \tag{3.37}$$

$$\begin{aligned} sysinner(s) &= \frac{T}{1+T} = \\ &= K3\ K \\ &\frac{s+a}{(R_{bat} + R_{line})\ C_2\ s^2 + (1 + K3\ K)\ s + K3\ K\ a} \end{aligned} \tag{3.38}$$

$$\begin{aligned} GT(s) &= sysinner\ Gv = \\ &= (R_{bat} + R_{line})\ K3\ K \\ &\frac{s+a}{(R_{bat} + R_{line})\ C_2\ s^2 + (1 + K3\ K)\ s + K3\ K\ a} \end{aligned} \tag{3.39}$$

Therefore, from equation 3.39, GT(s) is a second order transfer function. Besides, this makes the PI design more difficult than before. However, some simplifications could be done:

1. On one hand, the coefficient $(1 + K3 \cdot K)$ is fixed by the equilibrium point. Therefore, it could not be said in advance how big it was going to be. Nevertheless, it could be delimited. First, $K3 \cdot K$ was going to be always positive. Secondly, in worst case ($D = 0.5$ and $K3 = 0$), $(1 + K3 \cdot K) = 1$. In consequence, $(1 + K3 \cdot K)$ was always $>= 1$.

2. On the other hand, the coefficient $(R_{bat} + R_{line}) \cdot C_2$ is fixed by design. As it was explained, this values were really low and positive, so $0 < (R_{bat}+R_{line})\cdot C_2$ $<< 1$.

Finally,

$$(R_{bat} + R_{line})\ C_2 << (1 + K3\ K) \tag{3.40}$$

And then,

$$GT_{simplified}(s) = (R_{bat} + R_{line})\ K3\ K\ \frac{s+a}{(1 + K3\ K)\ s + K3\ K\ a} \tag{3.41}$$

Which is a first order system and the PI controller was easier to design.

Besides, it is important to remark that the simplified GT(s) is still causative since both numerator and denominator's order are the same.

However, it was necessary to check if both systems, GT and $GT_{simplified}$, behaved the same way. First, from Figure 3.27, it could be seen that both systems had the same dominant pole.

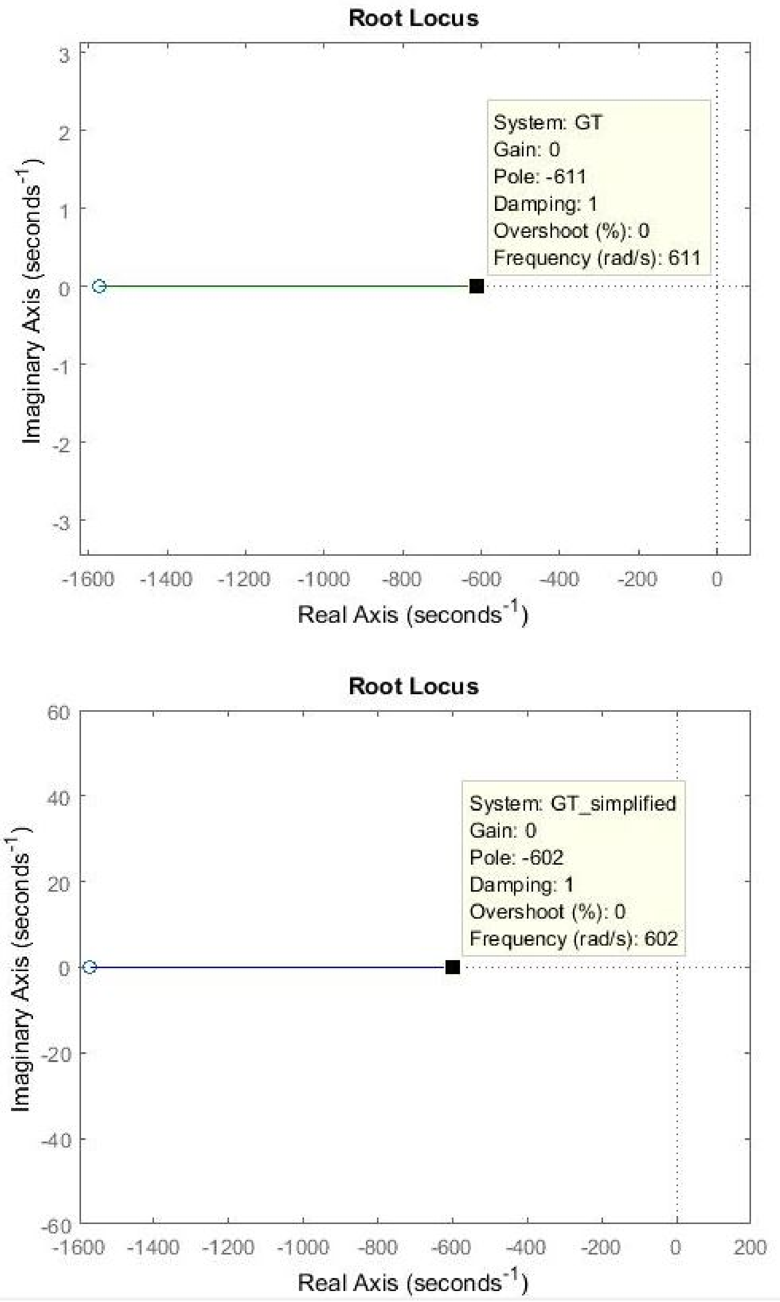

Figure 3.27: Rote locus of GT, the first one, and $GT_{simplified}$, the second one.

Moreover, it can be seen in Figure 3.28, that both systems reacted the same way with a step entrance.

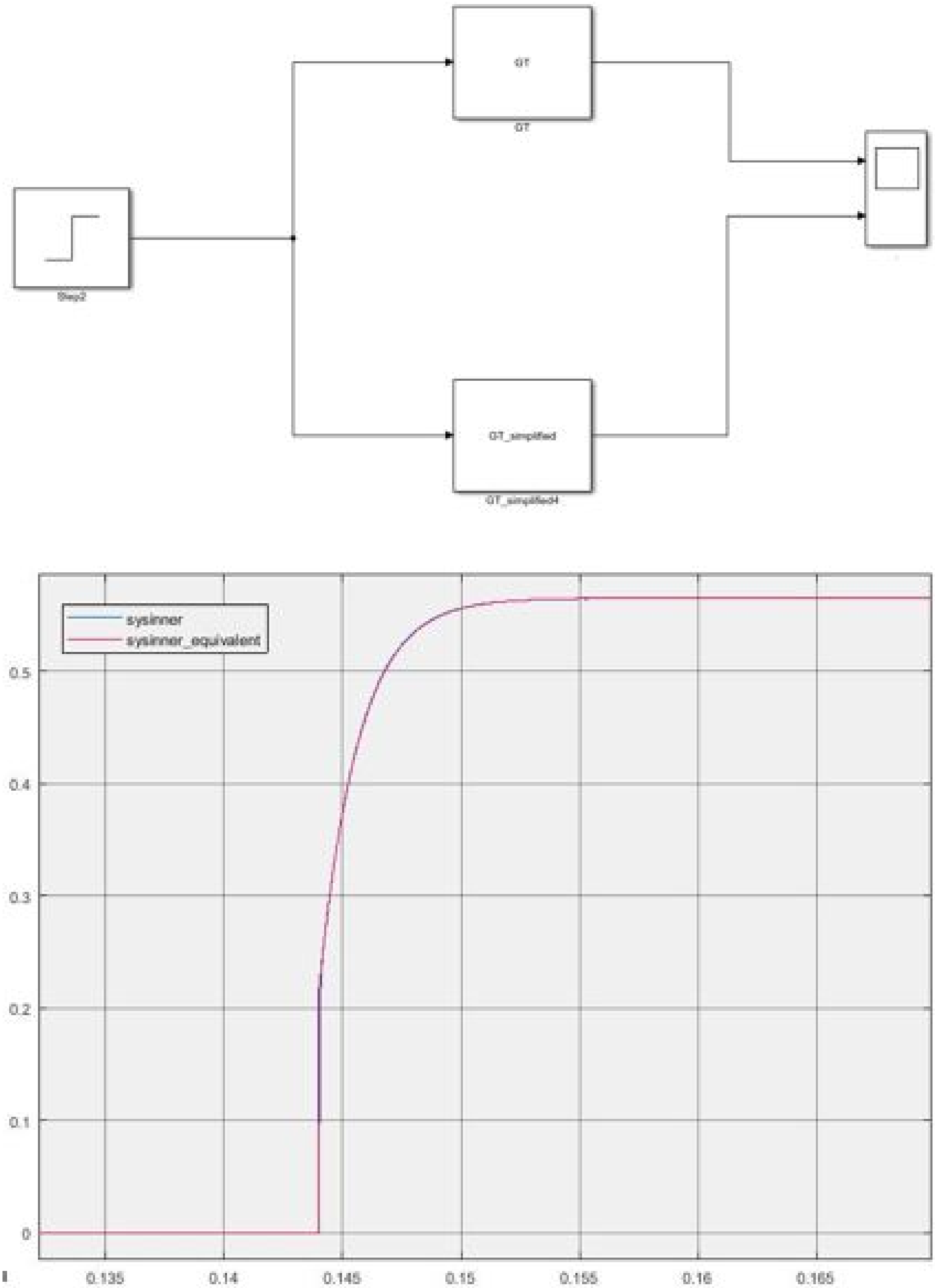

Figure 3.28: Step response of GT and $GT_{simplified}$.

In conclusion, $GT_{simplified}$ accurately represents GT.

Once it was demonstrated that $GT_{simplified}$ could be used, designing the PI controller was easier since the same procedure as before was used. These were the parameters obtained for it:

1. $K = 0.4071$
2. $w_L = 265.52$

Besides, the PI controller was:

$$RI(s) = 0.4071\ (1 + 265.52\ \frac{1}{s}) \tag{3.42}$$

According to the Phase Margin Theorem, previously discussed to study the stability of the system, and based on equation 3.23 and Figure 3.29, it can be guaranteed that the system was stable since φ_m is 103°, positive.

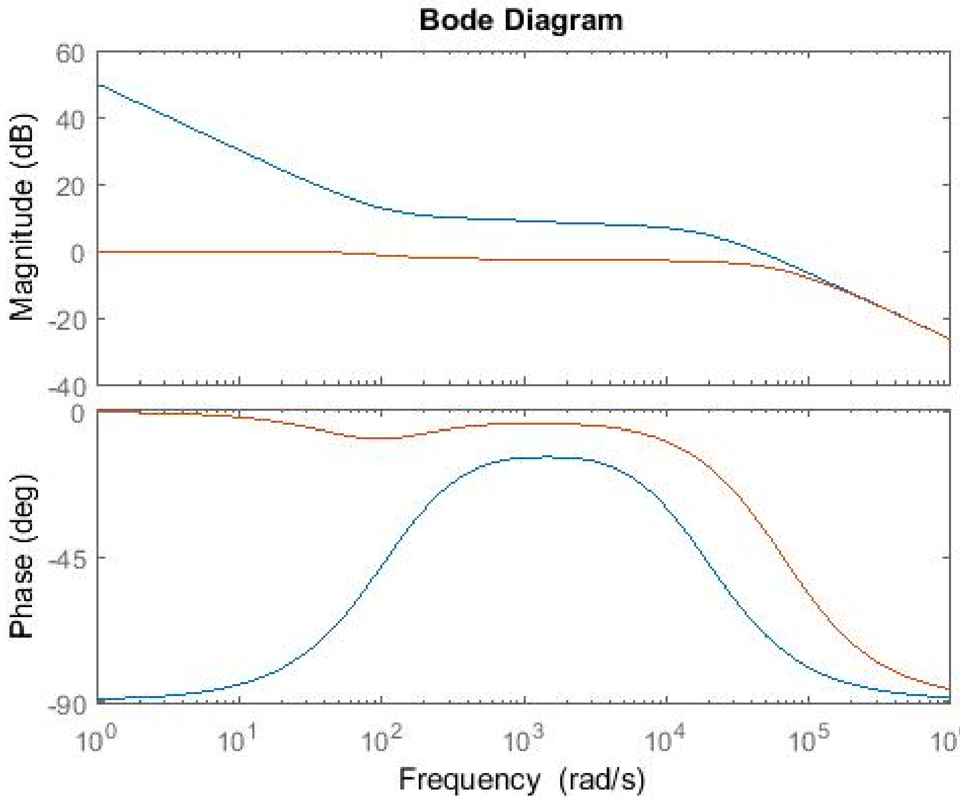

Figure 3.29: Bode diagram of T and total system in the outer loop. Case: one module and cascade control.

Once all the PI controllers were tuned, the transfer function system was tested. However, its behaviour is going to be shown together with the real system in the next section.

3.4.3.1.3 Closed loop cascade control. Comparison

The systems were tested in Simulink, as it is shown in Figure 3.30.

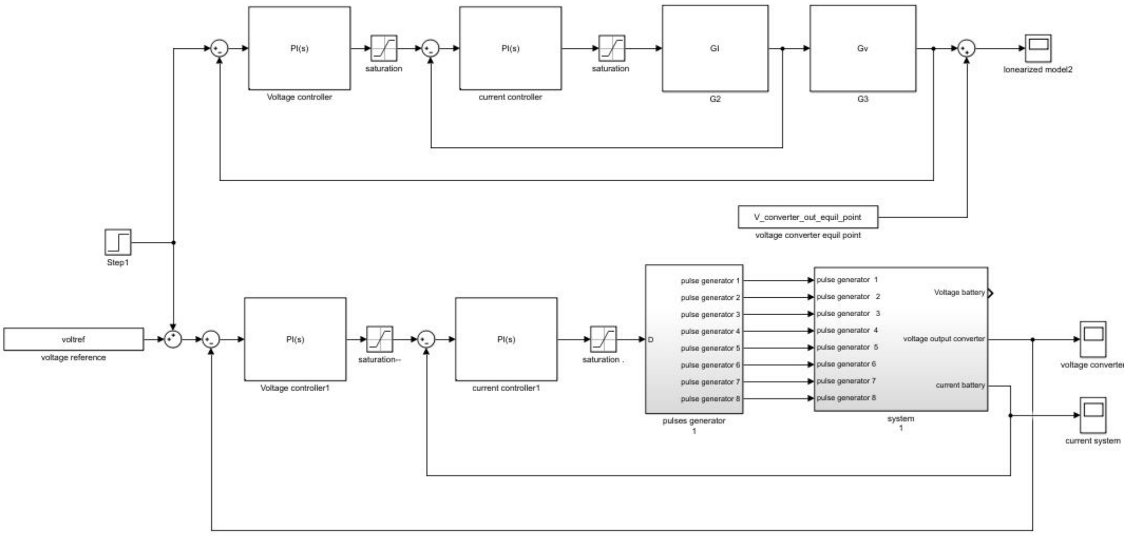

Figure 3.30: Simulink block for a one module DAB DC-DC converter of the cascade control.

Obviously, here the real transfer function GT was used.

This time, all the PI controllers and its stability was studied in the previous section. Consequently, the Simulink program from Figure 3.30 was run around the equilibrium point from the second phase of the charging strategy. This time, both current and voltage were controlled.

A small disturbance around the equilibrium point was introduced to observe the behaviour of both systems, obtaining the next results:

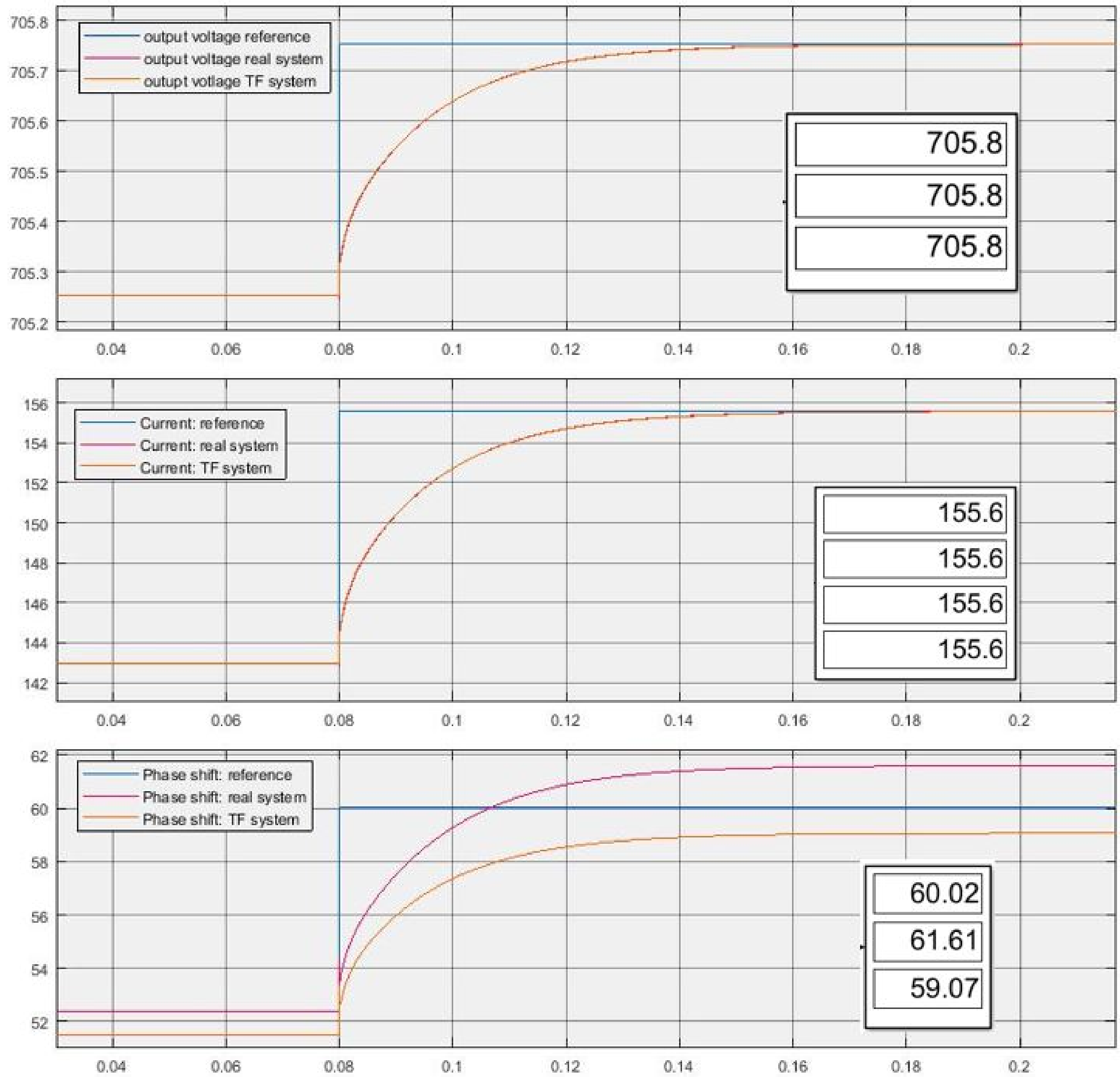

Figure 3.31: Simulink results of the cascade control for a one module DAB DC-DC converter. First graph is the output voltage, second one the current output and third one the phase shifts. Blue curves are the references, red curves the output from the real system and yellow ones the output from the transfer function system.

In Figure 3.31, it can be seen that both systems followed perfectly the voltage and current references, with just slight differences in the phase shift, since the real system had a difference of 2.65 % respect to the reference from formulas and the transfer function system a difference of -1.58 %. However, again, this differences were expected and it behaved as it had to do: on one hand, the real system, since it considers the looses, it needed a higher phase shift to achieve the same power. On the other hand, the transfer function is based on the loosless model, as the formulas do, but also it had the assumption of constant input voltage, and that is why it needed less phase shift to achieve the same current.

3.4.3.2 Digital control

Once again, after developing the analog control, it is time to focus on the digital control. Similar procedure as the one shown in section 3.4.1.2 is followed.

First, the structure used this time is the one shown in Figure 3.32.

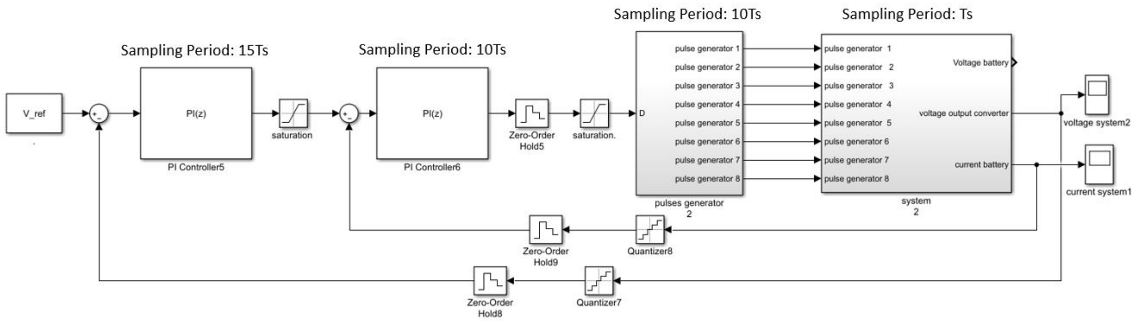

Figure 3.32: Simulink block of the digital cascade control strategy for a one module DAB bidirectional DC-DC converter.

As it was explained in the previous section, first, the inner loop is tuned and then the outer loop is studied and its PI(z) tuned. Finally, the whole system is analyzed.

Inner loop

The structure of the inner loop is shown in Figure 3.33.

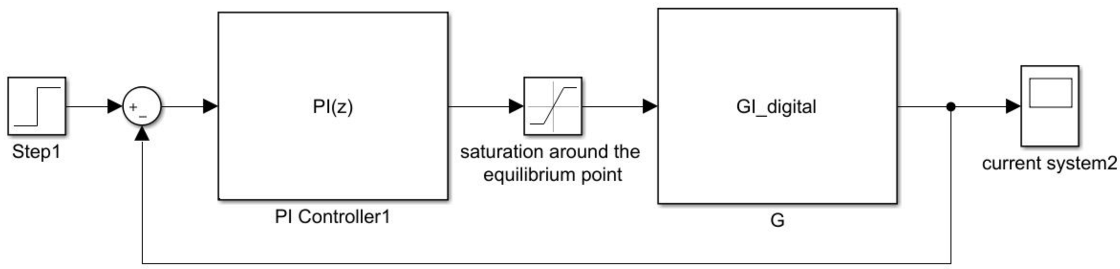

Figure 3.33: Inner loop in the discrete mode.

Where GI(z) is the discrete-time transfer function obtained from GI(s) from formula 3.32.

The step response is not needed in this case since it is the same transfer function as in section 3.4.2.2. However, the equilibrium point is different since the aim is the constant voltage mode. Besides, the PI(z) controller for the inner loop, based on formulas 3.26 and 3.27, is this time:

1. $V_p = 0.0021$
2. $V_i = 4.5572$

Thus, the PI(z) is:

$$R(z) = 0.0021 + 4.5572\,\frac{1}{z-1} \tag{3.43}$$

Besides, the output from Figure 3.33 is shown in Figure 3.34.

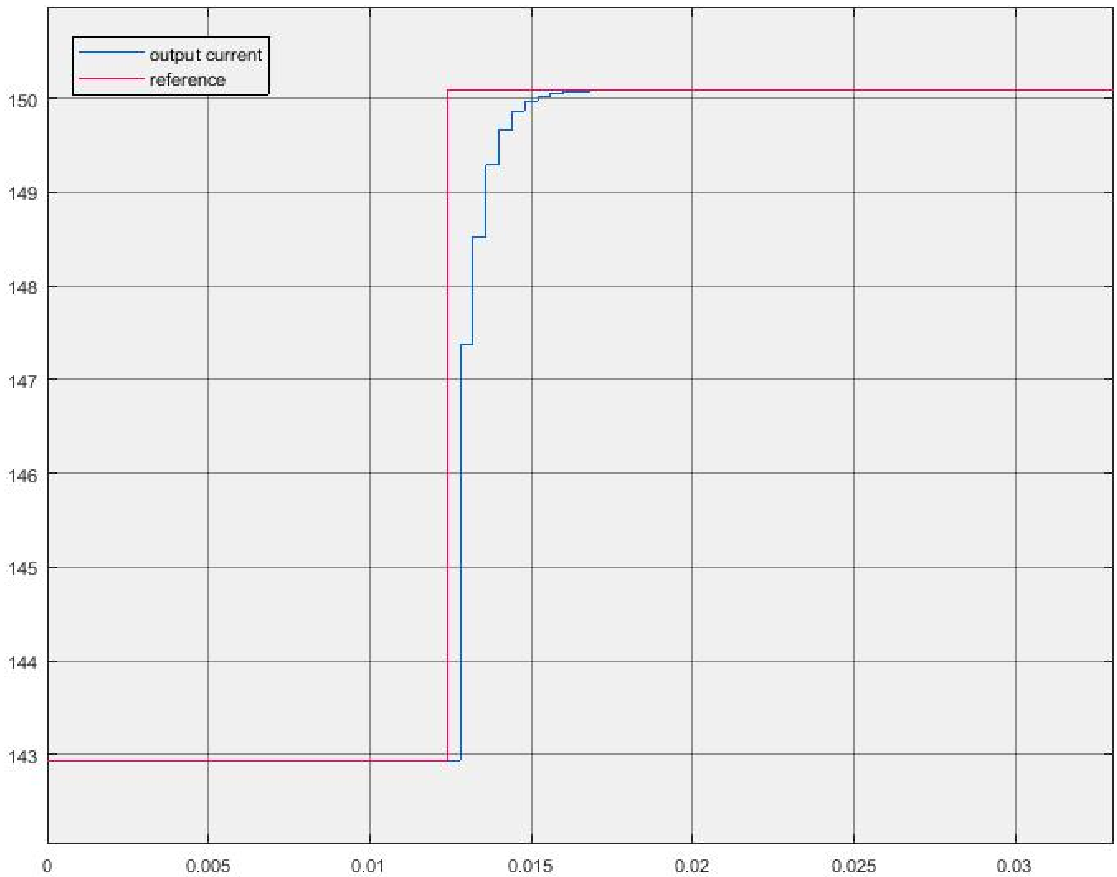

Figure 3.34: Discrete mode. Cascade control for a one module DAB bidirectional DC-DC converter. Inner loop design. Results.

Where it can be seen that the output current follows perfectly the reference.

Outer loop

The structure of the outer loop is shown in Figure 3.35.

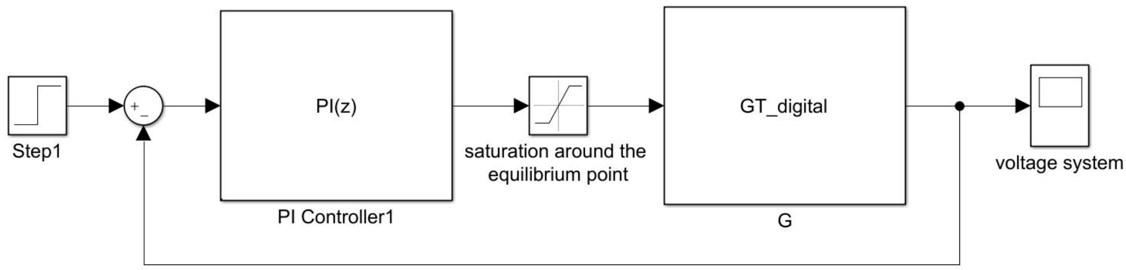

Figure 3.35: Outer loop. Discrete mode.

Where GT(z) is the discrete-time transfer function obtained from GT(s) from formula 3.39.

The step response cannot be implemented since there is no reference from the real system of GT because it includes not only the transfer function from the system but also the PI controller from the inner loop and the inner loop itself.

Therefore, going straight forward to the PI(z) design, based on formulas 3.26 and 3.27, the PI(z) controller is:

1. $V_p = 0.4071$
2. $V_i = 3458.5$

Thus, the PI(z) is:

$$R(z) = 0.4071 + 3458.5 \, \frac{1}{z-1}. \tag{3.44}$$

Besides, the output from Figure 3.35 is shown in Figure 3.36.

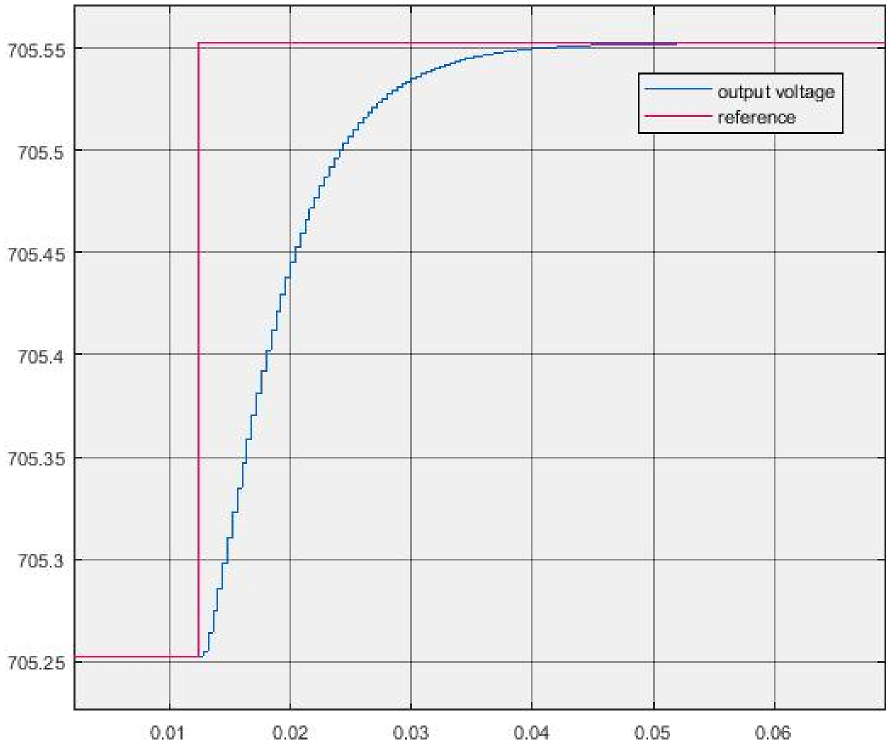

Figure 3.36: Results of the discrete mode. Cascade control for a one module DAB bidirectional DC-DC converter. Outer loop design.

Where it can be seen that the output voltage follows perfectly the reference.

Total system

Finally, the whole system was studied.

All in all, considering the structure from Figure 3.32 and the PI(z) controllers from 3.43 and 3.44, the system was tested. For that purpose, a small step disturbance was introduced to observe the systems behaviour. Moreover, again, it was compared with some other structures, as it is going to be explained. The results are shown in Figure 3.37.

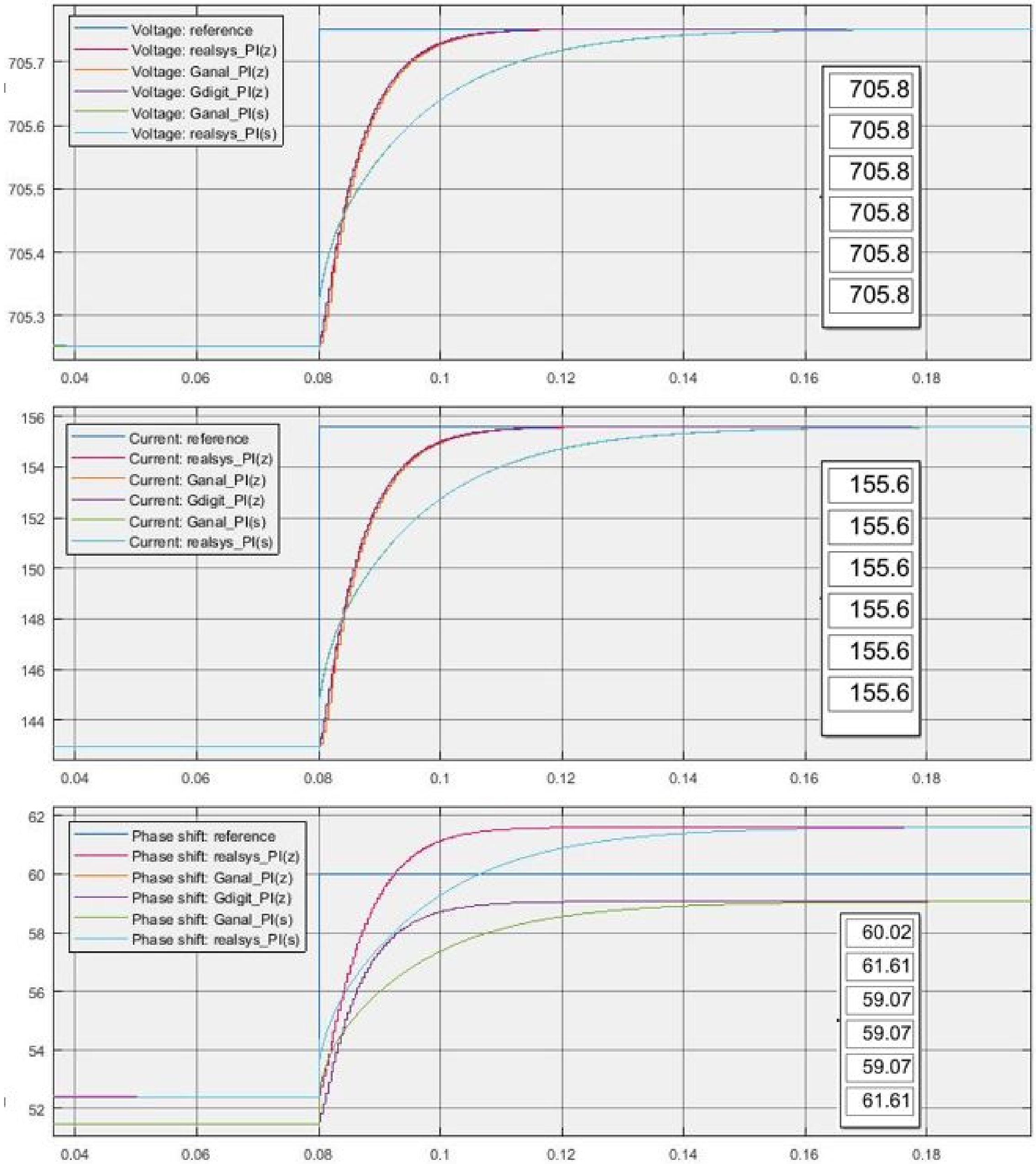

Figure 3.37: Results of the digital cascade control strategy for a one module DAB bidirectional DC-DC converter. First graph is the output voltage, second one is the output current and the third one the phase shift. Curves in order, according to the legend: 1. Output converter reference. 2. Output from a real system model controlled with a PI(z). 3. Output from a continuous-time transfer function model controlled with a PI(z). 4. Output from a discrete-dime transfer function model controlled with a PI(z). 5. Output from a continuous-time transfer function model controlled with a PI(s). 6. Output from a real system model controlled with a PI(s).

Once again, as it can be seen in Figure 3.37, it is totally coherence. On one hand, all the models controlled with a discrete PI(z), reaches the new steady state at the same time. Same happens with the continuous-time PI(s), but with different setting time, related to the controller used. On the other hand, those based on the real system, reach the same phase shift and higher (deviation of 2.65 %) than the one expected from formulas, as explained before. Also, those based on a transfer function system, reach the same phase shift and lower (deviation of -1.58 %) than the expected from formulas, also explained before.

4

Digital control of a three parallel connected DC/DC modules

Once it was demonstrated that controlling a one-module converter was possible, the 300 kW DC/DC converter was developed. With three modules parallel connected in the output, it was supposed to be possible to obtain 300 kW in the output. However, there were some doubts regarding if that was possible, as it will be discuss later on.

The first decision made was how the input port of the converters should be connected. Several configurations were studied, as it is shown in figures 4.1, 4.2 and 4.3.

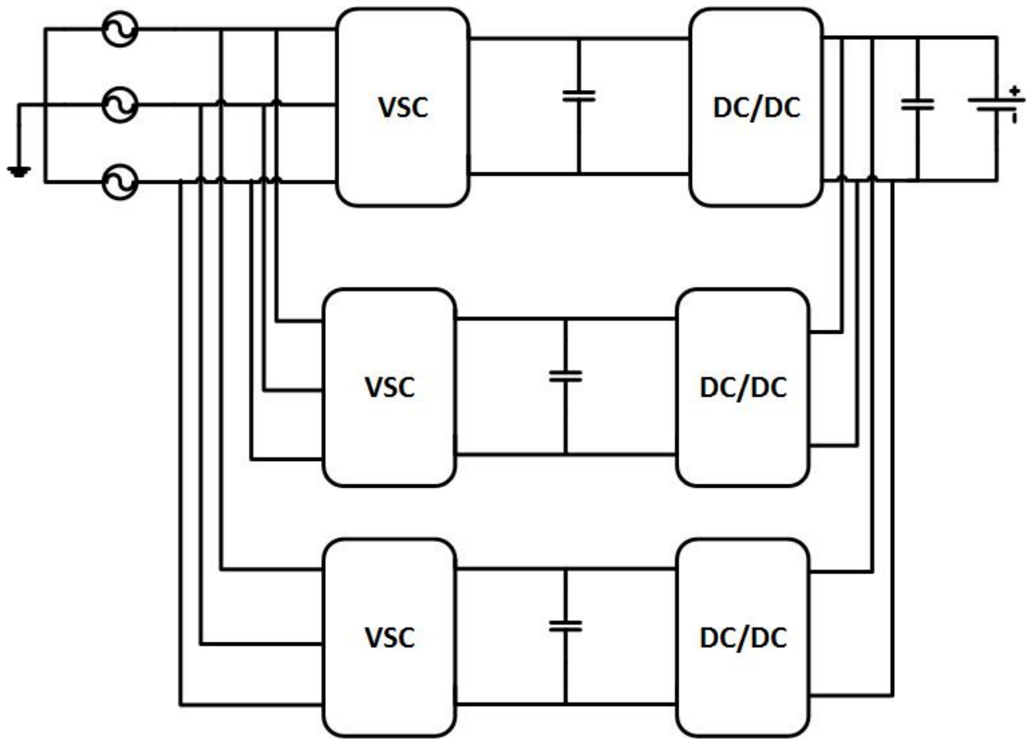

Figure 4.1: Parallel strategy I: isolated inputs.

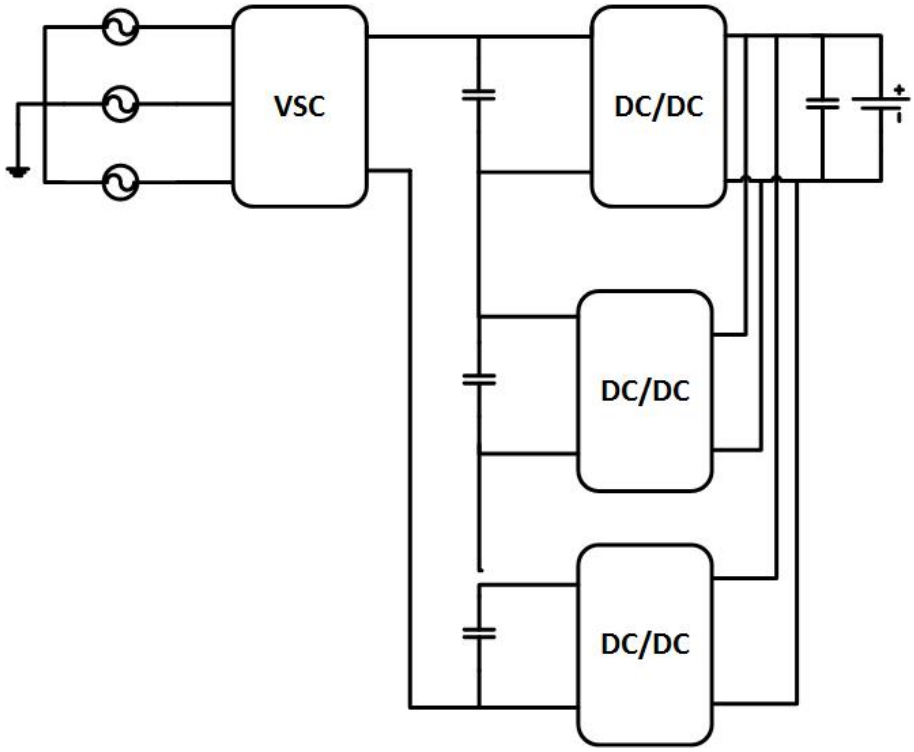

Figure 4.2: Parallel strategy II: ISOP configuration.

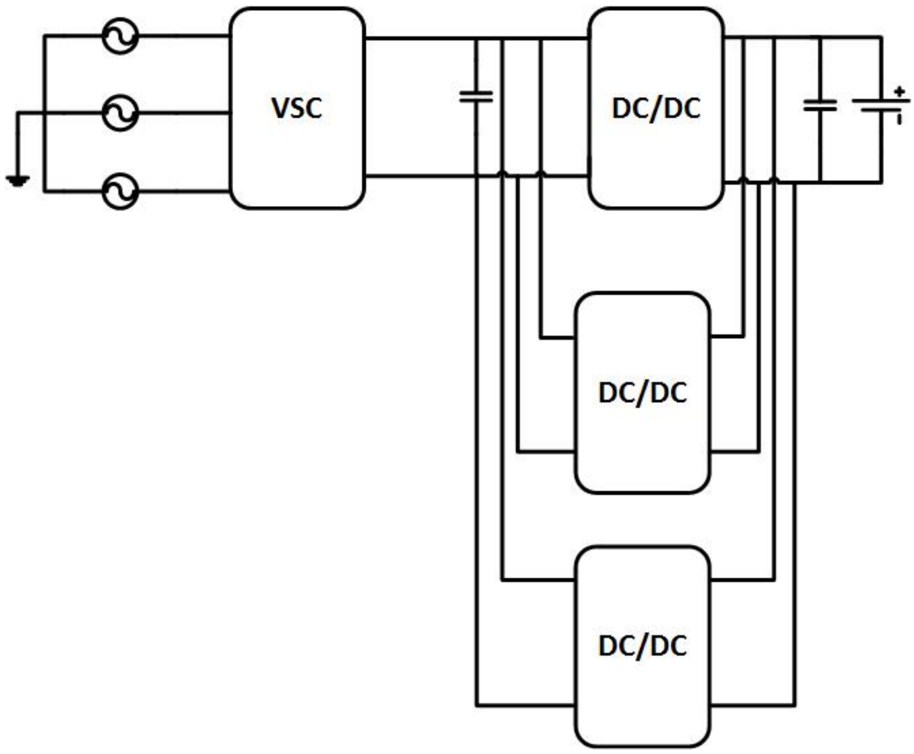

Figure 4.3: Parallel strategy III: IPOP configuration.

The first one, each one with their own isolated input, was discarded. It was the most expensive solution, since three different VSC and DC-links were needed and the power density was lower.

The second one, the input-series output-parallel configuration (ISOP) was considered [16]. The power density was higher than the first option and cheaper. However, in this case, the output voltage from the VSC was necessary higher than in any of the other solutions. This solution was still more expensive than the last one, since three capacitors were needed in the input ports.

Finally, the input-parallel output-parallel (IPOP) configuration was studied. This topology was the one chosen for several reasons. First, the interleaving technique allowed to reduce the size and the losses of the input and output filters. Also, just one filter is needed. Moreover, it has a better dynamic performance and higher power density [9]. Finally, it was the cheapest solution since it needs less components. Therefore, it was the best option.

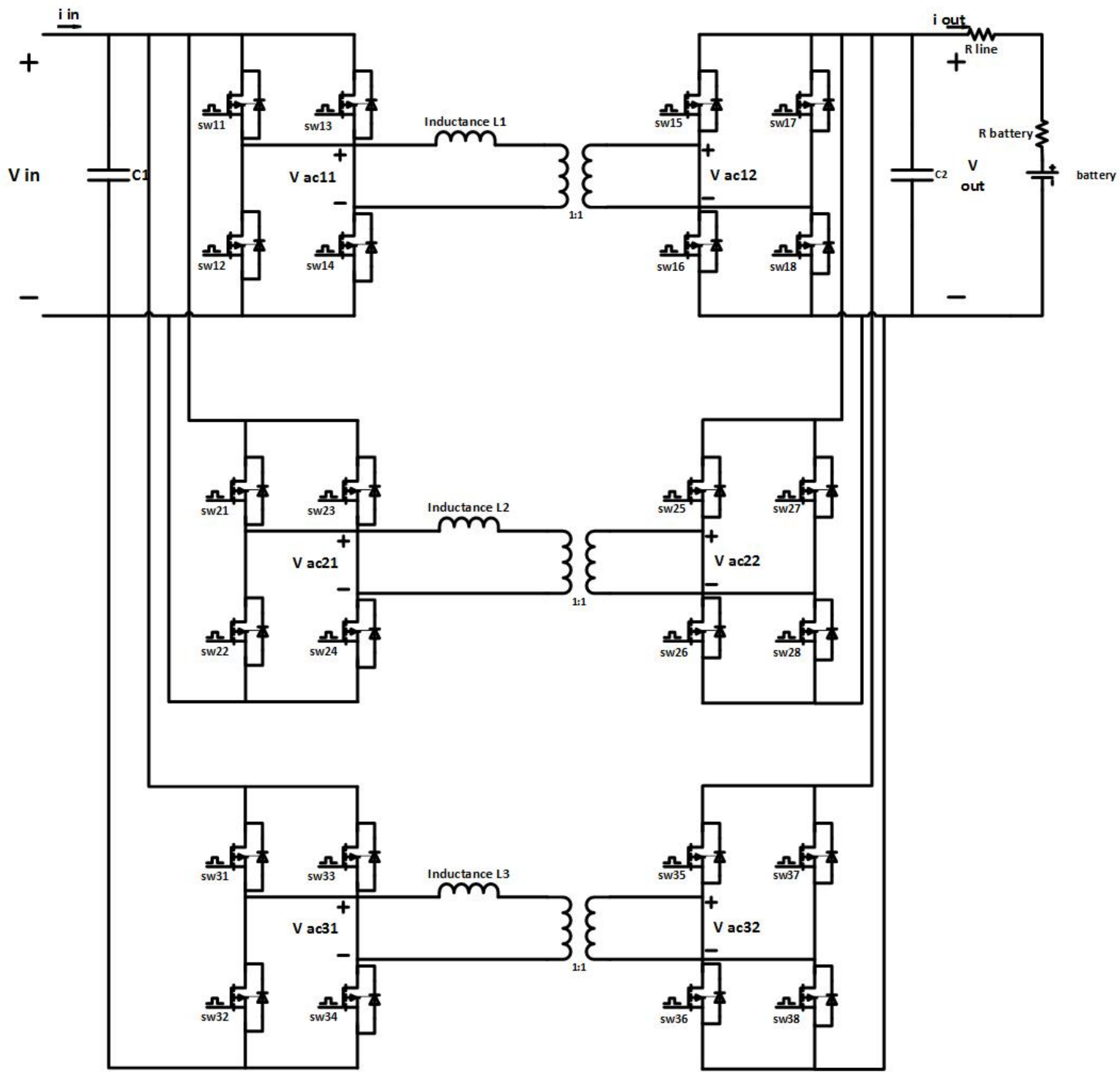

Figure 4.4: IPOP configuration of the 300 kW DC/DC converter.

For the Simulink model, the structure from Figure 4.4 was used in this case. There, it can be seen that the input is the phase shift which, trough the pulse generators, produce the pulses for the system. Then, inside the block 'system', the configuration from figure 4.4 is implemented, obtaining as outputs the followings: battery voltage, converter output voltage, converter current 1, converter current 2, converter current 3, total battery current and converter output power.

4.1 Parallel connection and control strategy

As it was said, there were some questions regarding the reliability of connecting in parallel several DC/DC modules. Were all of them going to provide the same power? Does it appear any recirculating current through the converters that does not go to the battery but to other converters? Specifically, there were some doubts on how any mismatches in the converter parameters, such as phase shift or inductance and transformer impedances, could affect to the operation of the whole converter.

For this purpose, the analysis from reference [9] is totally clarifier. In [9], two converter in IPOP configuration was studied and the common-phase-shift strategy was implemented. By this strategy, both converters received the same phase shift, according to the expected total current needed.

In [9], a steady state and dynamic analysis was realized to evaluate how mismatches in different modules parameters could affect the output current. In the steady-state analysis, it was shown that the variations in the output currents could be obtained as 4.1 shows:

$$\frac{\Delta I_{tot}}{I_{tot}} = \frac{I_{1a} - I_{1b}}{I_{1a} + I_{1b}} = \frac{1-2D}{2(1-D)} \cdot \frac{\Delta D}{D} - \frac{1}{2} \cdot \frac{\Delta L}{L} = \frac{1-2D}{2(1-D)} \cdot \alpha - \frac{1}{2} \cdot \beta. \tag{4.1}$$

Where I_{1a} and I_{1b} are the input currents of both DC/DC converters. Therefore, 4.1 shows the mismatches between converters' currents as function of mismatches in the phase shift and in the inductance, including there the transformer parameters. This formula is represented in Figure 4.5.

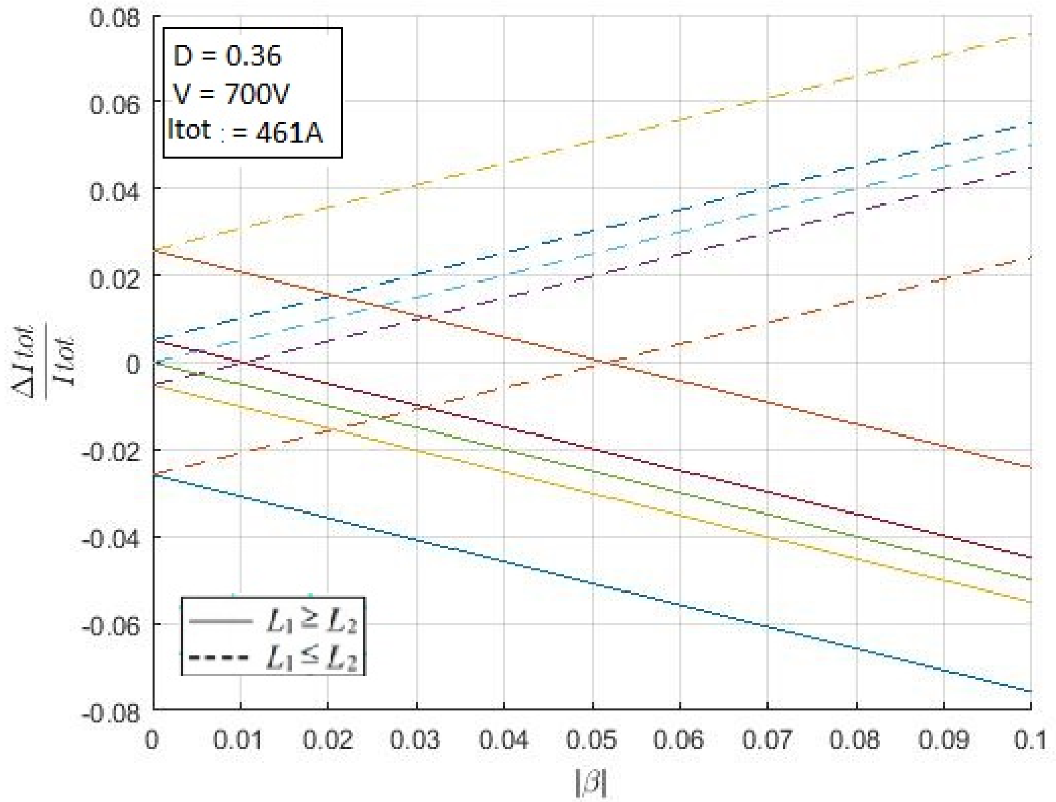

Figure 4.5: $\frac{\Delta I_{tot}}{I_{tot}}$ as a function of α and β. The one with the lowest starting point corresponds to α = -0.1. Then the others are, in order: -0.02, 0, 0.02 and 0.1.

As a consequence of that, considering mismatches at the same time in both phase shift and inductance parameters and both as big as 10%, the $\frac{\Delta I_{tot}}{I_{tot}}$ was, in worst case, lower than 0.08 which means that $I_{1a} - I_{1b}$ is, in worst case, lower than 8% from total current. However, it is important to remark that with the advance of modern manufacturing techniques, both mismatches can be practically neglected. So, therefore, the steady state analysis showed that mismatches in phase shift, leakage inductances or in transformer turn ratios have slight effect on the sharing of input currents [9].

In respect of dynamic analysis, reference [9] showed that mismatches in phase shift, leakage inductances or in transformer turn ratios slightly affects the dynamic sharing of input currents. But again, this mismatches are almost neglected with new manufacturing techniques.

Finally, some experiments were held in [9], which showed that common-phase-shift control guarantees that the IPOP converter achieves a totally acceptable performance of current sharing even if there are mismatches of 10% in different converter parameters.

In conclusion, as it was shown in [9] and endorsed by [10], [11] and [12], common-phase-shift control is absolutely acceptable for IPOP converters if maximum mismatches in parameters of 10% is ensured, which is, in practice, guaranteed. However, if more general methods were required, references [10] [11] [12] show also more general control techniques. Nevertheless, those are not considered for this purpose since mismatches lower that 10% are guaranteed.

In addition, to demonstrate that there is no recirculating current between converters, a simulation with the total system from Figure 4.4 was held. In this experiment, the following mismatches were introduced:

Converter	Inductance	Phase shift
Converter 1	Le	phi
Converter 2	Le*1.06	phi*1.06
Converter 3	Le*0.96	phi*0.96

Table 4.1: Mismatches introduced in the different modules.

Obtaining the following results:

Converter	Current from real system	Current expected from formula
Converter 1	141	142.9
Converter 2	136.1	139.5
Converter 3	146.7	145.2

Table 4.2: Results obtained from mismatches introduced in the different modules.

Where it can be observed that the results are coherent. On one hand, the higher the impedance is, the lower current is obtained. On the other hand, since the real system takes into account all the losses, the higher the inductance is the higher is the difference with respect to the expected value from formulas. Also, when the inductance is lower than Le, the current obtained is higher than the expected from formulas. Finally, the current that feeds the battery is the sum of the three of them in steady state.

4.2 Average model

Once it was demonstrated that the parallel connection was possible, the same process as before was followed, with a one module converter, to be able to develop the digital control of the total converter. For that purpose, first it is necessary to obtain a model of the system. Therefore, the first step is obtaining the average model of the total converter.

The average model was based on the lossless converter model [3] shown in figure 4.4. Each module provides the following power:

$$P_i = P_{i1} = P_{i2} = \frac{n\, V_1\, V_2\, D\, (1 - |D|)}{2\, f_s\, L_i}. \tag{4.2}$$

Where the sub-index i represents each converter: $i = 1, 2, 3$.

As it was explained in section 3.1, the DC current that flows in both sides of each module are shown in formulas 4.3 and 4.4.

$$I_{i1} = \frac{P_{i1}}{V_1} = \frac{n\, V_2\, D\, (1 - |D|)}{2\, f_s\, L_i} \tag{4.3}$$

$$I_{i2} = \frac{P_{i2}}{V_2} = \frac{n\, V_1\, D\, (1 - |D|)}{2\, f_s\, L_i}. \tag{4.4}$$

With equations 4.3 and 4.4 and Figure 4.4, the average circuit could be obtained, as shown in Figure 4.6.

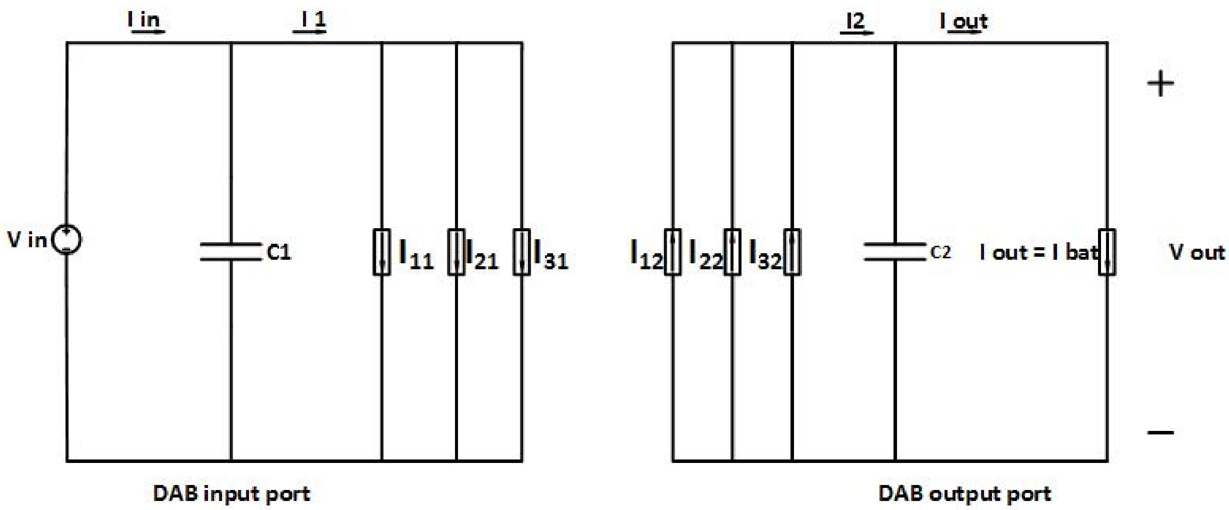

Figure 4.6: Average circuit model of a 3 modules DAB bidirectional DC/DC converter.

4.3 Small-signal model

According to the previous experience from section 3.2, it is only necessary to develop the equivalent DAB output port from Figure 3.4. Considering again that the voltage in the input side is constant ($\widehat{v}_{in} = 0$), the expected small-signal model of the 3 modules DC/DC converter is the one shown in Figure 4.7.

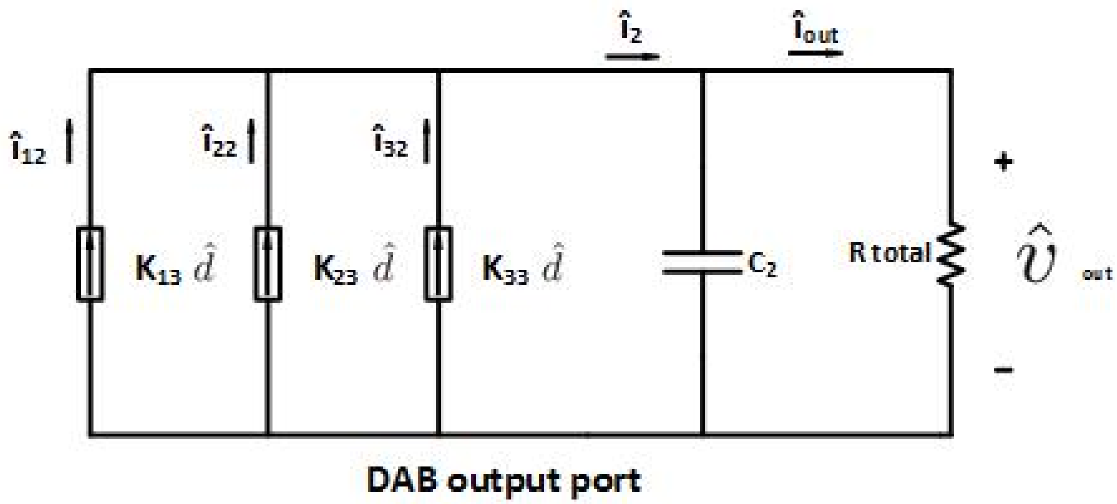

Figure 4.7: Simplified output port of the small-signal circuit model of a 3 modules DAB bidirectional DC/DC converter.

Where the constants K_{13}, K_{23} and K_{33} are:

$$K_{13} = \left.\frac{\partial i_{12}}{\partial d}\right|_{Eq.P} = \frac{(1-2\ |D|)\ n\ V_{in}}{2\ f_s\ L_1} \tag{4.5}$$

$$K_{23} = \left.\frac{\partial i_{22}}{\partial d}\right|_{Eq.P} = \frac{(1-2\ |D|)\ n\ V_{in}}{2\ f_s\ L_2} \tag{4.6}$$

$$K_{33} = \left.\frac{\partial i_{32}}{\partial d}\right|_{Eq.P} = \frac{(1-2\ |D|)\ n\ V_{in}}{2\ f_s\ L_3} \tag{4.7}$$

4.4 Simulink Block

For the Simulink model, the structure from Figure 4.8 was used in this case. There, it can be seen that the input is the phase shift which, trough the pulse generators, produce the pulses for the system. Then, inside the block "system", the configuration from figure 4.4 is implemented, obtaining as outputs the followings: battery voltage, converter output voltage, converter current 1, converter current 2, converter current 3, total battery current and converter output power.

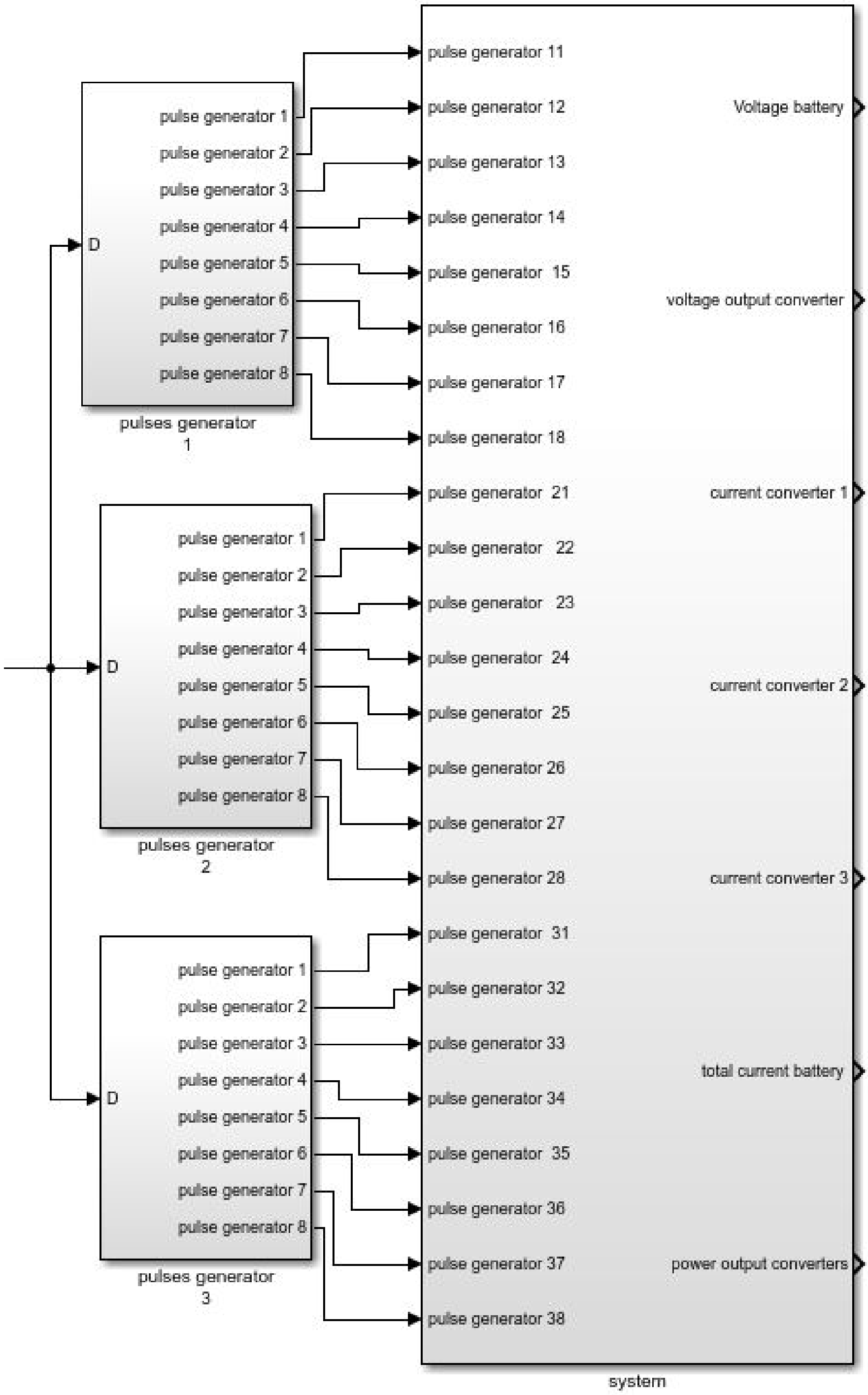

Figure 4.8: Simulink block for the 3 modules DAB DC/DC converter.

4.5 Control methods

In this section the different control methods are presented. First a simple voltage control is developed. Then, the current control method is shown followed, finally, by the cascade control.

The three methods had the same structure, which is the one followed in this report:

1. Development of the transfer function desired.

2. Step response and comparison between real system and transfer function.

3. Closed loop control, PI controller development, analysis of stability and Comparison between formulas, transfer function and real system.

Equilibrium points

In this case, the equilibrium points are different from before.

For the first phase, in the constant current mode, the current is fixed. Since in this phase the voltage is still not a problem, the maximum current can be applied until battery's voltage reaches its upper limit. Therefore, the next equilibrium point was assumed:

1. $i_{bat} = i_{out} = 461.47\,A$

2. $phase\,shift = 58.69°$

3. $V_{initial}\,battery = 650\,V$

4. $Power_{output\,converter} = 307.84\,kW$

This mode can last more or less, depending on the initial SOC of the battery and how far is its voltage away from its nominal value.

However, when the charging mode was switched to constant voltage mode, the next equilibrium point was used:

1. $i_{bat} = i_{out} = 428.82\,A$

2. $phase\,shift = 51.48°$

3. $V_{initial}\,battery = 700\,V$

4. $Power_{output\,converter} = 307.27\,kW$

4.5.1 Voltage control

The first control strategy developed is the voltage control. First, the analog development is presented. Then, the digital implementation of the previous system is shown.

4.5.1.1 Analog development

In this section, the transfer function, step response and close loop control for the voltage control is presented.

4.5.1.1.1 Transfer function

Based on the small signal model from Figure 4.7, the transfer function that relates voltage with phase shift is:

$$G = \frac{\widehat{v}_{out}}{\widehat{d}} = (K_{13} + K_{23} + K_{33}) \, \frac{Rline + Rbattery}{1 + s \, C_2 \, (Rline + Rbattery)}. \tag{4.8}$$

4.5.1.1.2 Step response and comparison

Before doing any control strategy, the previous transfer function is tested to check if the linearized model behaves as the real system does.

For that purpose, the Simulink model from Figure 4.9 was developed, obtaining the results shown in Figure 4.10.

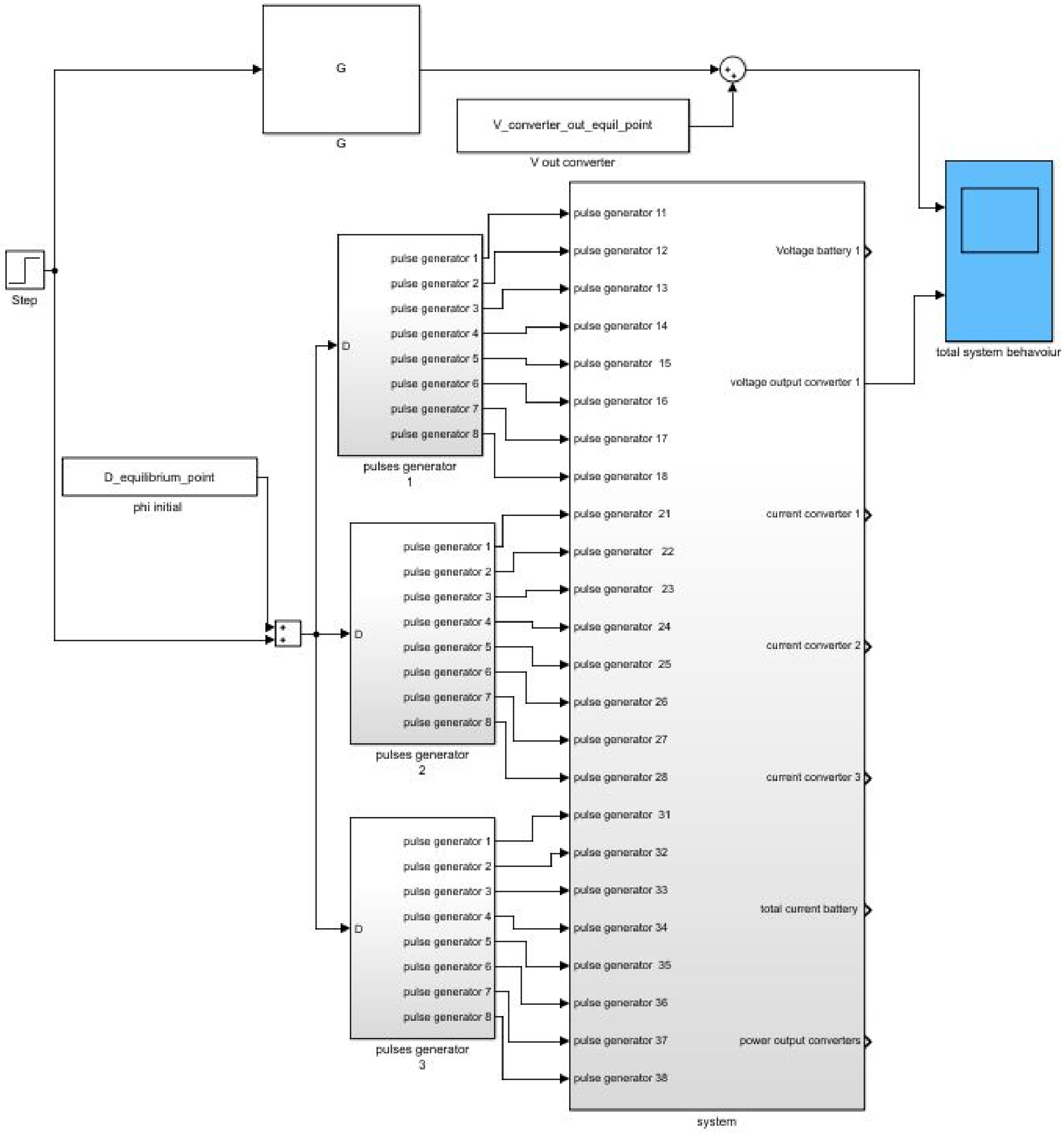

Figure 4.9: Simulink program of the step response for voltage control for a 3 modules DAB bidirectional DC-DC converter.

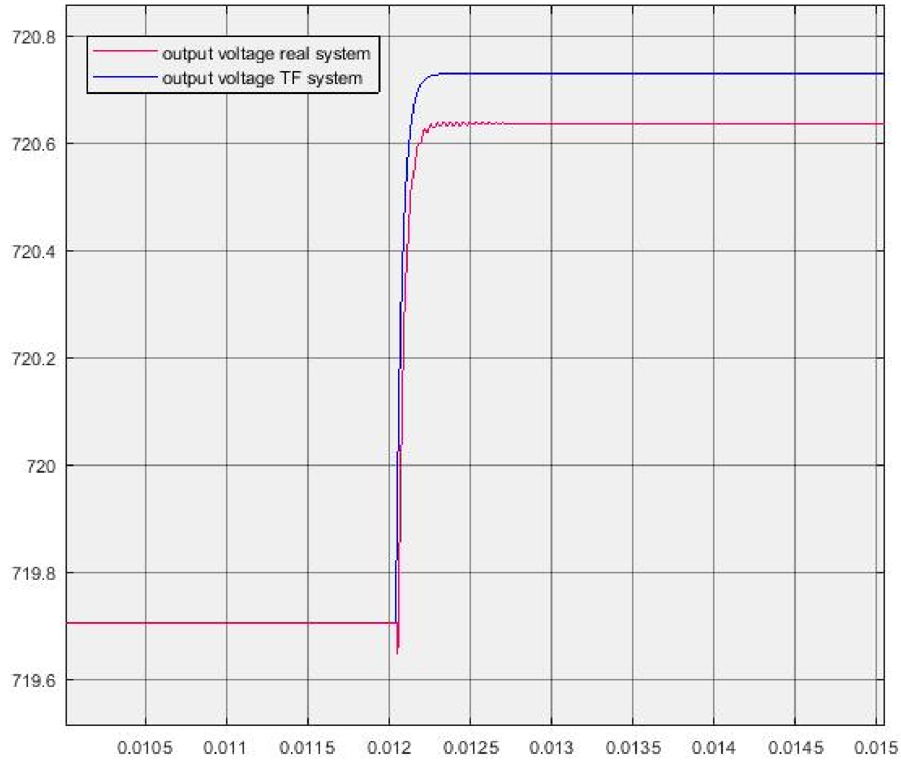

Figure 4.10: Results of the step response for voltage control for a 3 modules DAB bidirectional DC-DC converter.

As it can be observed, both systems behave similar to each other (deviation lower than 10 %). At this point it is important to remember that the real system takes into account the system losses meanwhile the transfer function is based on the lossless model and the assumption of constant voltage in the input. Therefore, the similarity was even better than expected.

Once it was demonstrated that the linearized system was accurate enough, the control system based on the linearized system was developed.

4.5.1.1.3 Closed loop voltage control and comparison

The control strategy followed here is the one used before and shown in Figure 4.11.

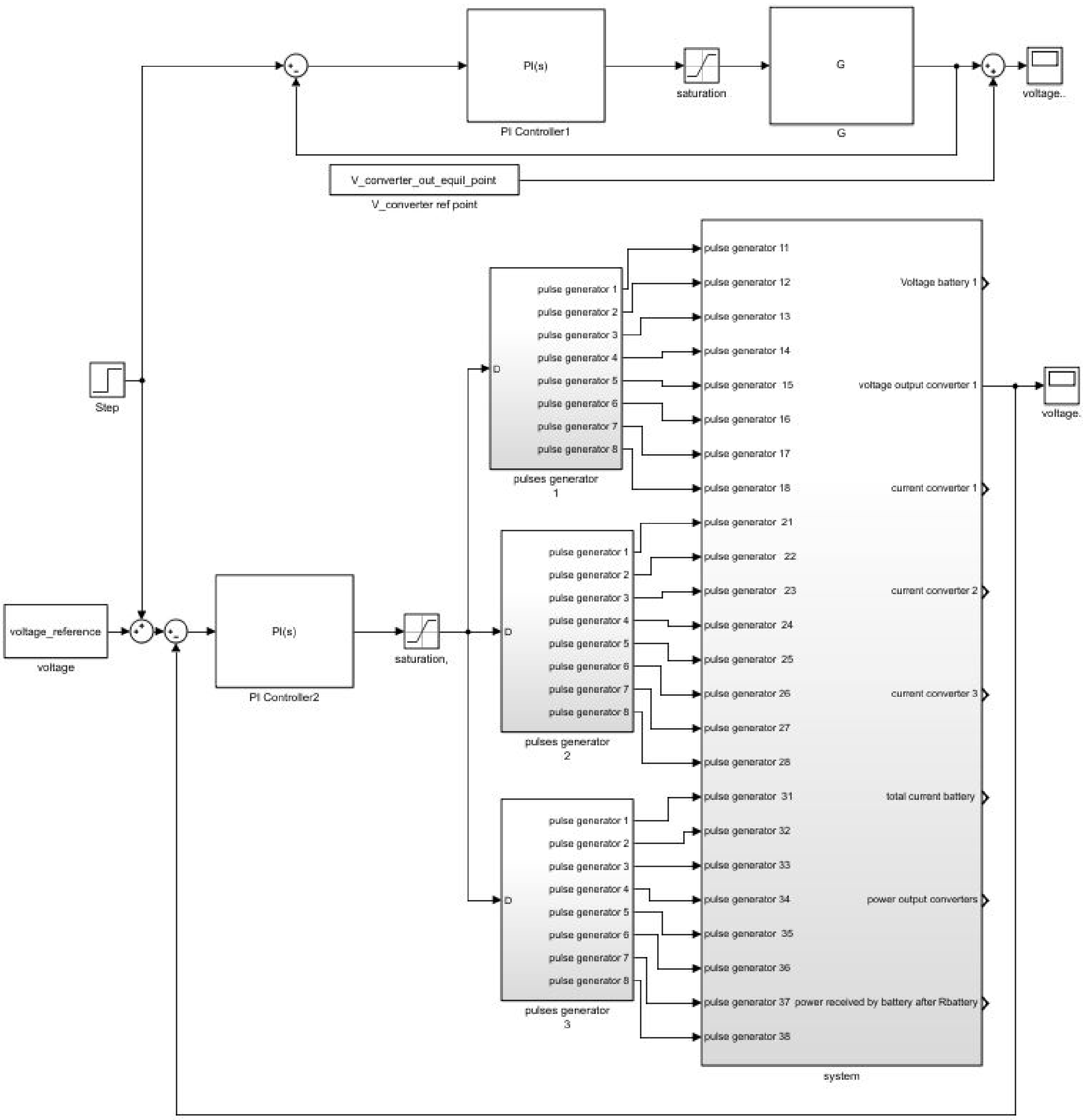

Figure 4.11: Simulink model of the voltage control strategy for a 3 modules converter.

The steps and theory behind how the PI controller was defined are the same as explained in section 3.4.1.

Therefore, the PI parameters obtained are:

1. $K = 0.000687$
2. $w_L = 15780$

Besides, the PI controller is:

$$R(s) = 0.000687 \cdot (1 + 15780 \cdot \frac{1}{s}) \tag{4.9}$$

According to the Phase Margin Theorem, previously discussed to study the stability of the system, and based on equation 3.23 and Figure 4.12, it can be guaranteed that the system was stable since φ_m is 82°, positive.

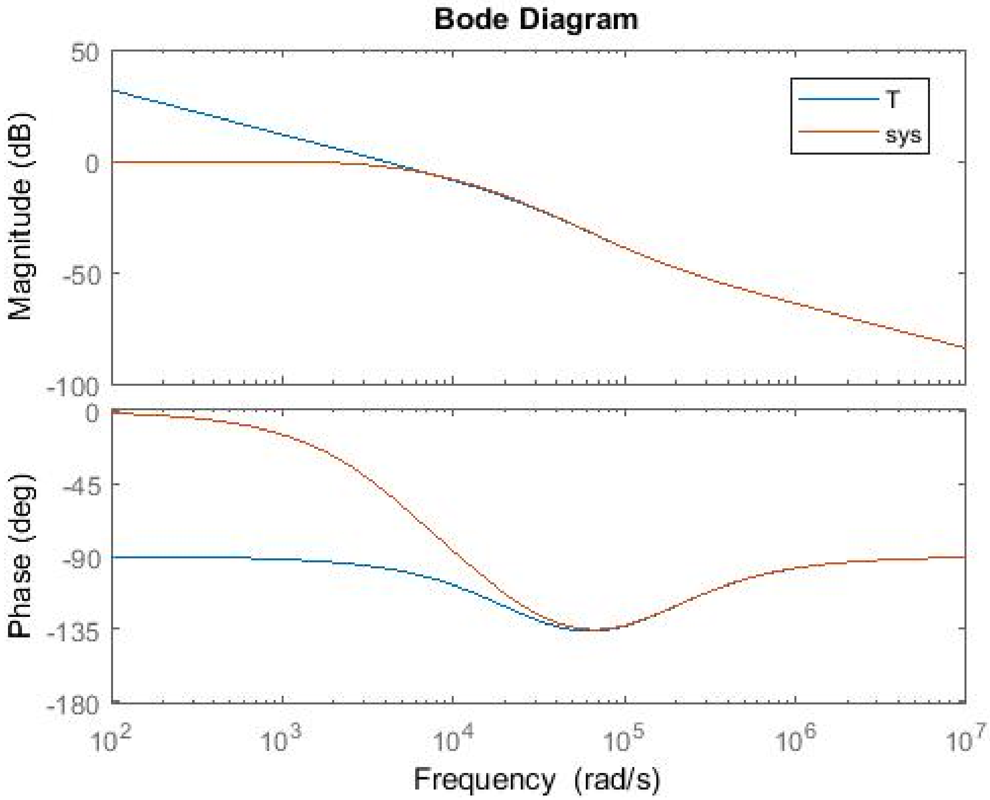

Figure 4.12: Bode diagram of T and total system (sys). Case: 3 modules and current control.

Once it was demonstrated that the system was stable, the controller was configured and the Simulink program from Figure 4.13 was run around the equilibrium point previously defined in this report.

A small disturbance around the equilibrium point was introduced to observe the behaviour of both systems, and this were the results obtained:

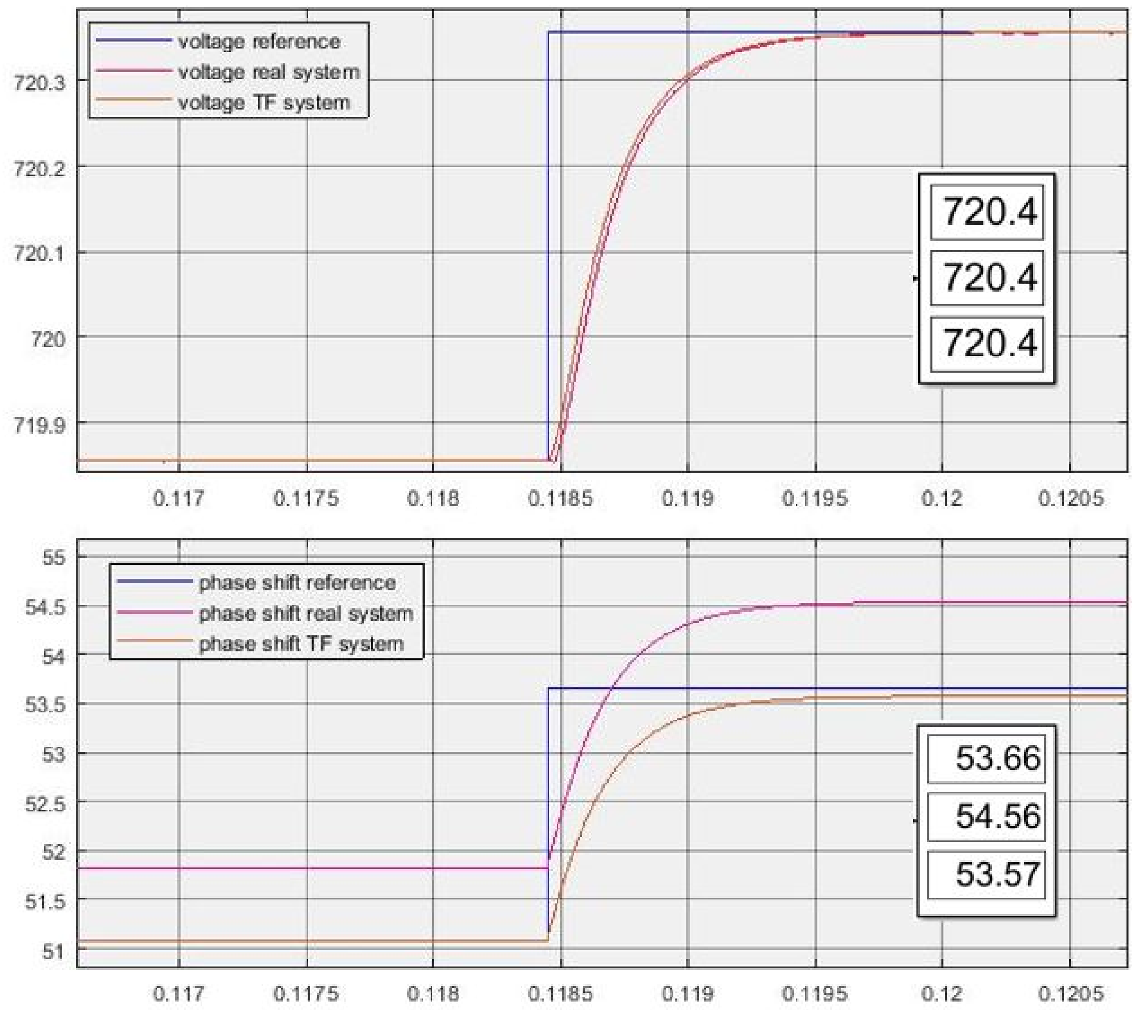

Figure 4.13: Results of the voltage control strategy for a 3 modules DAB bidirectional DC-DC converter.

In Figure 4.13 it is shown, in the first graph, the output voltage and, in the second graph, the phase shift. Blue curves are the references from formulas, red curves the output from the real system and the yellow curves the output from the transfer function system. As it can be seen, both systems followed perfectly the voltage reference, with just slight differences in the phase shift, since the real system has a difference of 1.68% respect to the reference from formulas and the transfer function system a difference of -0.17%. However, again, this differences were expected and it behaves as it has to do: on one hand, the real system, since it considers the looses, it needed a higher phase shift to achieve the same voltage. On the other hand, the transfer function is based on the loosless model, as the formulas do, but also it had the assumption of constant input voltage, and that is why it needed less phase shift to achieve the same voltage.

4.5.1.2 Digital control

Once the analog control is accomplished, the digital control is developed. The same procedure as the one shown in section 3.4.1.2 is followed.

Thus, the structure followed is the one shown in Figure 4.14.

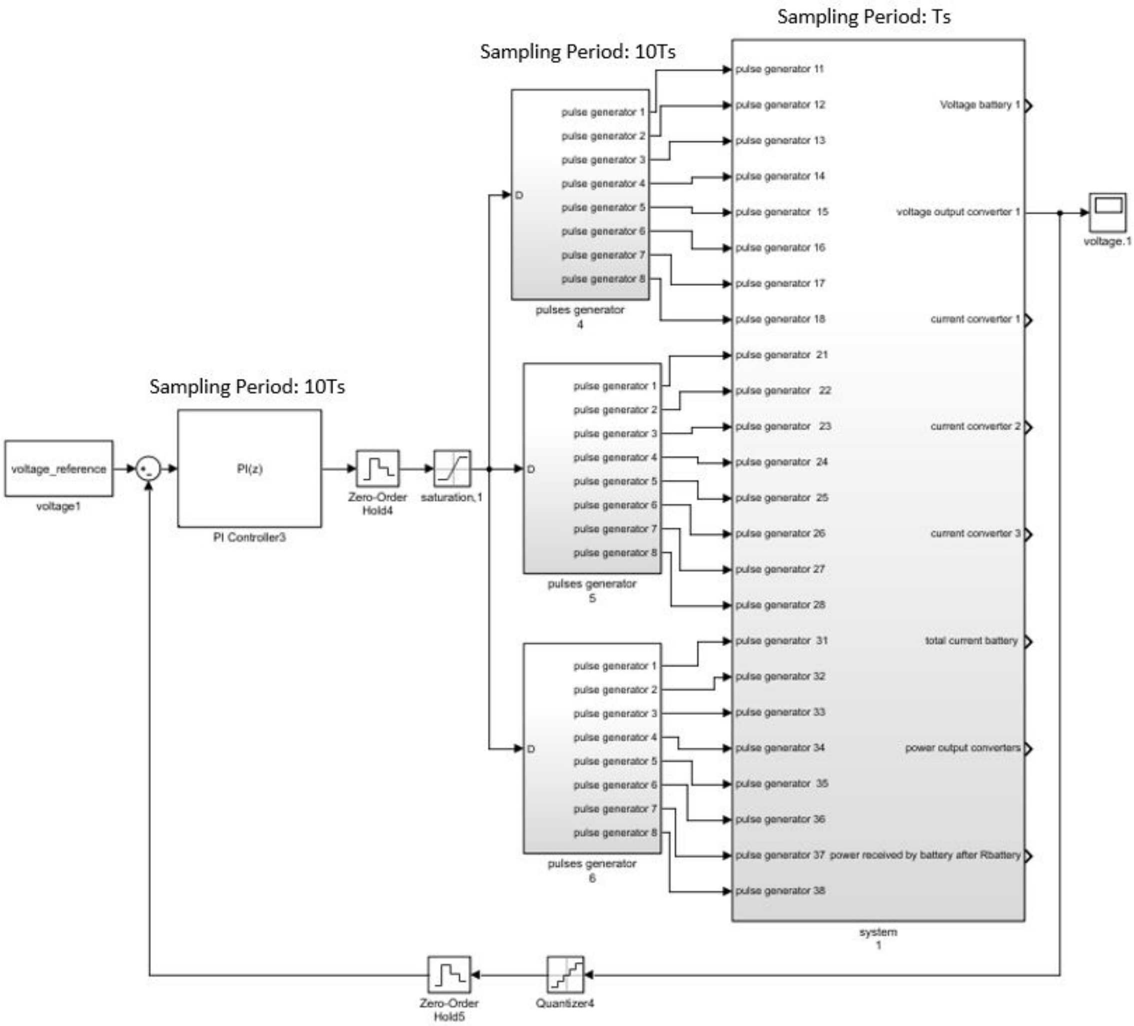

Figure 4.14: Simulink block of the digital voltage control strategy for a 3 modules DAB bidirectional DC-DC converter.

First, the transfer function G(z) was obtained from the one discussed in section 4.5.1.1.1. To guarantee that it behaves as the continuous-time transfer function, the step-response was studied and shown in Figure 4.15.

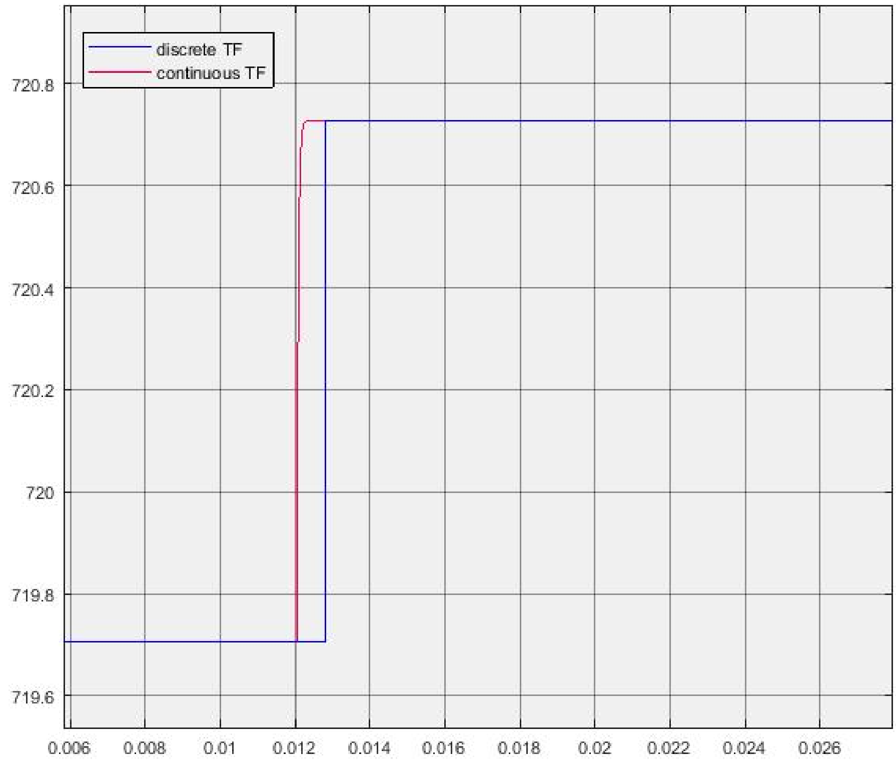

Figure 4.15: Results of the step response for voltage control for a 3 modules DAB bidirectional DC-DC converter. Comparison between G(s) and G(z).

Following the formulas 3.26 and 3.27, the parameters of the PI(z) used this time were:

1. $V_p = 0.000687$
2. $V_i = 21.59$

Thus, the PI(z) is:

$$R(z) = 0.000687 + 21.59\,\frac{1}{z-1} \tag{4.10}$$

All in all, with the structure from Figure 4.14 and the PI(z) controller, the system was tested. For that purpose, a small step disturbance was introduced to observe the systems behaviour. Moreover, it was compared with some other structures, as it is going to be explained. The results are shown in Figure 4.16.

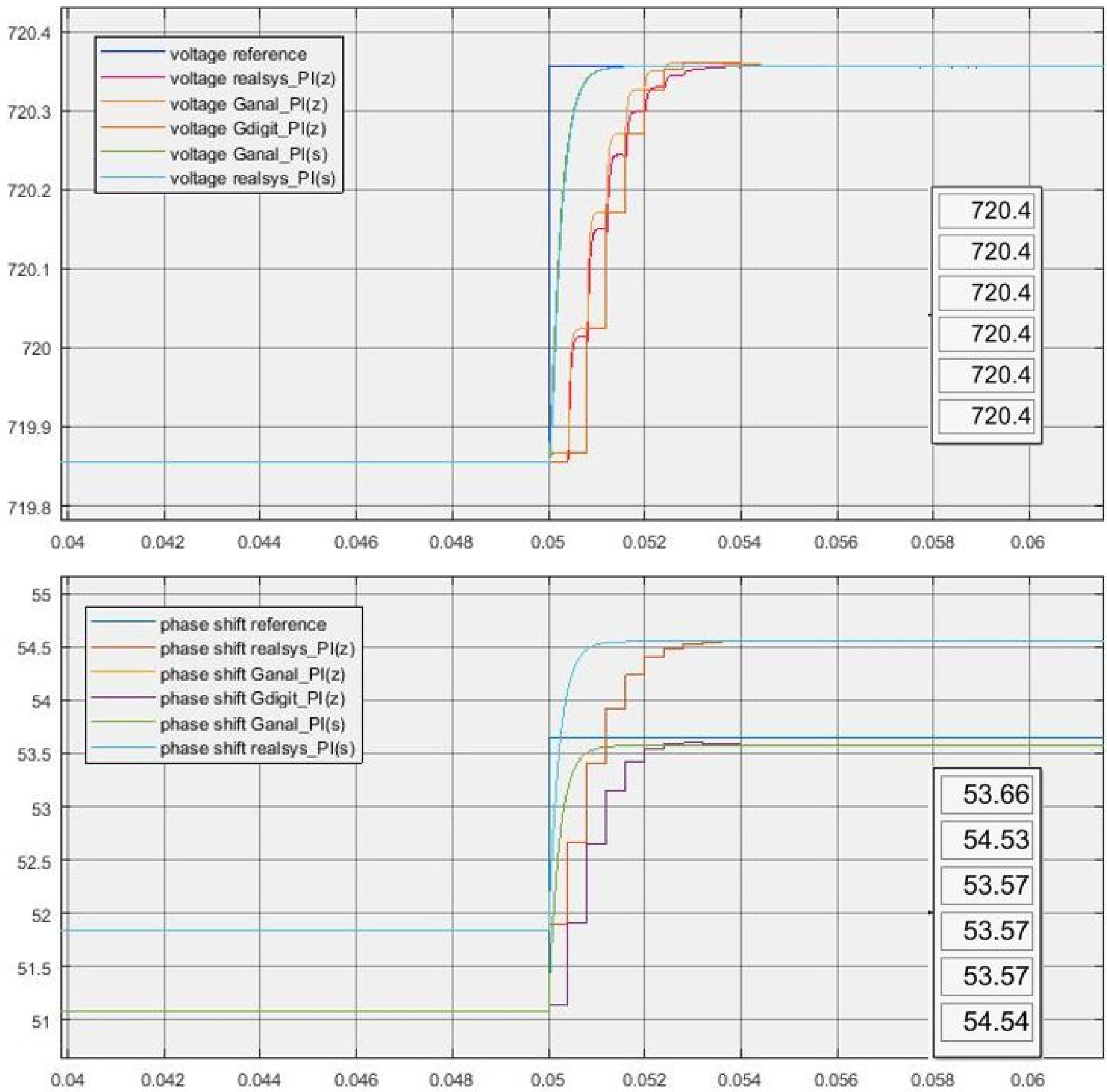

Figure 4.16: Results of the digital voltage control strategy for a 3 modules DAB bidirectional DC-DC converter. First graph is the output voltage and second one the phase shift. Curves, in order, according to the legend: 1. Output converter reference. 2. Output from a real system model controlled with a PI(z). 3. Output from a continuous-time transfer function model controlled with a PI(z). 4. Output from a discrete-dime transfer function model controlled with a PI(z). 5. Output from a continuous-time transfer function model controlled with a PI(s). 6. Output from a real system model controlled with a PI(s).

As it can be seen in Figure 4.16, it is totally coherent. On one hand, all the models controlled with a discrete PI(z), reaches the new steady state at one time. Same happens with the continuous-time PI(s), but with different setting time, related to the controller used. On the other hand, those based on the real system, reach the same phase shift and higher (deviation of 1.68 %) than the one expected from formulas, as explained before. Also, those based on a transfer function system, reach the same phase shift and lower (deviation of -0.17 %) than the expected from formulas, also explained before.

4.5.2 Current control

The next control strategy developed is the current control. First, the analog development is presented. Then, the digital implementation of the previous system is shown.

4.5.2.1 Analog development

In this section, the transfer function, step response and close loop control for the current control is presented.

4.5.2.1.1 Transfer function

Based on the small signal model from Figure 4.7, the transfer function that relates voltage with phase shift is:

$$G = \frac{\widehat{i}_{out}}{\widehat{d}} = (K_{13} + K_{23} + K_{33}) \, \frac{1}{1 + s \, C_2 \, (Rline + Rbattery)}. \tag{4.11}$$

4.5.2.1.2 Step response and comparison

Before doing any control strategy, the previous transfer function is tested to check if the linearized model behaves as the real system does.

For that purpose, the Simulink model from Figure 4.17 was developed, obtaining the results shown in Figure 4.18.

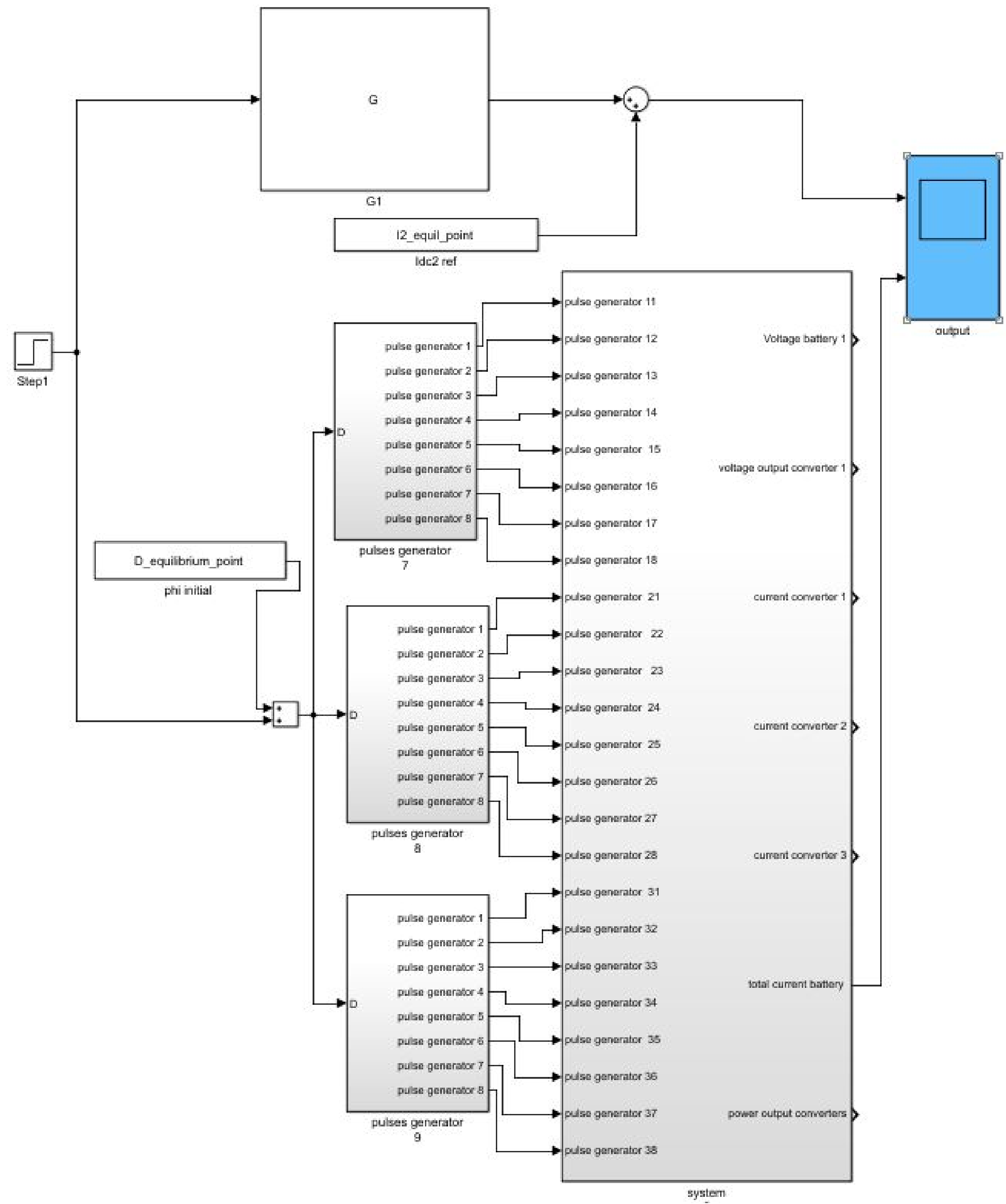

Figure 4.17: Simulink program for the step response for current control for a 3 modules DAB bidirectional DC-DC converter.

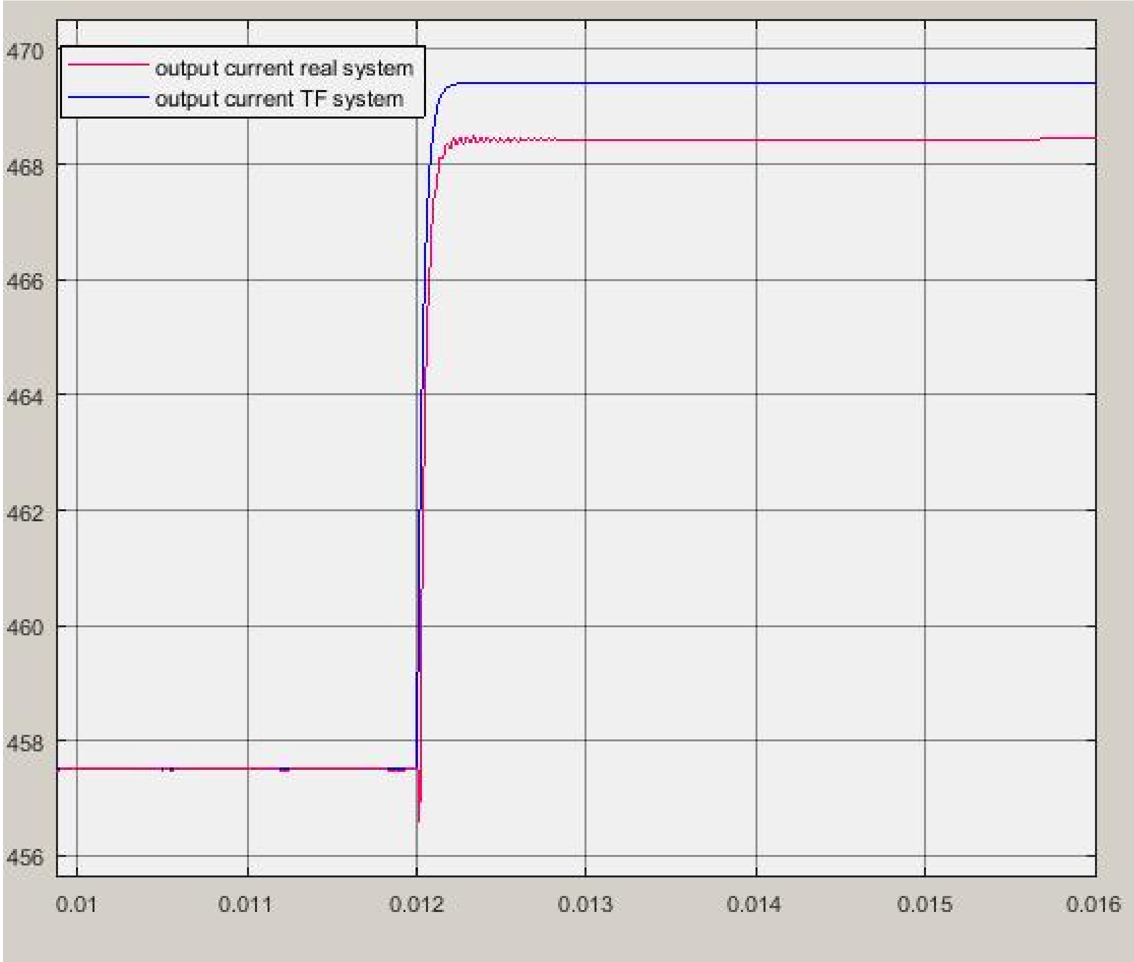

Figure 4.18: Results for the step response for current control for a 3 modules DAB bidirectional DC-DC converter.

As it can be observed, both systems behave similar to each other (deviation of 8.7 %). At this point it is important to remember that the real system takes into account the system losses meanwhile the transfer function is based on the lossless model and the assumption of constant voltage in the input. Therefore, the similarity was even better than expected.

Once it was demonstrated that the linearized system was accurate enough, it was time to develop the control system based on the linearized system.

4.5.2.1.3 Closed loop current control and comparison

The control strategy followed is the one used before and shown in Figure 4.19.

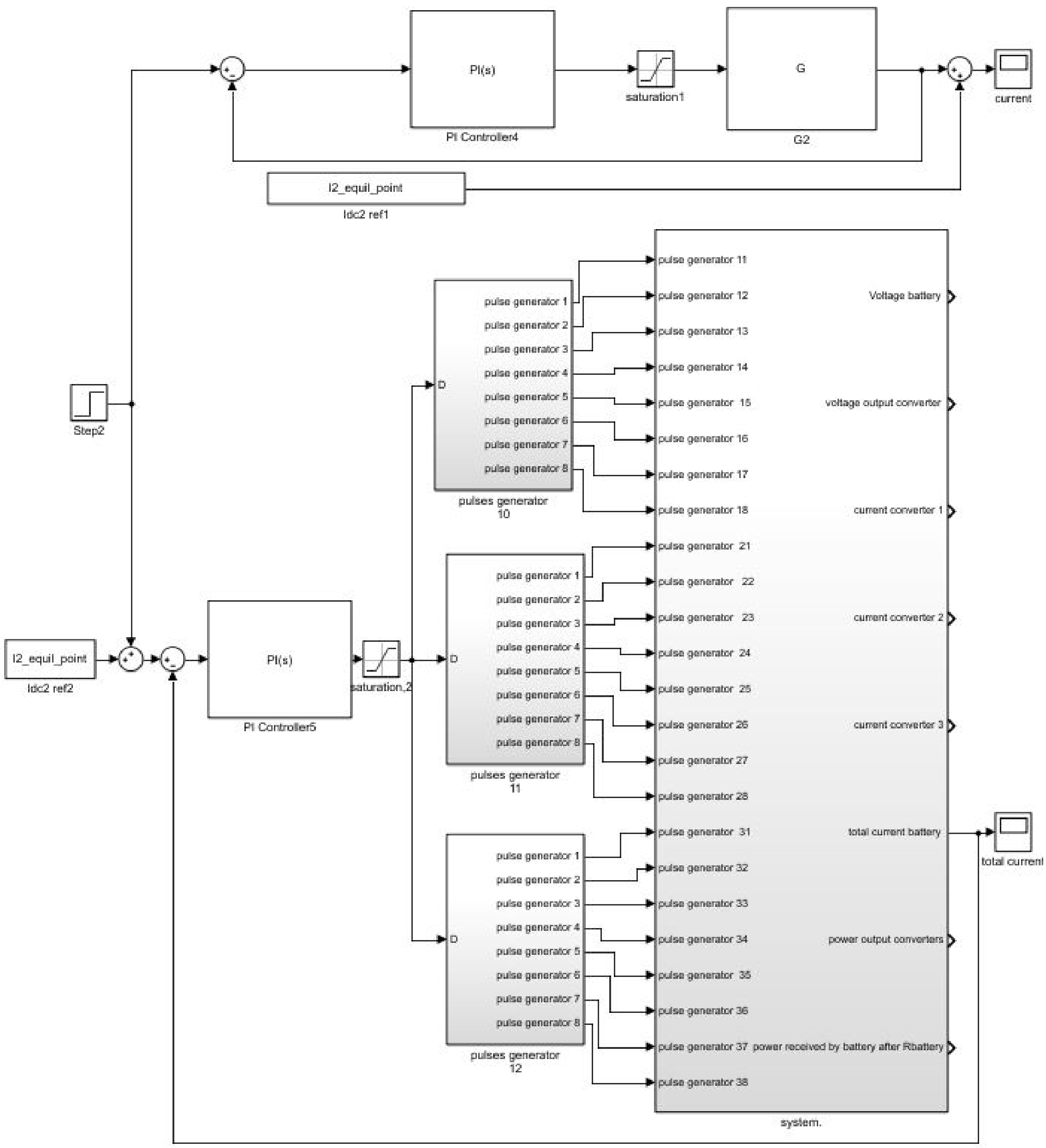

Figure 4.19: Simulink model for the current control strategy for a 3 modules converter.

The steps and theory behind how the PI controller was defined are the same as explained in section 3.4.1.

Therefore, the PI parameters obtained are:

1. $K = 0.0005278$
2. $w_L = 1047.2$

Besides, the PI controller is:

$$R(s) = 0.0005278 \cdot (1 + 1047.2 \cdot \frac{1}{s}) \tag{4.12}$$

According to the Phase Margin Theorem, previously discussed to study the stability of the system, and based on equation 3.23 and Figure 4.20, it can be guaranteed that the system was stable since φ_m is 104°, positive.

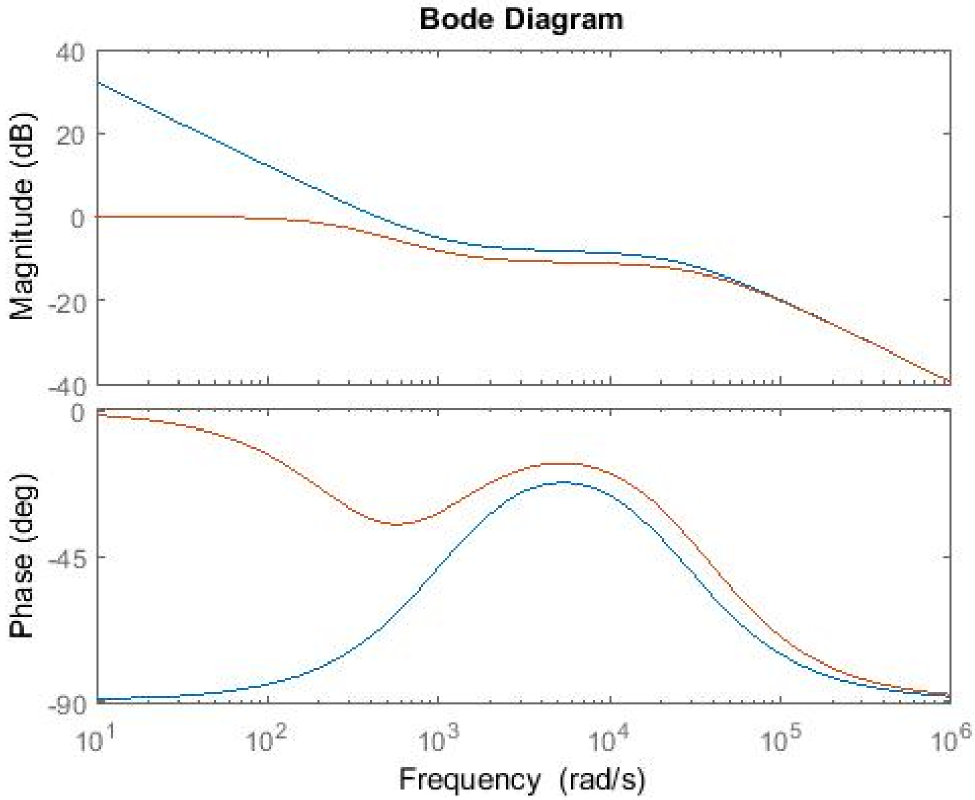

Figure 4.20: Bode diagram of T and total system (sys) for the case of 3 modules and current control.

Once it was demonstrated that the system was stable, the controller was configured and the Simulink program from Figure 4.21 was run around the equilibrium point previously defined in this report.

A small disturbance around the equilibrium point was introduced to observe the behaviour of both systems, and this were the results obtained:

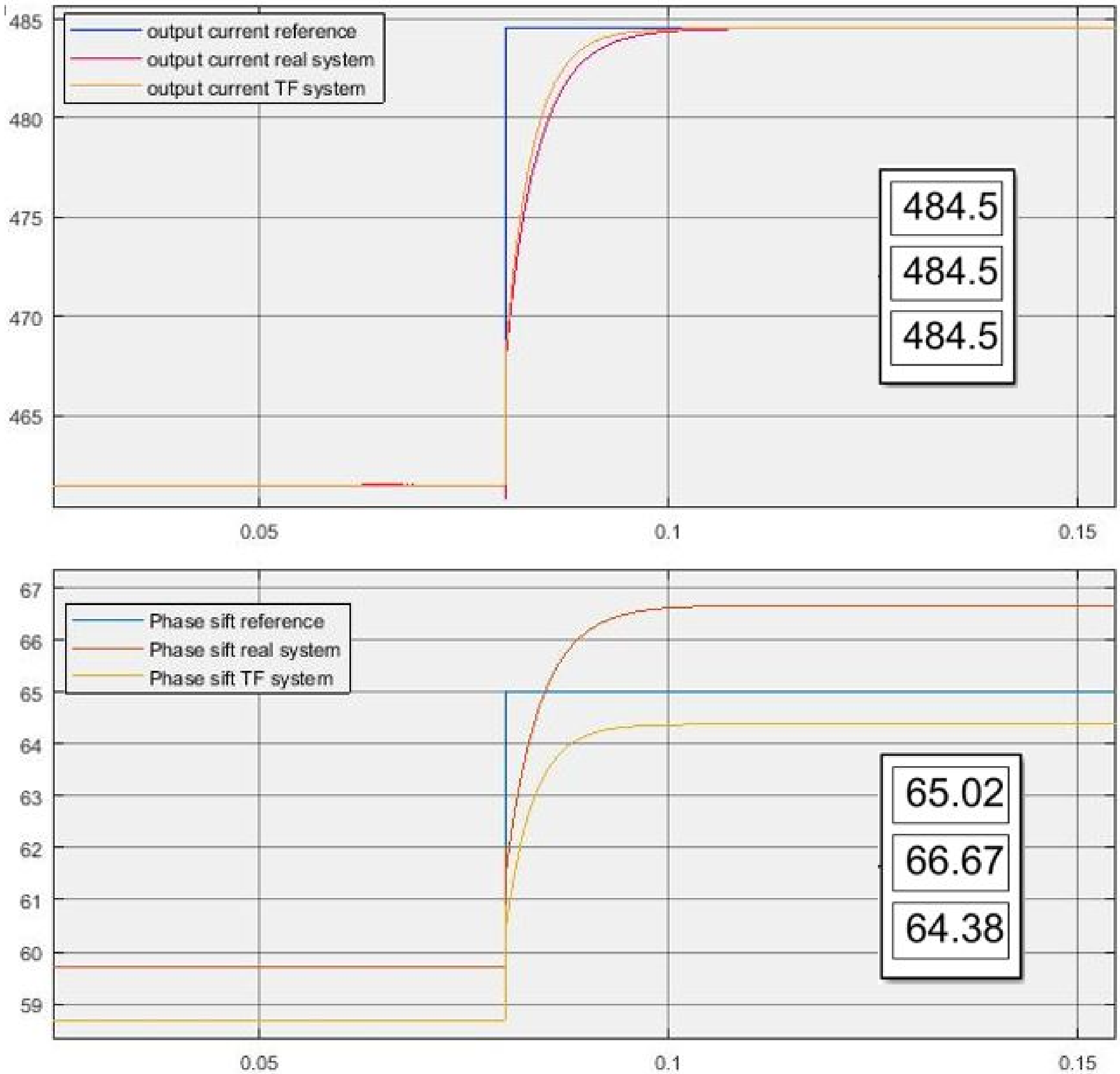

Figure 4.21: Results of the current control strategy for a 3 modules DAB bidirectional DC-DC converter.

In Figure 4.21 it is shown, in the first graph, the output current and, in the second graph, the phase shift. Blue curves are the references from formulas, red curves the output from the real system and the yellow curves the output from the transfer function system. As it can be seen, both systems followed perfectly the current reference, with just slight differences in the phase shift, since the real system has a difference of 2.54% respect to the reference from formulas and the transfer function system a difference of -0.98%. However, again, this differences were expected and it behaves as it has to do: on one hand, the real system, since it considers the looses, it needed a higher phase shift to achieve the same voltage. On the other hand, the transfer function is based on the loosless model, as the formulas do, but also it had the assumption of constant input voltage, and that is why it needed less phase shift to achieve the same voltage.

4.5.2.2 Digital control

Once the analog control is accomplished, the digital control is developed. The same procedure as the one shown in section 3.4.1.2 is followed.

Thus, the structure followed is the one shown in Figure 4.22.

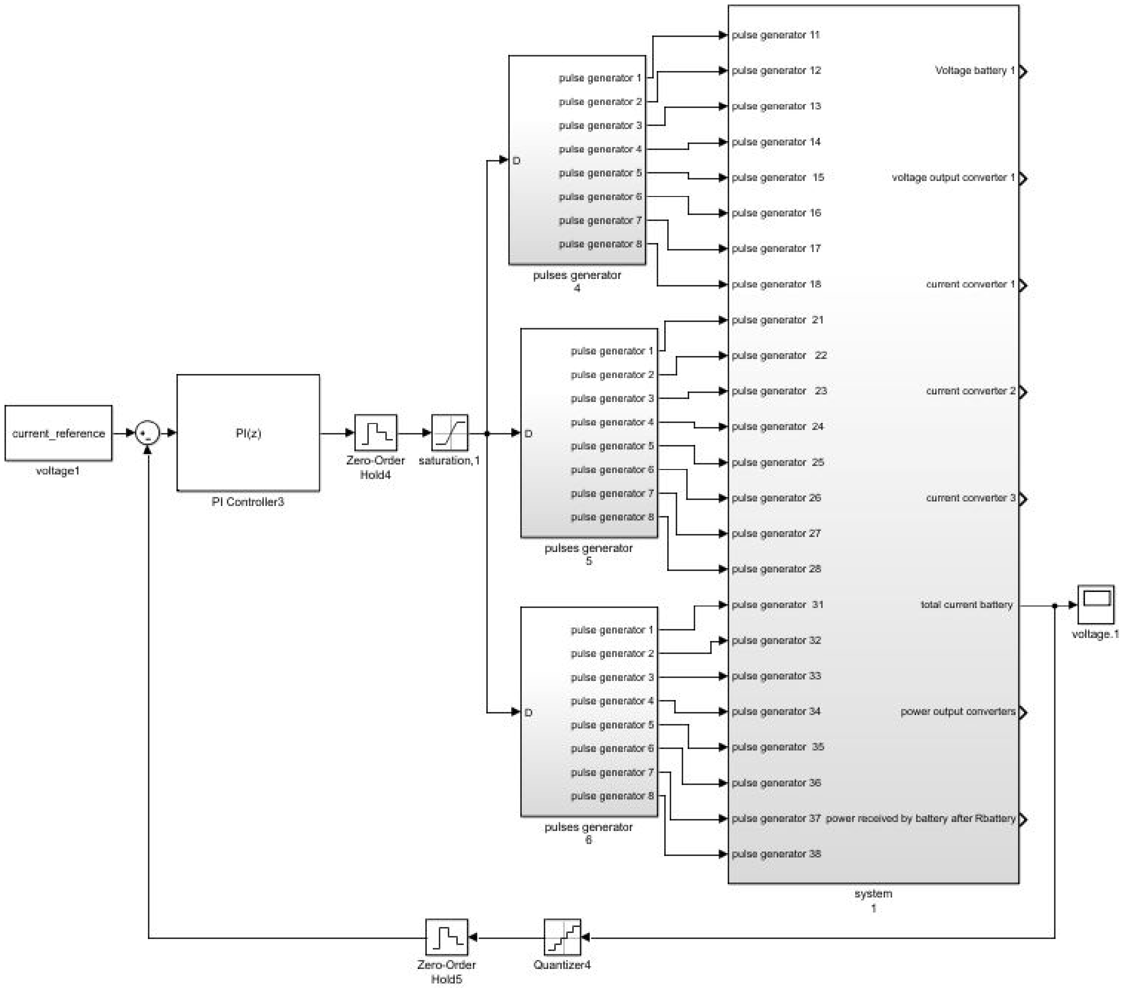

Figure 4.22: Simulink block of the digital current control strategy for a 3 modules DAB bidirectional DC-DC converter.

First, the transfer function G(z) was obtained from the one discussed in section 4.5.2.1.1. To guarantee that it behaves as the continuous-time transfer function, the step-response was studied and shown in Figure 4.23.

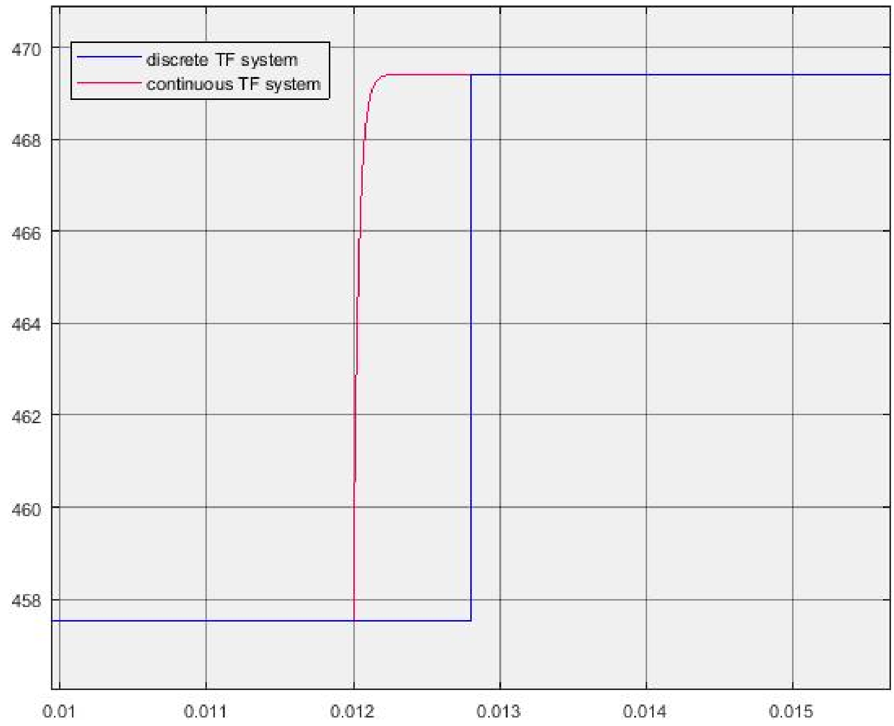

Figure 4.23: Results of the step response for current control for a 3 modules DAB bidirectional DC-DC converter. Comparison between G(s) and G(z).

Following the formulas 3.26 and 3.27, the parameters of the PI(z) used this time were:

1. $V_p = 0.0005278$
2. $V_i = 0.7732$

Thus, the PI(z) is:

$$R(z) = 0.0005278 + 0.7732\,\frac{1}{z-1} \tag{4.13}$$

With the structure from Figure 4.22 and the PI(z) controller, the system was tested. For that purpose, a small step disturbance was introduced to observe the systems behaviour. Moreover, it was compared with some other structures, as it is going to be explained. The results are shown in Figure 4.24.

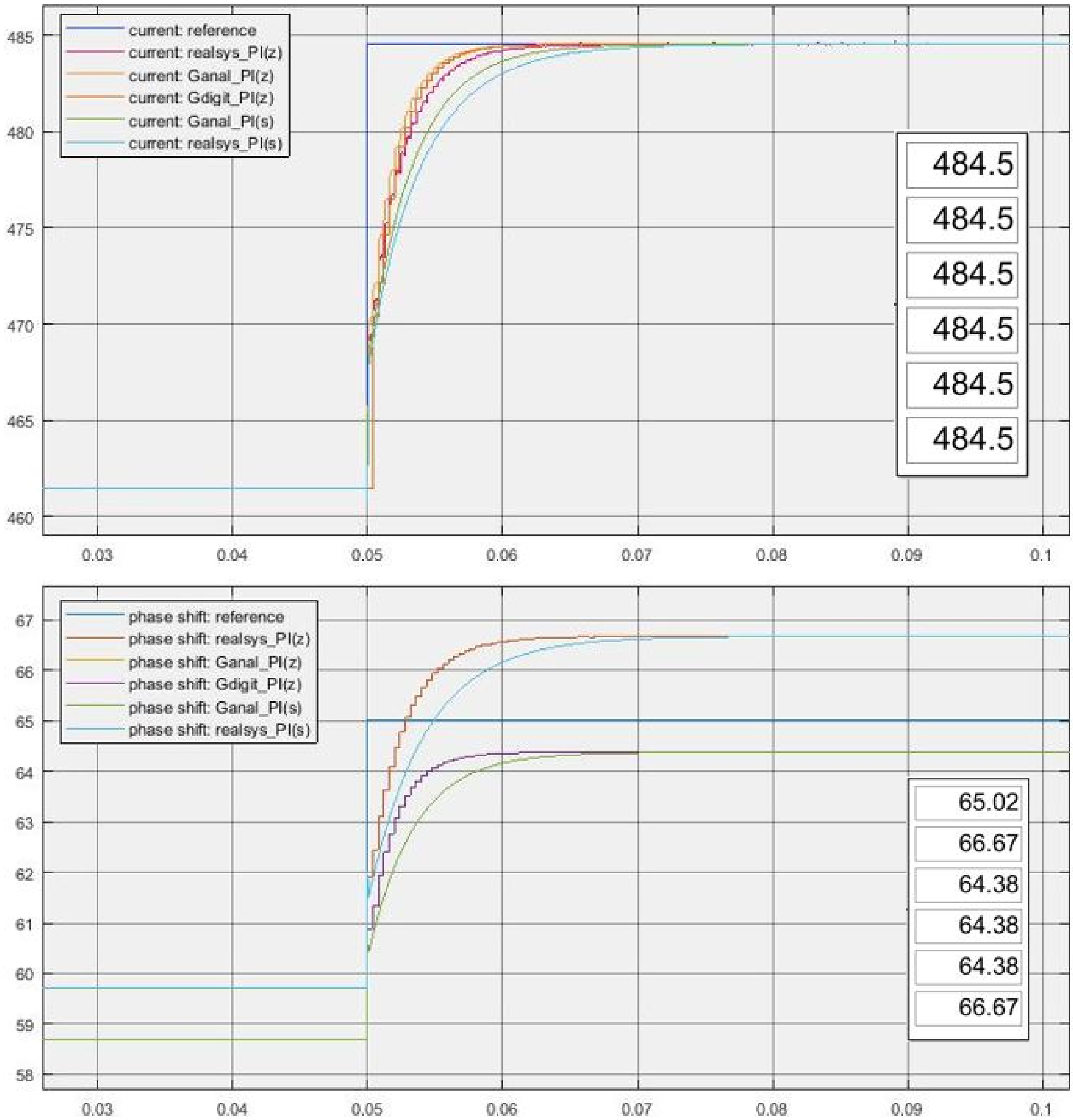

Figure 4.24: Results of the digital current control strategy for a 3 modules DAB bidirectional DC-DC converter. First graph is the output current and second one the phase shift.

In Figure 4.16 the curves are, in order, according to the legend: 1. Output converter reference. 2. Output from a real system model controlled with a PI(z). 3. Output from a continuous-time transfer function model controlled with a PI(z). 4. Output from a discrete-dime transfer function model controlled with a PI(z). 5. Output from a continuous-time transfer function model controlled with a PI(s). 6. Output from a real system model controlled with a PI(s).

As it can be seen in Figure 4.16, it is totally coherent. On one hand, all the models controlled with a discrete PI(z), reaches the new steady state at one time. Same happens with the continuous-time PI(s), but with different setting time, related to the controller used. On the other hand, those based on the real system, reach the same phase shift and higher (deviation of 2.54 %) than the one expected from formulas, as explained before. Also, those based on a transfer function system, reach the same phase shift and lower (deviation of -0.98 %) than the expected from formulas, also explained before.

4.5.3 Cascade control

Finally, the third control strategy developed was the cascade control strategy, corresponding to constant voltage mode.

First, the analog development is presented. Then, the digital implementation of the previous system is shown.

4.5.3.1 Analog development

In this section, the transfer function, tuning phase and close loop control for the current control is presented.

This control system is based on the one shown previously in Figure 3.22, where the master controller controls the output voltage meanwhile the slave controller is in charge of the output current.

4.5.3.1.1 Transfer function

In this special case, first GV(s) and GI(s) are defined:

$$GI = \frac{\widehat{i}_{out}}{\widehat{d}} = \frac{\widehat{i}_{bat}}{\widehat{d}} = (K_{13} + K_{23} + K_{33}) \frac{1}{1 + s\, C_2\, (Rline + Rbattery)} \tag{4.14}$$

$$GV = \frac{\widehat{v}_{out}}{\widehat{i}_{out}} = Rline + Rbattery \tag{4.15}$$

Where GI(s) is the transfer function of the inner loop and GV(s) completes the total system.

The process here is slightly different from before: first, the inner loop had to be tuned and, after that, it was possible to tun the outer loop.

4.5.3.1.2 Tuning phase

Inner loop

The inner loop has the same structure as shown in Figure 3.23. As it was said in section 3.4.3.1.2, the inner loop is the same system as in section 4.5.2 and, therefore, the transfer function represents the real system. However, the equilibrium point here is different since it is in the second phase of the charging strategy. Besides, a different PI controller was defined. In this case, the PI parameters were:

1. $K = 0.000691$
2. $w_L = a = 1570.8$

Thus, the PI controller was:

$$RI(s) = K(1 + a\frac{1}{s}) = 0.000691 \cdot (1 + 1570.8 \cdot \frac{1}{s}) \tag{4.16}$$

According to the Phase Margin Theorem, previously discussed to study the stability of the system, and based on equation 3.23 and Figure 4.25, it can be guaranteed that the system was stable since φ_m is 98°, positive.

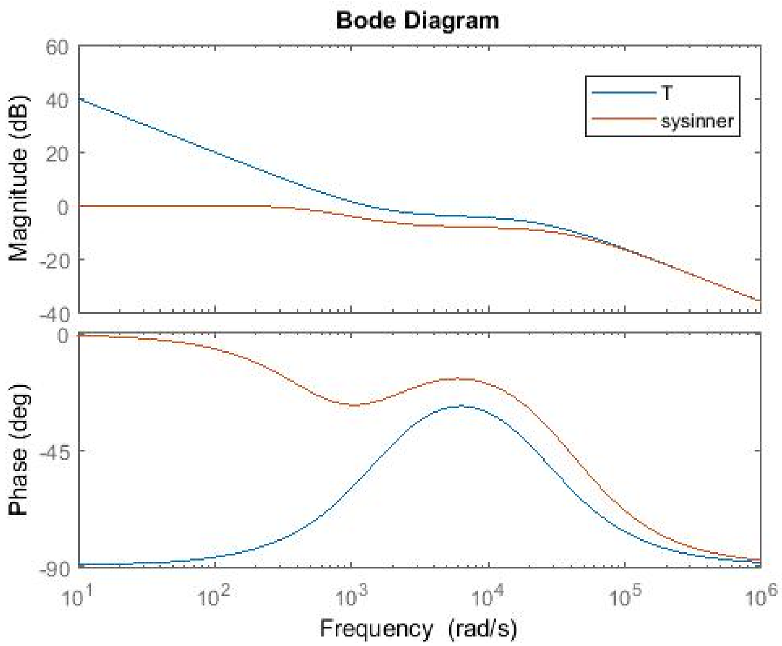

Figure 4.25: Bode diagram of T and total system in the inner loop for the case of 3 modules and cascade control.

Where T and sysinner represents:

$$T(s) = RI(s) \cdot GI(s) \tag{4.17}$$

And, then, the close loop transfer function is:

$$sysinner = \frac{T}{1+T} \tag{4.18}$$

And applying the PI controller to the system from Figure 3.23 it can be seen in Figure 4.26 that the inner loop was correctly tuned.

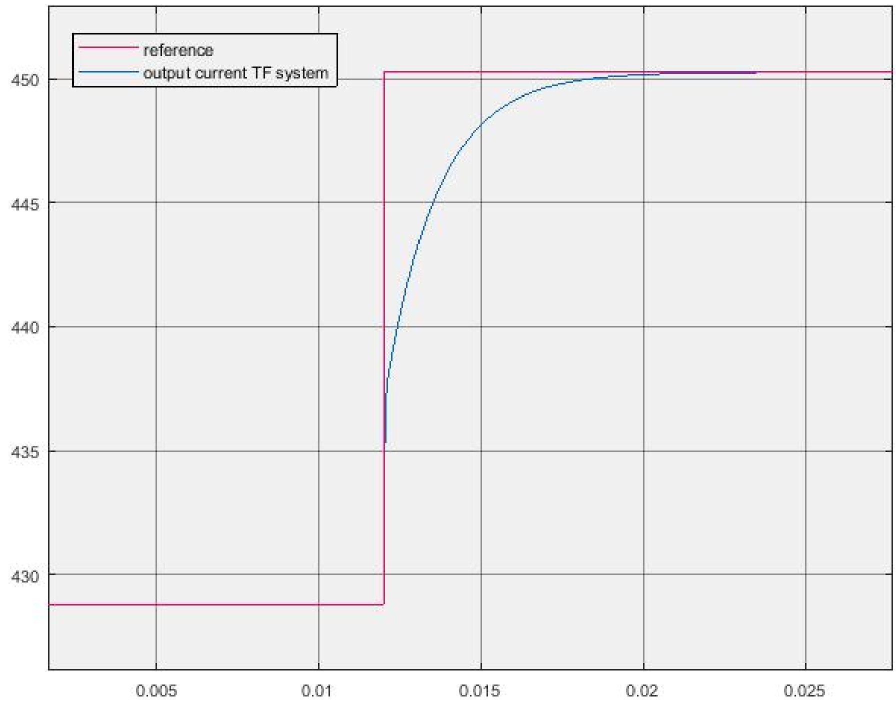

Figure 4.26: Results of the cascade control for a 3 modules DAB bidirectional DC/DC converter. Inner loop design.

Outer loop

The structure followed here is the same as in Figure 3.26.

This time, according to formulas 3.37, 3.38 and 3.39, the transfer function GT(s) is the one that follows:

$$GT(s) = sysinner\ Gv = \\ = (R_{bat} + R_{line})\ (K_{13} + K_{23} + K_{33})\ K \cdot \\ \frac{s + a}{(R_{bat} + R_{line})\ C_2\ s^2 + (1 + (K_{13} + K_{23} + K_{33})\ K)\ s + (K_{13} + K_{23} + K_{33})\ K\ a} \tag{4.19}$$

According to the theory exposed in section 4.1 and the theory development shown in section 3.4.3.1.2, the simplification from equation 3.40 applies in this case as well. Therefore,

$$GT_{simplified}(s) = (R_{bat} + R_{line})\ (K_{13} + K_{23} + K_{33})\ K \cdot \\ \frac{s + a}{(1 + (K_{13} + K_{23} + K_{33})\ K)\ s + (K_{13} + K_{23} + K_{33})\ K\ a}. \tag{4.20}$$

Which is a first order system and the PI controller was easier to design.

Besides, it is important to remember that the simplified GT(s) is still causative since both numerator and denominator's order are the same.

However, it was necessary to check if both systems, GT and $GT_{simplified}$, behaved the same way. The same process was followed as in section 3.4.3.1.2, concluding that both systems are totally equivalent. Therefore, $GT_{simplified}$ accurately represents GT.

Here again, designing the PI controller was easier since the same procedure as before was used. These were the parameters obtained for it:

1. $K = 40.71$
2. $w_L = 398.289$

Besides, the PI controller was:

$$RI(s) = 40.71\ (1 + 398.289\ \frac{1}{s}) \tag{4.21}$$

According to the Phase Margin Theorem, previously discussed to study the stability of the system, and based on equation 3.23 and Figure 4.27, it can be guaranteed that the system was stable since φ_m is 106°, positive.

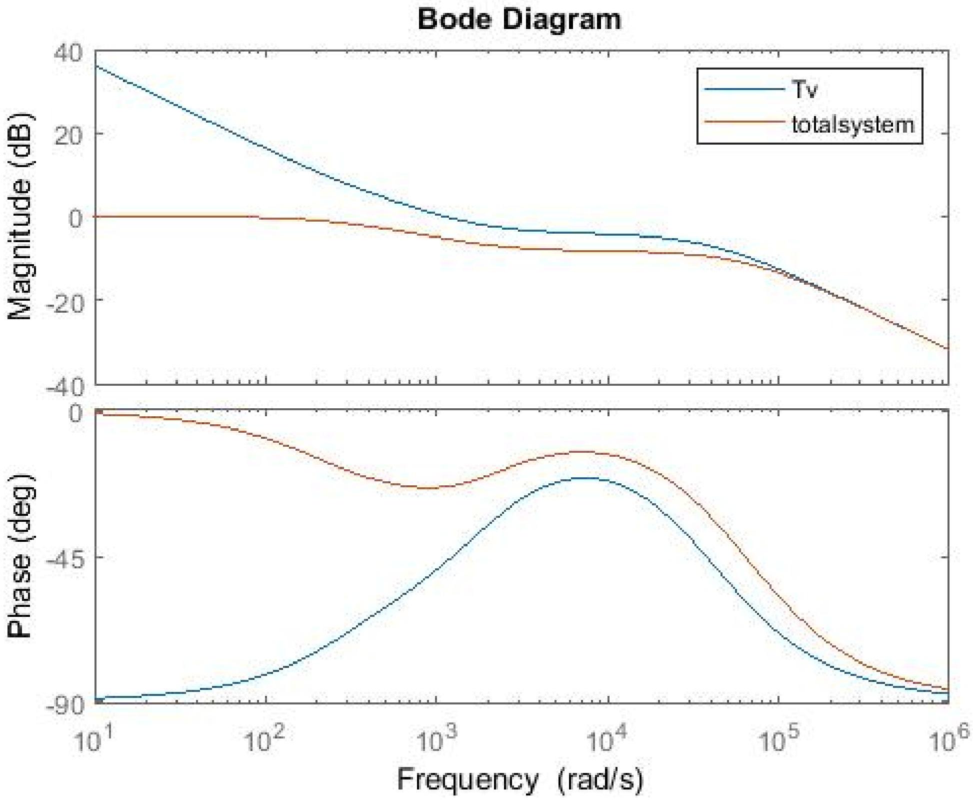

Figure 4.27: Bode diagram of T and total system in the outer loop for the case of one module and cascade control.

Once all the PI controllers were tuned, the transfer function system was tested. However, its behaviour is going to be shown together with the real system in the next section.

4.5.3.1.3 Closed loop cascade control and comparison

The systems were tested in Simulink, as it is shown in Figure 4.28.

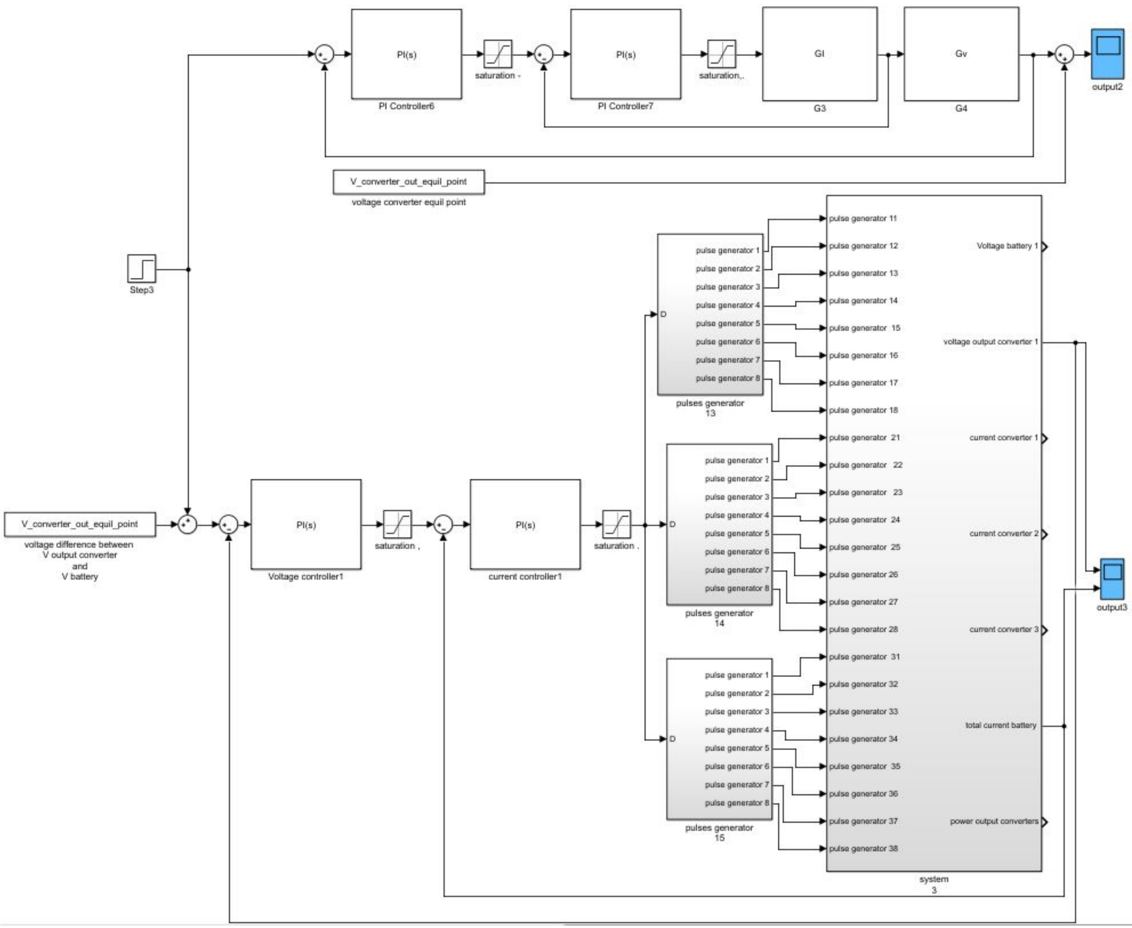

Figure 4.28: Simulink block for a 3 modules DAB DC-DC converter of the cascade control.

Here the real transfer function GT was used.

This time, all the PI controllers and its stability was studied in the previous section. Consequently, the Simulink program from Figure 4.28 was run around the equilibrium point from the second phase of the charging strategy. This time, both current and voltage were controlled.

A small disturbance around the equilibrium point was introduced to observe the behaviour of both systems, obtaining the next results:

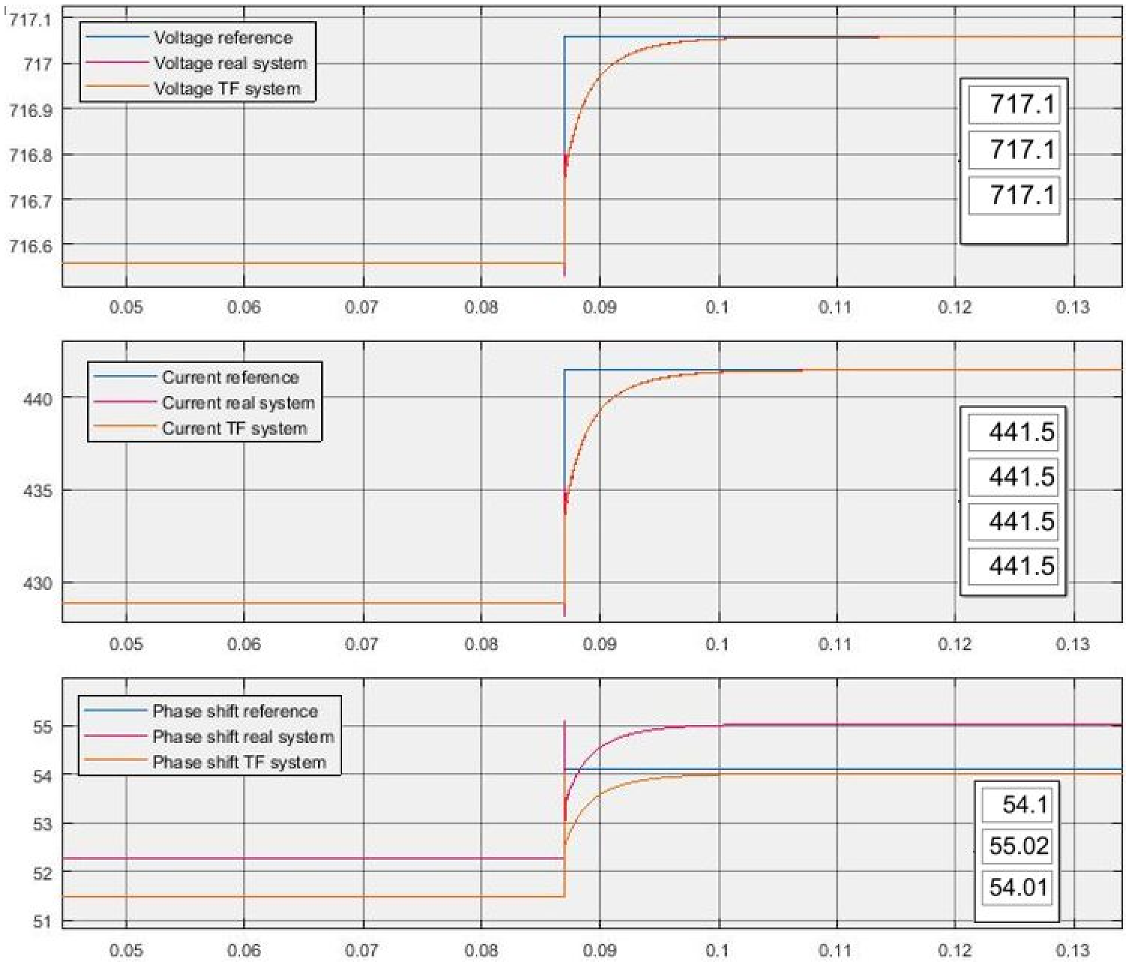

Figure 4.29: Simulink results for a 3 modules DAB DC-DC converter of the cascade control. First graph is the output voltage, second one the current output and third one the phase shifts. Blue curves are the references, red curves the output from the real system and yellow ones the output from the transfer function system.

In Figure 4.29, it can be seen that both systems followed perfectly the voltage and current references, with just slight differences in the phase shift, since the real system had a difference of 1.7 % respect to the reference from formulas and the transfer function system a difference of -0.17 %. However, again, this differences were expected and it behaved as it had to do: on one hand, the real system, since it considers the looses, it needed a higher phase shift to achieve the same power. On the other hand, the transfer function is based on the loosless model, as the formulas do, but also it had the assumption of constant input voltage, and that is why it needed less phase shift to achieve the same current.

4.5.3.2 Digital control

After developing the analog control, the digital control is developed. Similar procedure as before is followed.

First, the structure used this time is the one shown in Figure 4.30.

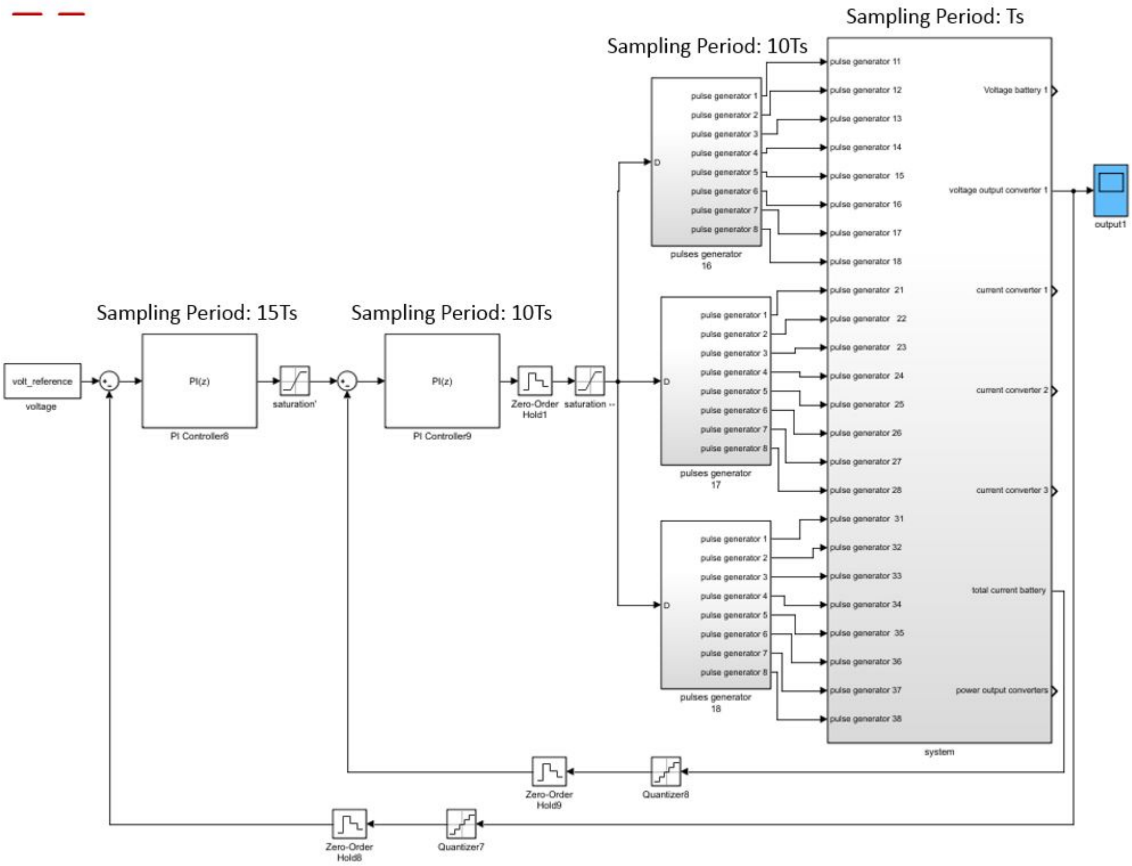

Figure 4.30: Simulink block of the digital cascade control strategy for a 3 modules DAB bidirectional DC-DC converter.

As it was explained in the previous section, first, the inner loop is tuned and, after it, the outer loop is studied and its PI(z) tuned. Finally, the whole system is analyzed.

Inner loop

The structure of the inner loop is the same as in Figure 3.33.

The step response is not needed in this case since it is the same transfer function as in section 4.5.2.2. However, the equilibrium point is different since the aim is the constant voltage mode. Besides, the PI(z) controller for the inner loop, based on formulas 3.26 and 3.27, is this time:

1. $V_p = 0.000197$

2. $V_i = 0.434$

Thus, the PI(z) is:

$$R(z) = 0.000197 + 0.434\,\frac{1}{z-1} \tag{4.22}$$

Besides, the output from this inner loop is shown in Figure 4.31.

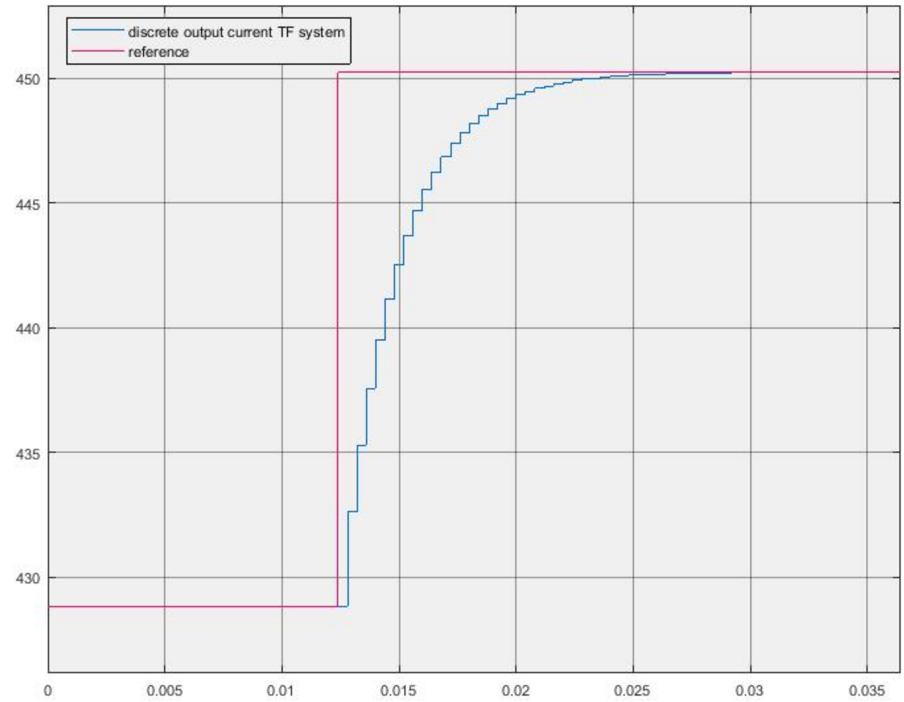

Figure 4.31: Results of the cascade control in the discrete mode for a 3 modules DAB bidirectional DC-DC converter. Inner loop design.

Where it can be seen that the output current follows perfectly the reference.

Outer loop

The structure of the outer loop is the same as the one shown in Figure 3.35.

In this case, the GT(z) is the discrete-time transfer function obtained from GT(s) from formula 4.19.

The step response cannot be implemented since there is no reference from the real system of GT because it includes not only the transfer function from the system but also the PI controller from the inner loop and the inner loop itself.

Therefore, going straight forward to the PI(z) design, based on formulas 3.26 and 3.27, the PI(z) controller is:

1. $V_p = 40.71$
2. $V_i = 12930$

Thus, the PI(z) is:

$$R(z) = 40.71 + 12930\,\frac{1}{z-1}. \tag{4.23}$$

Besides, the output from this outer loop is shown in Figure 4.32.

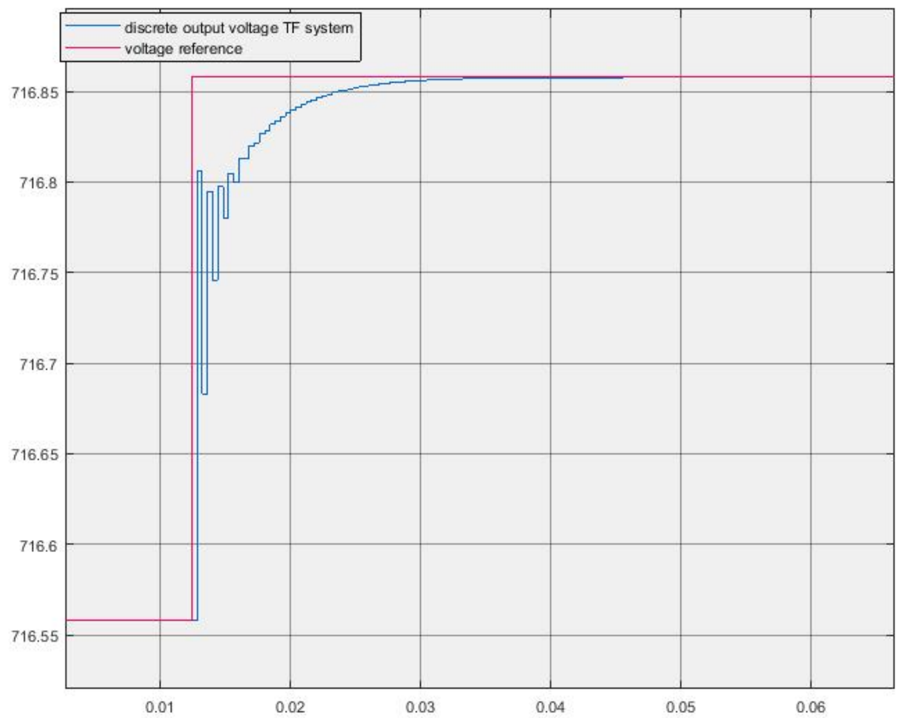

Figure 4.32: Results of the cascade control in the discrete mode for a 3 modules DAB bidirectional DC-DC converter. Outer loop design.

Where it can be seen that the output voltage follows perfectly the reference.

Total system

Finally, the whole system was studied.

Considering the structure from Figure 4.30 and the PI(z) controllers from 4.22 and 4.23, the system was tested. For that purpose, a small step disturbance was introduced to observe the systems behaviour. Moreover, again, it was compared with some other structures, as it is going to be explained. The results are shown in Figure 4.33.

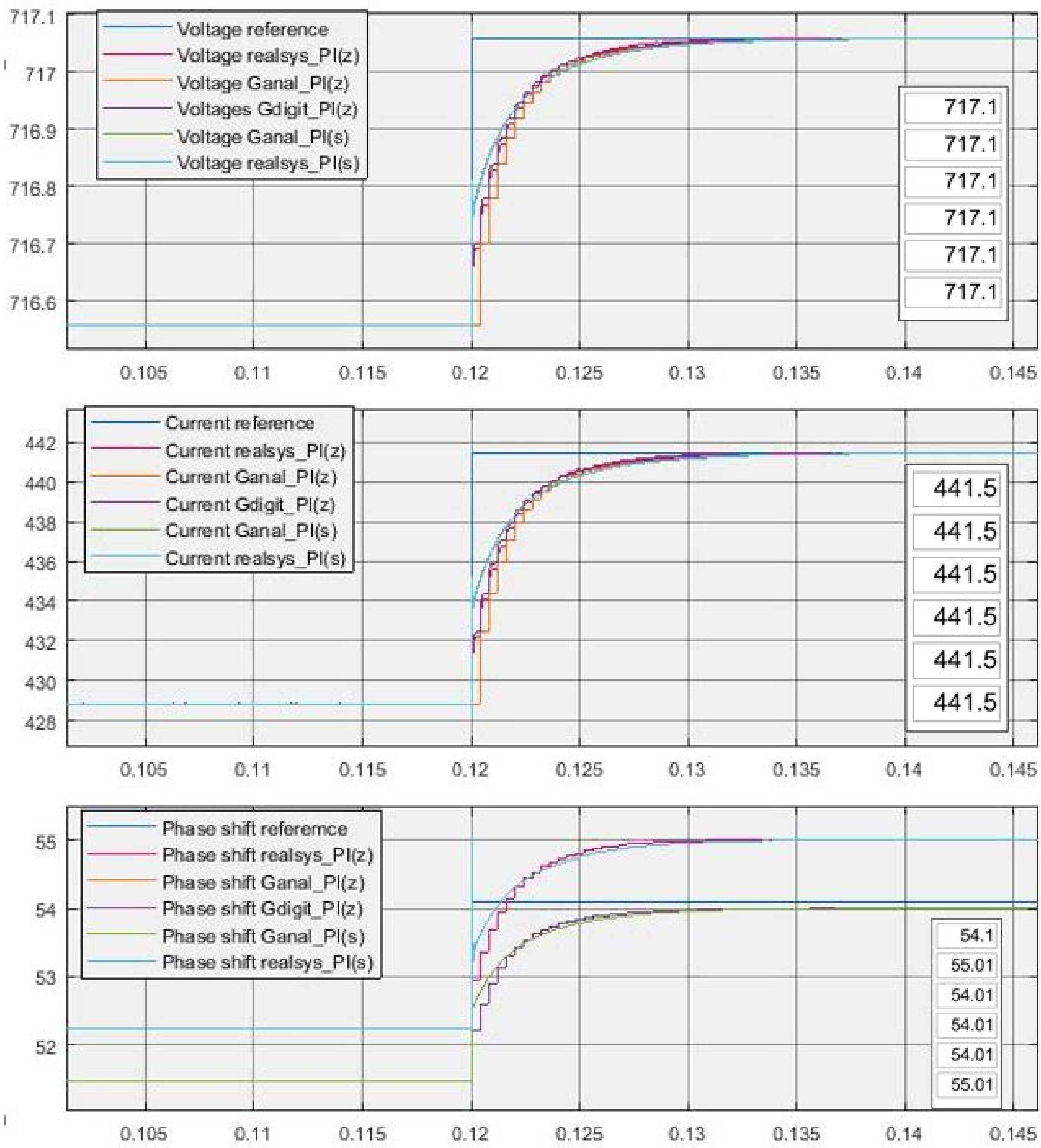

Figure 4.33: Results of the digital cascade control strategy for a 3 modules DAB bidirectional DC-DC converter.

First graph is the output voltage, second one is the output current and the third one the phase shift. Curves in order, according to the legend: 1. Output converter reference. 2. Output from a real system model controlled with a PI(z). 3. Output from a continuous-time transfer function model controlled with a PI(z). 4. Output from a discrete-dime transfer function model controlled with a PI(z). 5. Output from a continuous-time transfer function model controlled with a PI(s). 6. Output from a real system model controlled with a PI(s).

As it can be seen in Figure 4.33, it is totally coherence. On one hand, all the models controlled with a discrete PI(z), reaches the new steady state at the same time. Same happens with the continuous-time PI(s), related to the controller used. On the other hand, those based on the real system, reach the same phase shift and higher (deviation of 1.7 %) than the one expected from formulas, as explained before. Also, those based on a transfer function system, reach the same phase shift and lower (deviation of -0.17 %) than the expected from formulas, also explained before.

5

Results

In this chapter, the results from the previous chapter are presented. A digital control of the converter has been developed in this thesis. Now, the results from that control system are shown.

First, results from a one module DC/DC converter are presented and, after that, the results from a 3 modules DC/DC converter are shown.

5.1 Digital control of a one module converter

The first remarkable result is the small signal model of the one module DC/DC converter, shown in Figure 5.1.

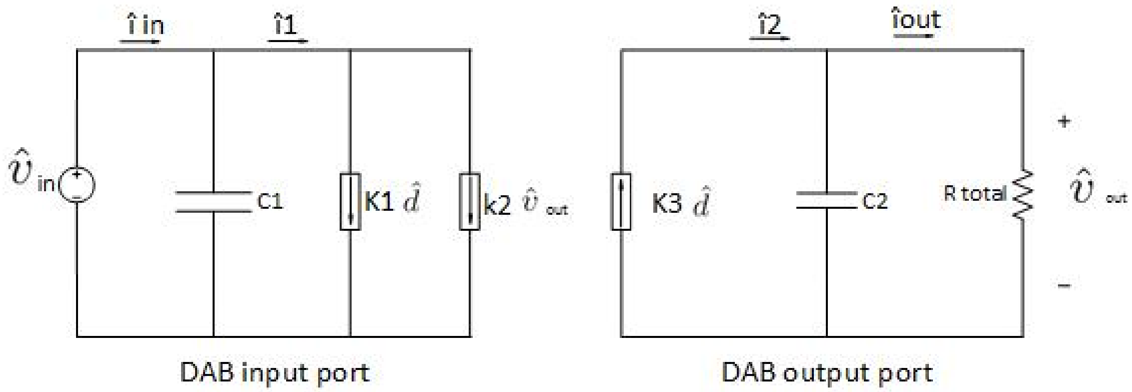

Figure 5.1: Simplified small-signal circuit model of a DAB bidirectional DC/DC converter.

Based on that circuit, the control system is developed. The control system developed had two phases: a constant current mode and a constant voltage mode.

5.1.1 Constant current mode with current control.

The control loop followed is the one shown in Figure 5.2.

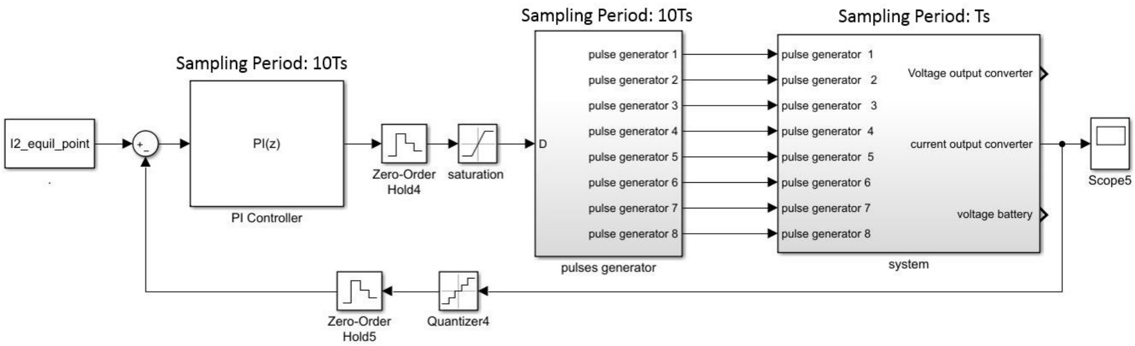

Figure 5.2: Simulink block of the digital current control strategy for a one module DAB bidirectional DC-DC converter.

Based on it, the results obtained for the constant current mode are shown in Figure 5.3. A small disturbance was introduced to observe how the control system behaves.

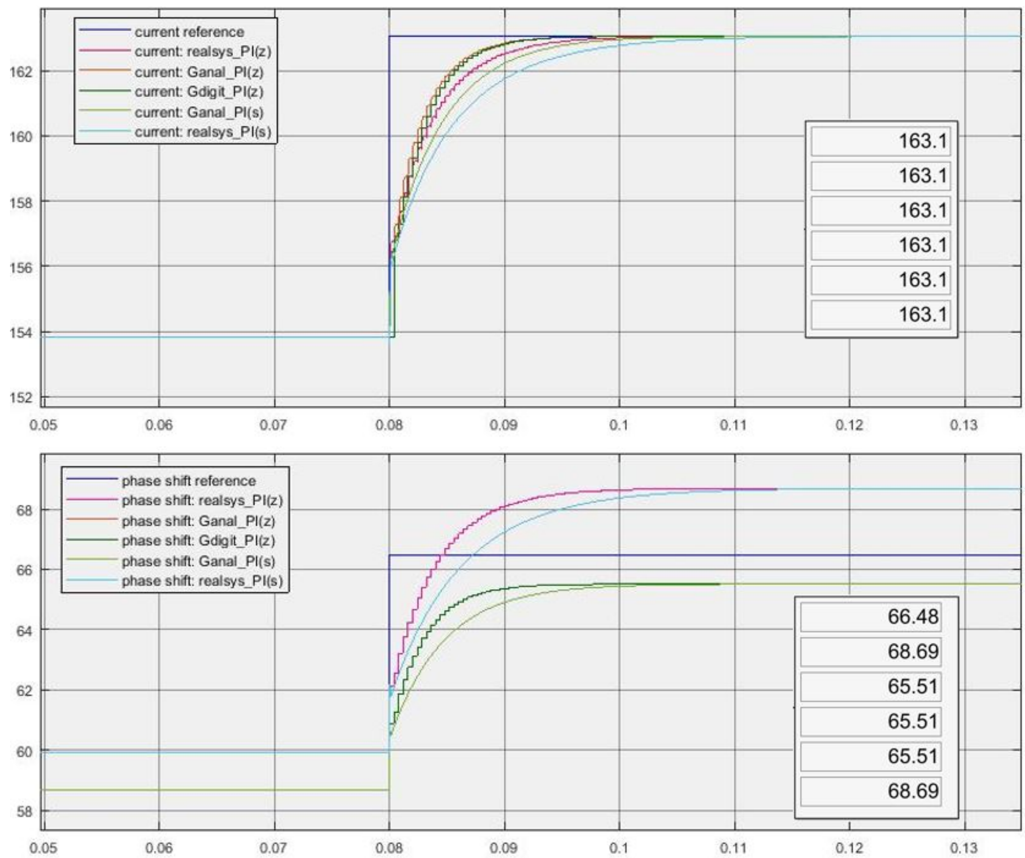

Figure 5.3: Results of the digital current control strategy for a one module DAB bidirectional DC-DC converter.

In Figure 5.3 the first graph is the output current and the second one the phase shift. The curves are in order, according to the legend: 1. Output converter reference. 2. Output from a real system model controlled with a PI(z). 3. Output from a continuous-time transfer function model controlled with a PI(z). 4. Output from a discrete-dime transfer function model controlled with a PI(z). 5. Output from a continuous-time transfer function model controlled with a PI(s). 6. Output from a real system model controlled with a PI(s).

As it can be seen in Figure 5.3, the results are totally coherent. On one hand, all the models controlled with a discrete PI(z), reaches the new steady state at the same time. Same happens with the continuous-time PI(s), but with different setting time, related to the controller used. On the other hand, those based on the real system, reach the same phase shift and higher (deviation of 2.98 %) than the one expected from formulas. Also, those based on a transfer function system, reach the same phase shift and lower (deviation of -0.98 %) than the expected from formulas. However, this difference were expected and it behaves as it had to do: on one hand, the real system, since it considers the looses, it needed a higher phase shift to achieve the same power. On the other hand, the transfer function is based on the loosless model, as the formulas do, but also it had the assumption of constant input voltage, and that is why it needed less phase shift to achieve the same voltage.

5.1.2 Constant voltage mode with cascade control.

The control loop followed is the one shown in Figure 5.4.

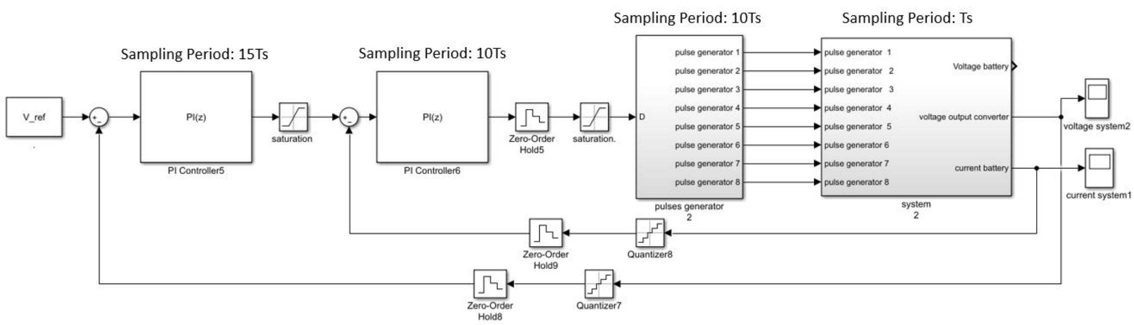

Figure 5.4: Simulink block of the digital cascade control strategy for a one module DAB bidirectional DC-DC converter.

Based on it, the results obtained for the constant voltage mode are shown in Figure 5.5. A small disturbance was introduced to observe how the control system behaves.

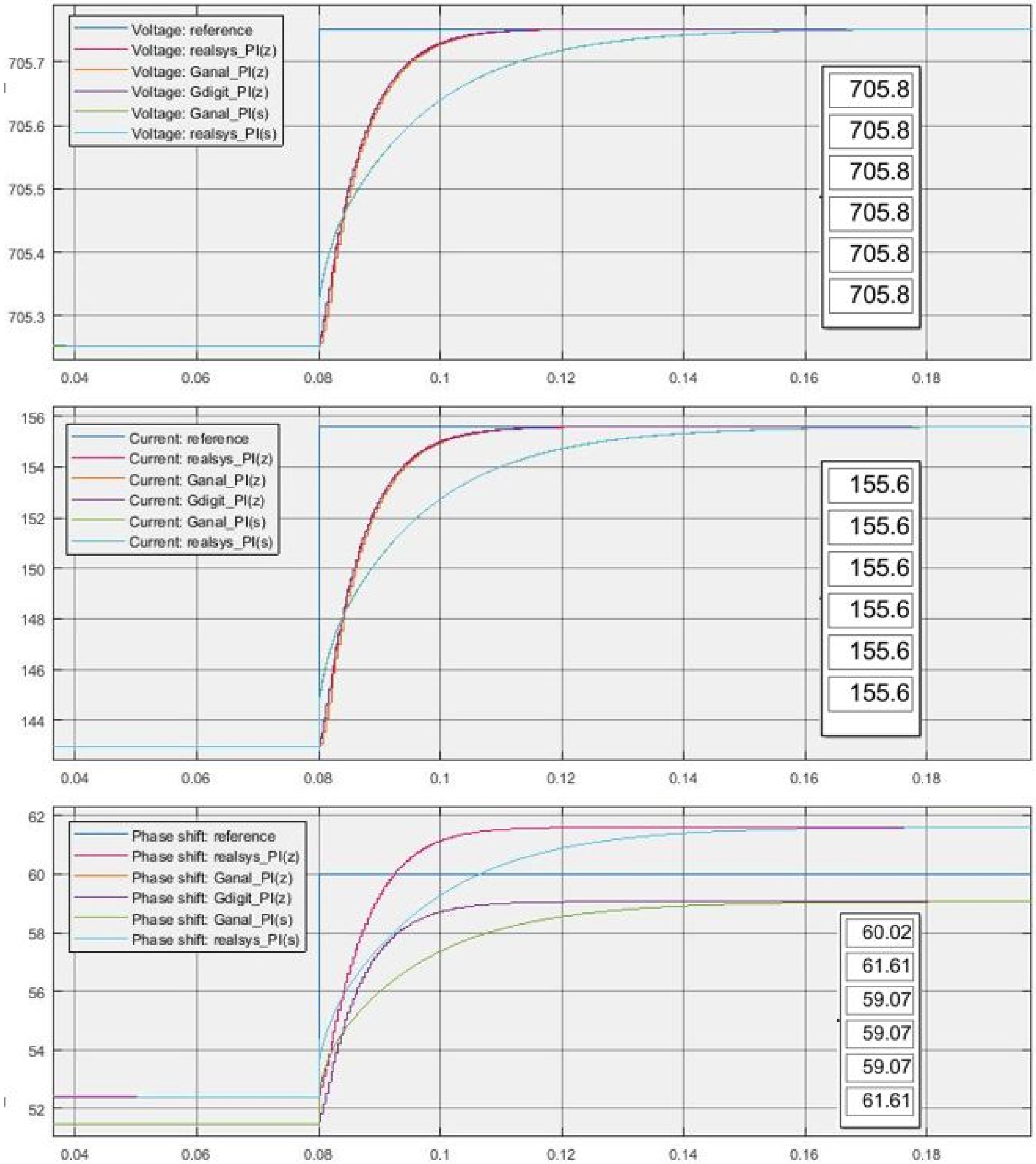

Figure 5.5: Results of the digital cascade control strategy for a one module DAB bidirectional DC-DC converter.

In Figure 5.5, first graph is the output voltage, second one is the output current and the third one the phase shift. The curves are, in order, according to the legend: 1. Output converter reference. 2. Output from a real system model controlled with a PI(z). 3. Output from a continuous-time transfer function model controlled with a PI(z). 4. Output from a discrete-dime transfer function model controlled with a PI(z). 5. Output from a continuous-time transfer function model controlled with a PI(s). 6. Output from a real system model controlled with a PI(s).

As it can be seen in Figure 5.5, it is totally coherent. On one hand, all the models controlled with a discrete PI(z), reaches the new steady state at the same time. Same happens with the continuous-time PI(s), but with different setting time, related to the controller used. On the other hand, those based on the real system, reach the same phase shift and higher (deviation of 2.65 %) than the one expected from formulas, as explained before. Also, those based on a transfer function system, reach the same phase shift and lower (deviation of -1.58 %) than the expected from formulas, also explained before.

5.2 Digital control of a 3 modules converter

The first important result in the section is the parallel configuration finally chosen, which is the input-parallel output-parallel (IPOP) configuration, as it can be seen in Figure 5.6.

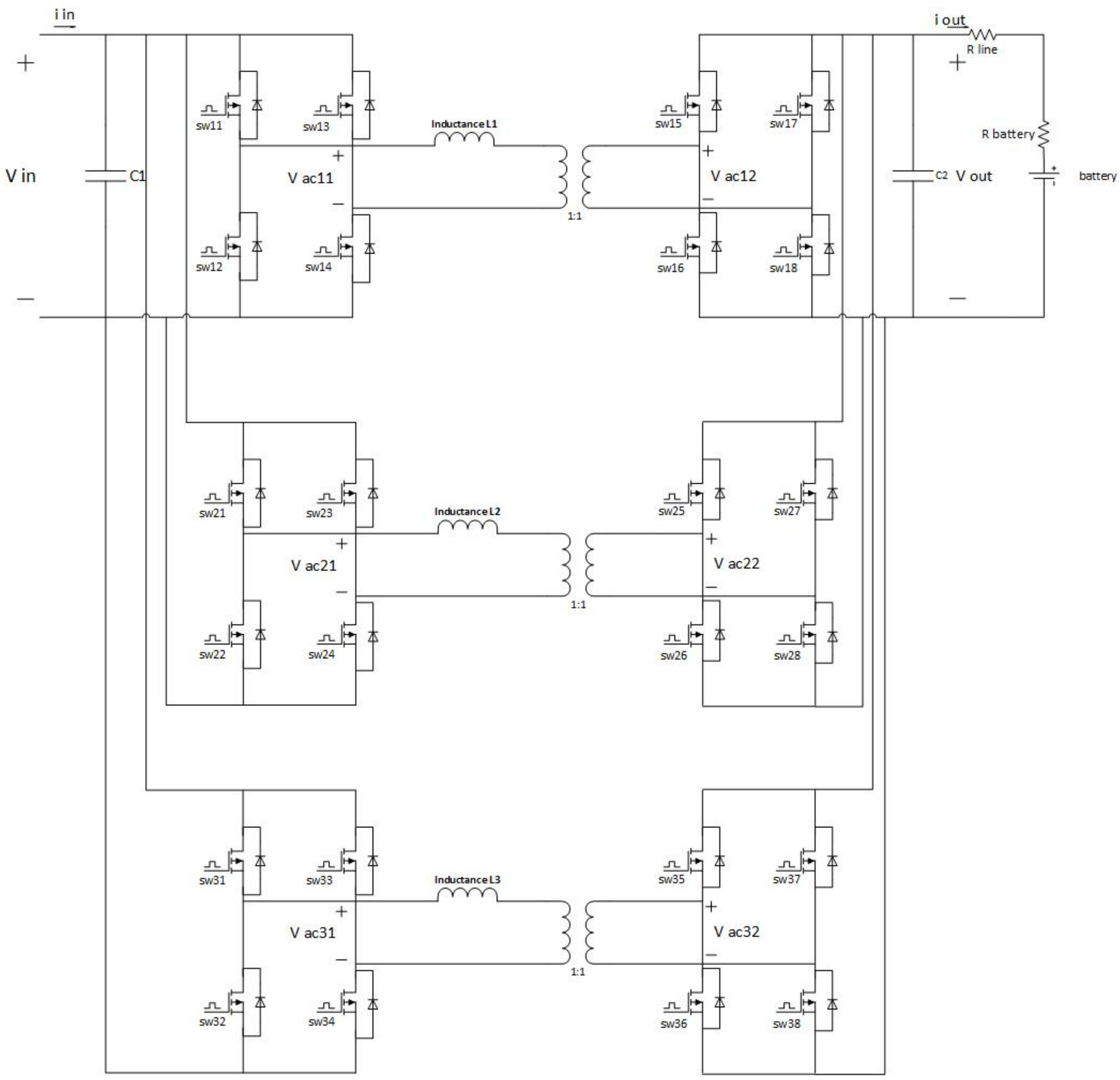

Figure 5.6: IPOP configuration of the 300 kW DC/DC converter.

Among other reasons, it is selected because the interleaving technique allowed to reduce the size and the losses of the input and output filters. Also, just one filter is needed. Moreover, it has a better dynamic performance and higher power density [9]. Finally, it is the cheapest solution since it needs less components.

The next relevant achievement is the control technique used. In this case, it is not as easy as controlling just one module, since three modules have to be controlled at the same time. Several strategies were studied, such as using independent control loops for each one. However, according to [9], using the technique of common phase shift for the three of them is reliable if maximum mismatches in modules parameters of 10% is ensured, which is, in practice, guaranteed, due to the advance of modern manufacturing techniques. Therefore, a common phase shift strategy is implemented.

Once the parallel configuration was settled and the control technique was decided, the small signal model of this new system was obtained, as shown in Figure 5.7.

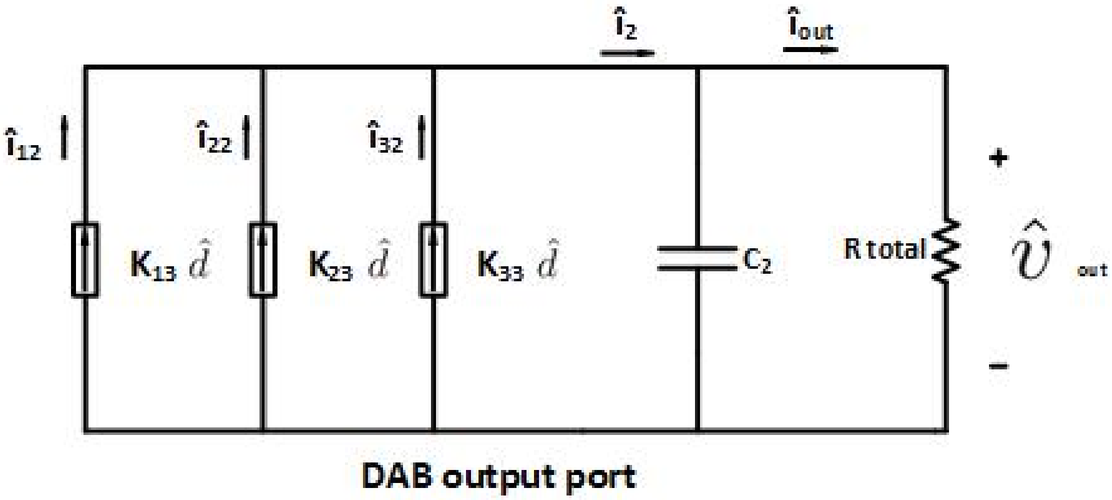

Figure 5.7: Simplified output port of the small-signal circuit model of a 3 modules DAB bidirectional DC/DC converter.

Based on that circuit, the control system is developed. First, the constant current mode is developed, followed by the constant voltage mode.

5.2.1 Constant current mode with current control.

The control loop followed is the one shown in Figure 5.8.

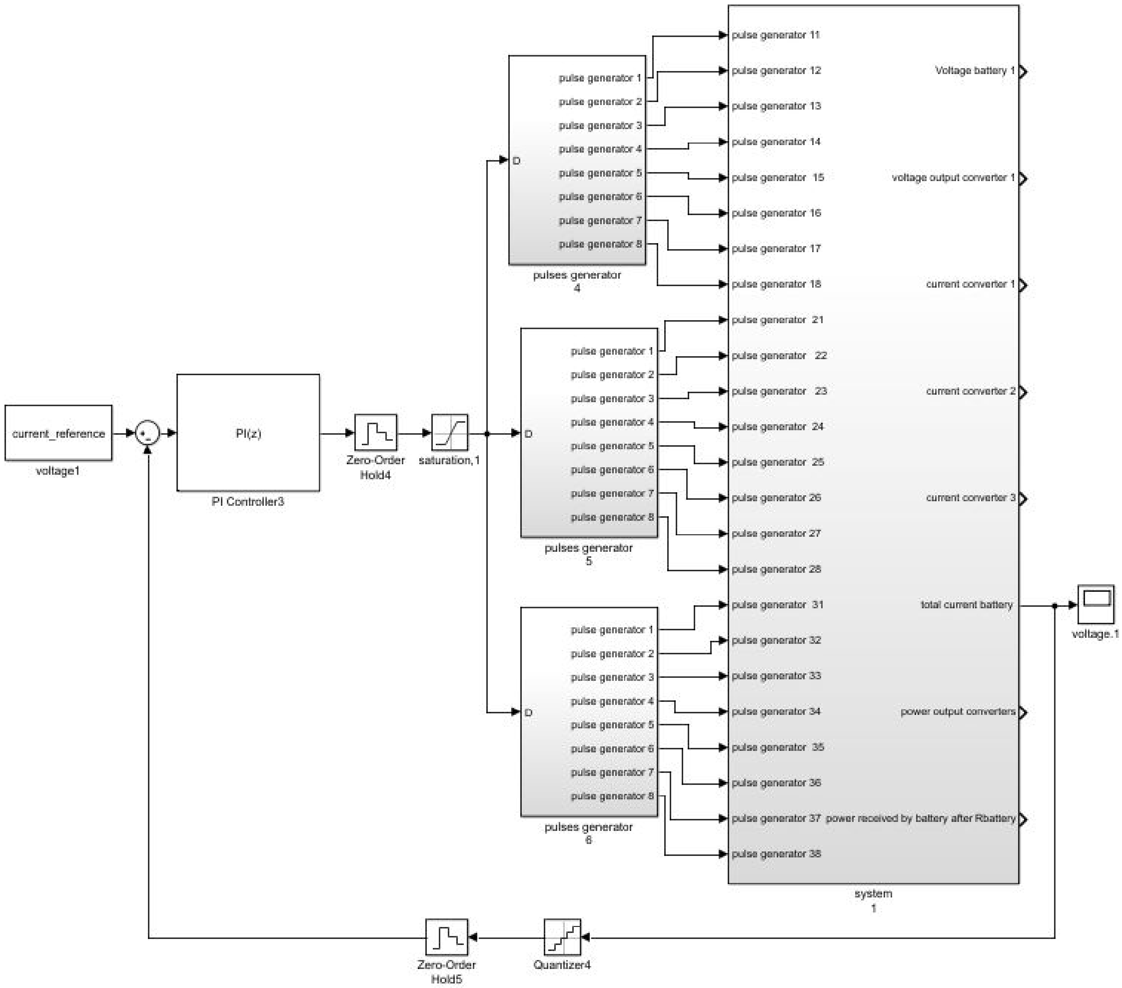

Figure 5.8: Simulink block of the digital current control strategy for a 3 modules DAB bidirectional DC-DC converter.

Based on it, the results obtained for the constant current mode are shown in Figure 5.9. A small disturbance was introduced to observe how the control system behaves.

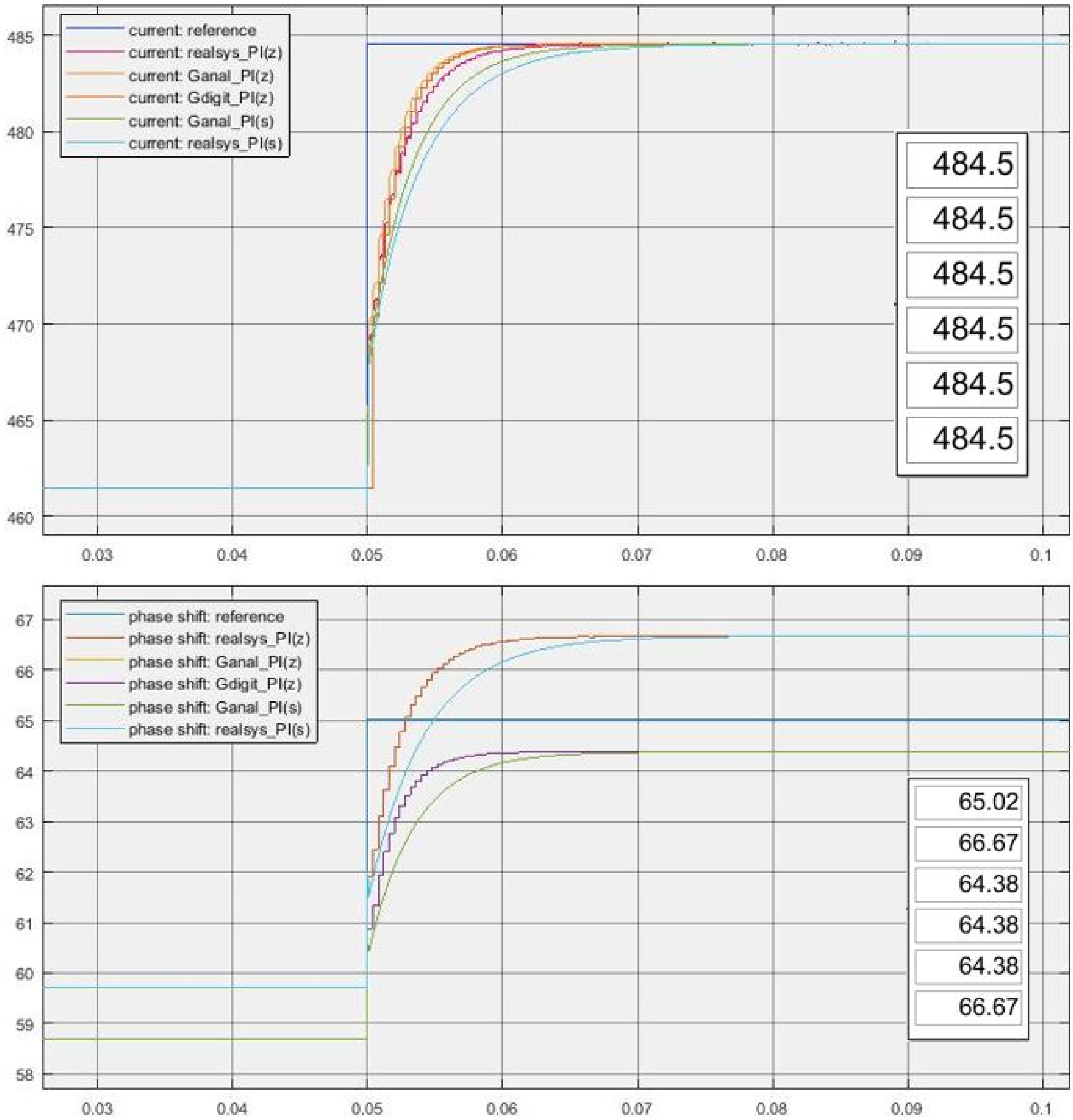

Figure 5.9: Results of the digital current control strategy for a 3 modules DAB bidirectional DC-DC converter.

In Figure 5.9 the first graph is the output current and the second one the phase shift. The curves are, according to the legend: 1. Output converter reference. 2. Output from a real system model controlled with a PI(z). 3. Output from a continuous-time transfer function model controlled with a PI(z). 4. Output from a discrete-dime transfer function model controlled with a PI(z). 5. Output from a continuous-time transfer function model controlled with a PI(s). 6. Output from a real system model controlled with a PI(s).

As it can be seen in Figure 5.9, the system is totally coherent. On one hand, all the models controlled with a discrete PI(z), reaches the new steady state at one time. Same happens with the continuous-time PI(s), but with different setting time, related to the controller used. On the other hand, those based on the real system, reach the same phase shift and higher (deviation of 2.54 %) than the one expected from formulas, as explained before. Also, those based on a transfer function system, reach the same phase shift and lower (deviation of -0.98 %) than the expected from formulas, also explained before.

5.2.2 Constant voltage mode with cascade control.

The control loop followed is the one shown in Figure 5.10.

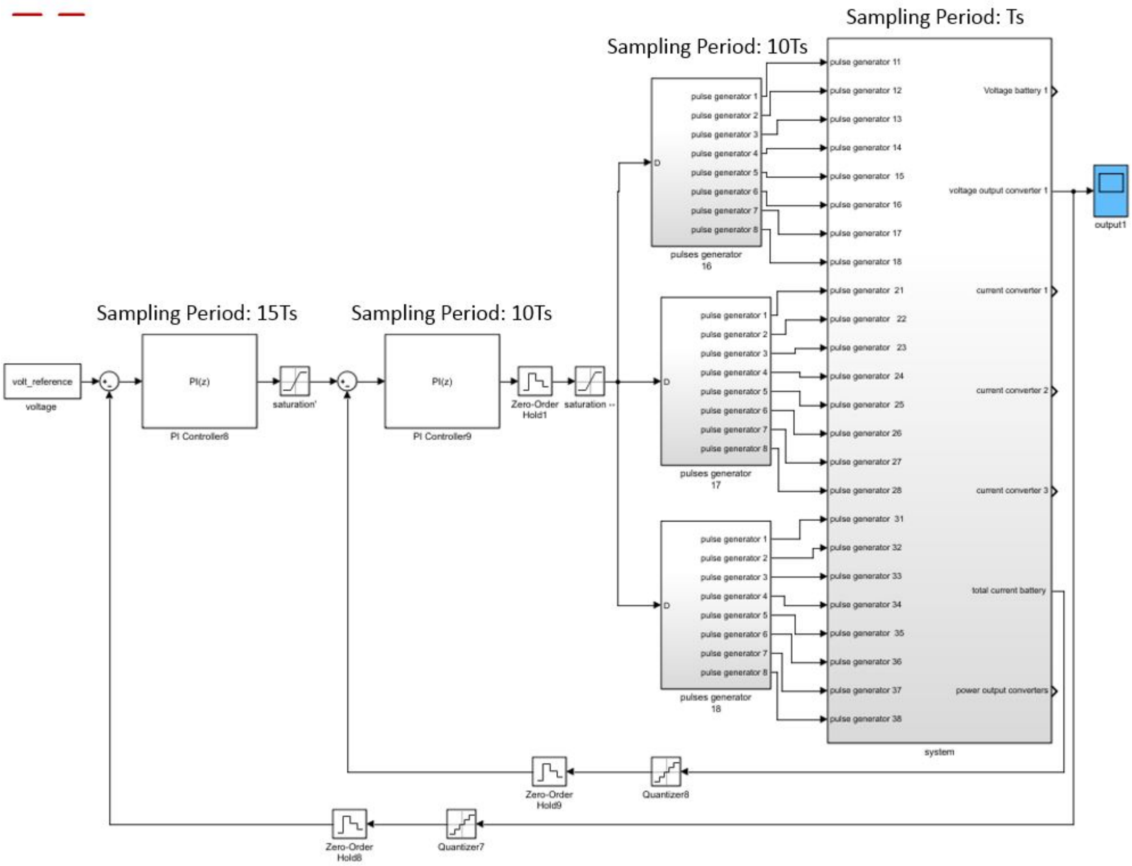

Figure 5.10: Simulink block of the digital cascade control strategy for a 3 modules DAB bidirectional DC-DC converter.

Based on it, the results obtained for the constant voltage mode are shown in Figure 5.11. A small disturbance was introduced to observe how the control system behaves.

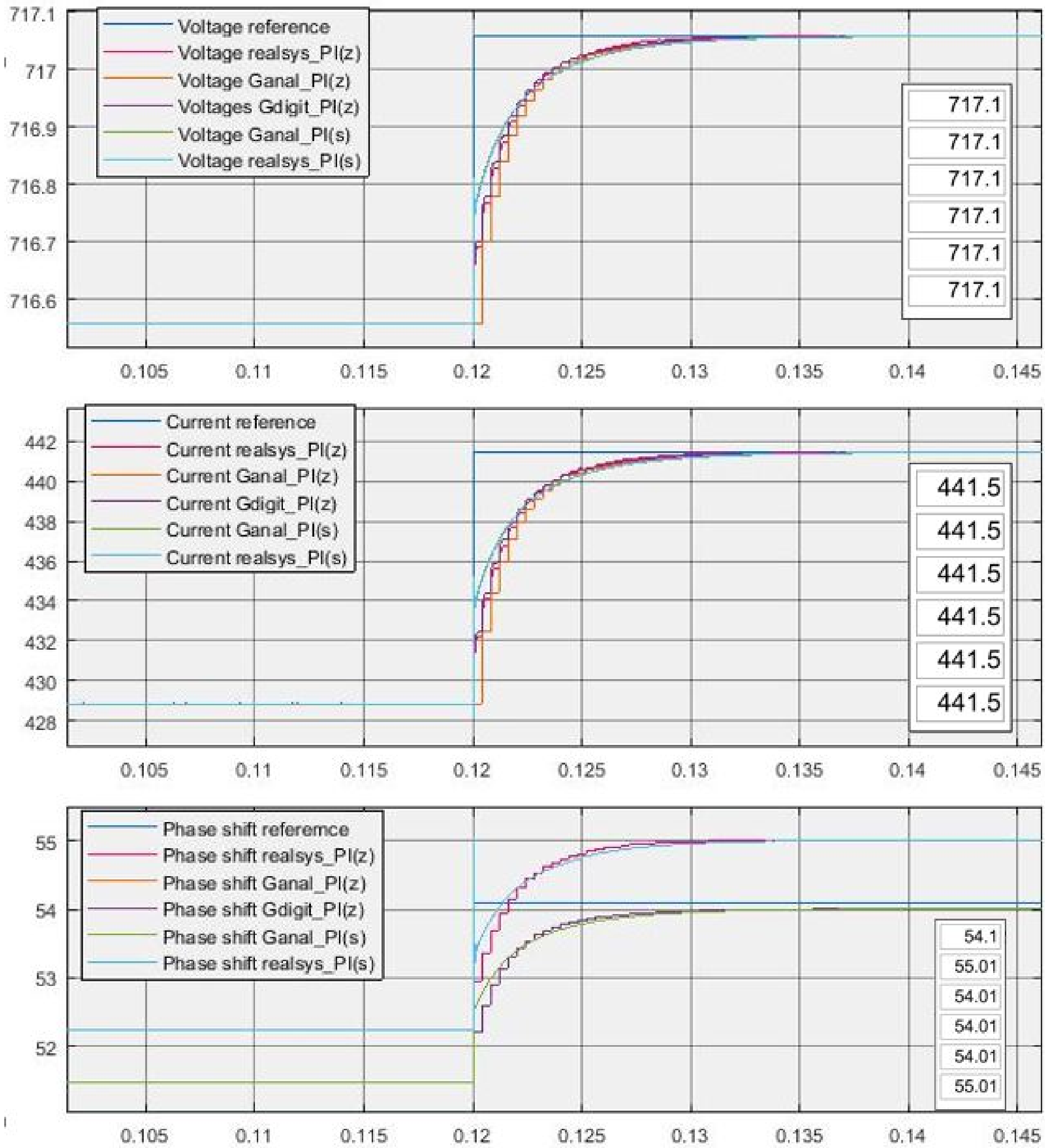

Figure 5.11: Results of the digital cascade control strategy for a 3 modules DAB bidirectional DC-DC converter.

In Figure 5.11, first graph is the output voltage, second one is the output current and the third one the phase shift. The curves are, according to the legend: 1. Output converter reference. 2. Output from a real system model controlled with a PI(z). 3. Output from a continuous-time transfer function model controlled with a PI(z). 4. Output from a discrete-dime transfer function model controlled with a PI(z). 5. Output from a continuous-time transfer function model controlled with a PI(s). 6. Output from a real system model controlled with a PI(s).

As it can be seen in Figure 5.11, the system is totally coherent. On one hand, all the models controlled with a discrete PI(z), reaches the new steady state at the same time. Same happens with the continuous-time PI(s), related to the controller used. On the other hand, those based on the real system, reach the same phase shift and higher (deviation of 1.7 %) than the one expected from formulas, as explained before. Also, those based on a transfer function system, reach the same phase shift and lower (deviation of -0.17 %) than the expected from formulas, also explained before.

Taking a look in all of them, it is important to highlight that the systems have such a smooth reaction to the disturbances because it is equivalent to a first order system, where the typical response in those cases is the one shown in all these results.

6

Conclusion and future work

In this chapter, the conclusions for this Master Thesis are presented.

A complete digital control of a DC/DC converter for a fast charger station of 300 kW for electric vehicles has been presented in this Master Thesis. Therefore, a contribution for reducing the charging time, one of the main drawbacks of electric vehicles, has been achieved.

Moreover, all the goals proposed for this Master Thesis have been accomplished:

1. A steady state analysis of the dc/dc converter was carried out.
2. The small signal modeling of the converter for digital control implementation was developed for both single module a 3 modules DC/DC converters.
3. The charging strategy has been selected.
4. The digital control of a single module DC/DC converter was obtained.
5. The parallel connection for the 3 modules DC/DC converter and its control strategy were decided. It is important to highlight that one of the main achievements of this thesis is that it was demonstrated that the parallel connection of several modules is totally possible and reliable.
6. The digital control of a 3 modules DC/DC converter was developed.

However, it has a weakness. Along this Master Thesis, only the charging mode has been studied. Therefore, the discharging process needs to be studied as well.

As an end for this report, possible future lines are proposed.

As a continuation of this Master Thesis, a DSP implementation of this control technique, for both types of converters, should be developed. As a suggestion, it could be implemented with an Infineon MCU, which are easier to work with than Texas Instruments ones.

Afterwards, it would be time to test it on a lab charger, already built in Chalmers. After that, it could be implemented in a real prototype.

Last but not least, it is important to study as well the uncharging process, since it is a bidirectional charger.

Bibliography

[1] F. Krismer, *“Modeling and optimization of bidirectional dual active bridge DC–DC converter topologies,”* Ph.D. dissertation, Dept. Swiss Federal Inst. Technol. Zurich, Univ. ETH Zürich, Zurich, Switzerland, 2010.

[2] R. W. Erickson and D. Maksimovic, *Fundamentals of power electronics*, second edition, Kluwer Academic, 2004.

[3] V. M. Iyer, S. Gulur, and S. Bhattacharya, *“Small-Signal Modeling and Stability Analysis of a Bidirectional Electric Vehicle Charger”*, vol. 5, pp. 1030–1035, 2017.

[4] V. M. Iyer, S. Gulur, and S. Bhattacharya, *“Optimal design methodology for dual active bridge converter under wide voltage variation”*, in 2017 IEEE Transportation Electrification Conference and Expo (ITEC), June 2017, pp. 413–420.

[5] Bo Feng, Yubin Wang, and Jingbin Man, *“A novel dual-phase-shift control strategy for dual-active-bridge DC-DC converter”*, in Industrial Electronics Society, IECON 2014 - 40th Annual Conference of the IEEE. 2014, pp. 4140–4145. DOI: 10.1109/IECON.2014.7049124.

[6] L. F. Marcelino, H. H. Sathler, T. R. de Oliveira and P. F. Donoso-Garcia, *"Modeling and Control of a Dual Active Bridge for Energy Storage in DC Microgrid Applications"*, in IEEE 8th International Symposium on Power Electronics for Distributed Generation Systems (PEDG), 2017.

[7] J. Guacaneme, G. Garceni, E. Figueres, I. Patrao and R. GonzalezMedina, *"Dynamic modeling of a dual active bridge DC to DC convel1er with average current control and 1oad-current feed-forward"*, in International Journal of Circuit Theory and Applications, vo!. 43, no. 10, pp. l 311-l 332, 2015.

[8] A. R. Alonso, J. Sebastian, D. G. Lamar, M. M. Hernando and A. Vazquez, *“An overall study of a dual active bridge for bidirectional dc/dc conversion,”* in in Proc. IEEE Energy Convers. Congr. Expo., 2010, pp. 1129–1135.

[9] J. Shi, L. Zhou, and X. He, *“Common-duty-ratio control of input-parallel output-parallel (IPOP) connected DC–DC converter modules with automatic sharing of currents,”* in IEEE Trans. Power Electron., vol. 27, no. 7, pp. 3277–3291, Jul. 2012.

[10] L. Yifei, W. Yubin and W. Shanshan, *"Sensorless Current Sharing in Two-Phase Input-Parallel Output-Parallel DC-DC Converters"* in 18th International Conference on Electrical Machines and Systems (ICEMS), IEEE, 2015.

[11] J. J. Shi, T. J. Liu, J, Cheng, and X. N. He, *“Automatic current sharing of an input-parallel output-parallel (IPOP)-connected DC–DC converter system with chain-connected rectifiers,”* in IEEE Trans. Power Electron., vol. 30, no. 6, pp. 2997–3016, Jun. 2015.

[12] L. Yifei, W. Yubin and W. Shanshan, *"Sensorless current estimation and sharing in multiphase input-parallel output-parallel DC-DC converters"* in 2nd International Future Energy Electronics Conference (IFEEC), 2015 IEEE.

[13] S.S. Zhang, *"The effect of the charging protocol on the cycle life of a Li-ion battery"* in Journal of Power Sources 161 2006.

[14] F. Najmabadi, *“Signal Circuit and Transistor Small-Signal Model.,”* Lecture notes.

[15] S. P. Kodali and S. Das, *“Implementation of five level charging scheme in lithium ion batteries for enabling fast charging in plug-in hybrid electric vehicles,”* in National Power Electronics Conference (NPEC), pp. 147–152, 2017.

[16] M. Sato, *“High efficiency design for ISOP converter system with dual active bridge DC-DC converter,”* in Proc. 2016 IEEE Appl. Power Electron. Conf. Expo., 2016, pp. 2465–2472.

[17] Franklin, Powell, and Workman, *Digital Control of Dynamic Systems,* , 3rd. Ed., 1997.

[18] J-P. Corriou, *Process Control. Theory and Applications* 2nd edition, Springer 2004.

[19] F. Haugen, *Discrete-time signals and systems* in TechTeach, 2005.